THE EVALUATION OF THE DAMPING CHARACTERISTICS OF A HARD COATING ON TITANIUM

THESIS

Christopher M. Blackwell, Captain, USAF
AFIT/GAE/ENY/04-M03

DEPARTMENT OF THE AIR FORCE
AIR UNIVERSITY

AIR FORCE INSTITUTE OF TECHNOLOGY

Wright-Patterson Air Force Base, Ohio

AFIT/GAE/ENY/04-M03

THE EVALUATION OF THE DAMPING CHARACTERISTICS OF A HARD COATING ON TITANIUM

THESIS

Presented to the Faculty

Department of Aeronautics and Astronautics

Graduate School of Engineering and Management

Air Force Institute of Technology

Air University

Air Education and Training Command

In Partial Fulfillment of the Requirements for the

Degree of Master of Science in Aeronautical Engineering

Christopher M. Blackwell, BS, MS

Captain, USAF

March 2004

AFIT/GAE/ENY/04-M03

THE EVALUATION OF THE DAMPING CHARACTERISTICS OF A HARD COATING ON TITANIUM

Christopher M. Blackwell, BS, MS
Captain, USAF

Approved:

/signed/

_____ _____

Prof. Anthony N. Palazotto (Chairman) date

/signed/

_____ _____

Major Richard Cobb (Member) date

/signed/

_____ _____

Dr. Peter J. Torvik (Member) date

Abstract

Engine failures due to fatigue have cost the Air Force an estimated $400 million dollars per year over the past two decades (Garrison, 2001). Damping treatments capable of reducing the internal stresses of fan and turbine blades to levels where fatigue is less likely to occur have the potential for reducing cost while enhancing reliability. This research evaluates the damping characteristics of magnesium aluminate spinel, $MgO+Al_2O_3$, (mag spinel) on titanium plates.

The material and aspect ratio were chosen to approximate the low aspect ratio blades found in military gas turbine fans. The plates were tested with a cantilevered boundary condition, using electrodynamic shaker excitation. The effective test area of each specimen was 4-1/2 in. x 4-1/2 in. The nominal plate thickness was 1/8 in. Mag spinel was applied to both sides of the plate, at a thickness of .01 in., and damping tests were run at room temperature. The effect of the coating was evaluated at the 2nd bending mode (mode 3) and the chordwise bending mode (mode 4).

A scanning laser vibrometer revealed the frequency and shape of each mode for the plates. Sine sweeps were used to characterize the damping of the coated and uncoated specimens for the modes tested. The coating increased damping nonlinearly for both modes tested. The test results are presented in this document.

Acknowledgements

I would first like to thank Dr. Anthony Palazotto for his tremendous influence in my AFIT education, both as an instructor and a mentor/friend. His acknowledgement that I had a life outside of the classroom was appreciated.

I also would like to thank Dr. Peter Torvik for focusing my work on the important aspects and warning me of potential pitfalls.

I have immense gratitude for the people of the Turbine Engine Fatigue Facility; Dr. Charles Cross, Gary Terborg, and Angela Smith. Most especially, I thank Dr. Tommy George and Brian Runyon. On more than one occasion it seemed that they were doing all the work and all I could do was watch. Without their willingness to help I could never have left the starting block.

I also would like to thank Captain Brian Lutz. His friendship helped me to maintain my focus on the most important aspect of my life, my relationship with Jesus.

My most humble and gracious wife, you can see the good in everything. I thank you for loving me and helping me to see the silver lining in the AFIT cloud. The anticipation of seeing your smiling face was (and still is) the highlight of my everyday. I love you.

My son the first time you smiled at me I finally understood the priceless joy of parenthood. I love you.

Most of all, I thank my Lord for his sacrifice. Without Him all things are done in vain.

> For the wisdom of this world is foolishness with God. For it is written, He taketh the wise in their own craftiness.
>
> **1Corinthians 3:19**

> The fear of the LORD is the beginning of wisdom: a good understanding have all they that do his commandments: his praise endureth for ever.
>
> **Psalms 111:10**

Table of Contents

Page

Abstract iv

Acknowledgements v

List of Figures viii

List of Tables x

I: Introduction 1

Fatigue 1
Damping 2
Damping Treatments 4
Mag Spinel 6
Application of Mag Spinel 6
Objective of Thesis 8
Related Work 10
Current Approach 11

II: Prediction Methods 16

Approximate Analytic Calculations for Natural Modes of Plates 16
Finite Element Models 19

III: Test Setup and Procedures 23

Test Fixture 23
Test Specimens 25
Uncoated Plates 25
Coated Plates 27
Data Collection 28
Strain Gages 29
Modal Characterization 30
Strain-Velocity-Displacement Calibration 33
Damping Characterization 36

IV: Results and Discussion 40

Resonant Frequencies 40
Comparison to Theoretical Predictions 40
Experimental Resonant Frequencies 41
Mode Shapes 50
Strain/Displacement Relationship 59
Damping 62

Page

V: Conclusions and Recommendations 75

Conclusions 75
Recommendations 77

Appendix A: Scanning Laser Vibrometer Mode Shapes 78

Plate T1 78
Plate T2 83
Plate T3 88

Appendix B: Experimental Data for Uncoated and Coated Plate Sine Sweeps 93

Plate T1 94
Plate T2 96
Plate T3 98

Bibliography 100

Vita 103

List of Figures

Figure Page

Figure 1. Effect of Damping 3

Figure 2. Schematic of Arc Plasma Spray Process (APS Materials, 2004) 7

Figure 3. First Five Plate Modes 9

Figure 4. Plate Geometry 11

Figure 5. Test Fixture 13

Figure 6. Nodal Lines for Cantilevered Square Plate 19

Figure 7. Mode 3 Displacement and Stresses 21

Figure 8. Mode 4 Displacement and Stresses 22

Figure 9. Test Fixture 24

Figure 10. Titanium Plate 26

Figure 11. Titanium Plate Specimen 28

Figure 12. Strain Gage Locations 30

Figure 13. Laser Vibrometry Setup 33

Figure 14. Shaker Table Setup 35

Figure 15. Laser Vibrometer Measurement Location 35

Figure 16. Half-power Bandwidth 37

Figure 17. Nonlinearity of h 39

Figure 18. Frequency Response from Laser Vibrometer for Plate T1 (Uncoated with and without Strain Gages and Coated) 43

Figure 19. Frequency Response from Laser Vibrometer for Plate T2 (Uncoated with and without Strain Gages and Coated) 44

Figure Page

Figure 20. Frequency Response from Laser Vibrometer for Plate T3 (Uncoated with and without Strain Gages and Coated) 45

Figure 21. FEM Solutions: Out-of-Plane Displacement 51

Figure 22. Laser Vibrometer Results: Out-of-Plane Displacement 51

Figure 23. Plate T1: Mode 3 Section Comparison..... 53

Figure 24. Plate T1: Mode 4 Section Comparison..... 54

Figure 25. Plate T2: Mode 3 Section Comparison..... 55

Figure 26. Plate T2: Mode 4 Section Comparison..... 56

Figure 27. Plate T3: Mode 3 Section Comparison..... 57

Figure 28. Plate T3: Mode 4 Section Comparison..... 58

Figure 29. Strain/Displacement Relationship for Plate T1 60

Figure 30. Strain/Displacement Relationship for Plate T2 61

Figure 31. Strain/Displacement Relationship for Plate T3 61

Figure 32. Sine Sweeps for Plate T1: Mode 3 Uncoated and Coated 64

Figure 33. Sine Sweeps for Plate T1: Mode 4 Uncoated and Coated 65

Figure 34. Sine Sweeps for Plate T2: Mode 3 Uncoated and Coated 66

Figure 35. Sine Sweeps for Plate T2: Mode 4 Uncoated and Coated 67

Figure 36. Sine Sweeps for Plate T3: Mode 3 Uncoated and Coated 68

Figure 37. Sine Sweeps for Plate T3: Mode 4 Uncoated and Coated 69

Figure 38. Q-Strain Relationship for Plate T1: Uncoated and Coated 70

Figure 39. Q-Strain Relationship for Plate T2: Uncoated and Coated 71

Figure 40. Q-Strain Relationship for Plate T3: Uncoated and Coated 72

List of Tables

Table Page

Table 1. Resonant Frequency Calculations 17

Table 2. FEM Calculations for Mode 3 20

Table 3. FEM Calculations for Mode 4 20

Table 4. Comparison of FEM to Mathematical Predictions 20

Table 5. Uncoated Plate Measurements 26

Table 6. Coated Plate Measurements 27

Table 7. Comparison of Theoretical to Experimental Mode 3 Natural Frequency for the Uncoated Plates without Strain Gages (Frequencies are in Hz) 41

Table 8. Comparison of Theoretical to Experimental Mode 4 Natural Frequency for the Uncoated Plates without Strain Gages (Frequencies are in Hz) 41

Table 9. Resonant Frequency from Laser Vibrometer Test for Plate T1 (Uncoated without Strain Gages) (Frequencies are in Hz) 46

Table 10. Resonant Frequency from Laser Vibrometer Test for Plate T2 (Uncoated without Strain Gages) (Frequencies are in Hz) 46

Table 11. Resonant Frequency from Laser Vibrometer Test for Plate T3 (Uncoated without Strain Gages) (Frequencies are in Hz) 46

Table 12. Resonant Frequency from Laser Vibrometer Test for Plate T1 (Uncoated with Strain Gages) (Frequencies are in Hz) 47

Table 13. Resonant Frequency from Laser Vibrometer Test for Plate T2 (Uncoated with Strain Gages) (Frequencies are in Hz) 47

Table 14. Resonant Frequency from Laser Vibrometer Test for Plate T3 (Uncoated with Strain Gages) (Frequencies are in Hz) 47

Table 15. Comparison of Resonant Frequencies from Laser Vibrometer for Plate T1: Uncoated with and without Strain Gages (Frequencies are in Hz) 48

Table Page

Table 16. Comparison of Resonant Frequencies from Laser Vibrometer for Plate T2: Uncoated with and without Strain Gages (Frequencies are in Hz) 48

Table 17. Comparison of Resonant Frequencies from Laser Vibrometer for Plate T3: Uncoated with and without Strain Gages (Frequencies are in Hz) 48

Table 18. Comparison of Uncoated Resonant Frequencies to Coated Resonant Frequencies from Laser Vibrometer for Plate T1 (Frequencies are in Hz) 49

Table 19. Comparison of Uncoated Resonant Frequencies to Coated Resonant Frequencies from Laser Vibrometer for Plate T2 (Frequencies are in Hz) 49

Table 20. Comparison of Uncoated Resonant Frequencies to Coated Resonant Frequencies from Laser Vibrometer for Plate T3 (Frequencies are in Hz) 49

Table 21. Uncoated versus Coated Q Comparison at Different Strains for Plate T1 73

Table 22. Uncoated versus Coated Q Comparison at Different Strains for Plate T2 73

Table 23. Uncoated versus Coated Q Comparison at Different Strains for Plate T3 74

Table 24. Average Uncoated versus Average Coated Q Comparison at Different Strains 74

THE EVALUATION OF THE DAMPING CHARACTERISTICS OF A HARD COATING ON TITANIUM

I: Introduction

Fatigue

Fatigue is the failure of material through cyclic loading at stresses below the ultimate stress. This occurs by the formation and growth of microscopic cracks during each load cycle. Fatigue is generally divided into two categories: low-cycle fatigue (LCF) and high-cycle fatigue (HCF). LCF is characterized by higher loads and fewer cycles to failure than HCF. The reason for this is that LCF strains are dominated by larger plastic regions for each cycle, whereas HCF strains are predominately elastic for each cycle (Grady, 1999).

Over the years, LCF failures in aircraft engines have been greatly reduced through the use of fracture mechanics and a retirement-for-cause management philosophy, leaving HCF as the primary cause of engine failures (Nicholas, 1996). There are many different sources of mechanical vibration that lead to HCF damage in turbine engines. Some of these sources are aerodynamic excitation, airfoil flutter, and acoustic fatigue. As improvements for increased performance and reduced weight have been implemented in engines, the operating temperatures, stresses, and stage loading have increased, making the HCF problem more acute (Cowles, 1996). Throughout the 1980s and 1990s, HCF

was the single largest cause of aircraft engine failure, resulting in lost aircraft and the expenditure of many millions of maintenance man-hours and dollars. Estimates put the cost of high cycle fatigue at over $400 million per year (Garrison, 2001). Fatigue in engine blades, what this research is trying to minimize through damping, is the result of stresses generated by unsteady aerodynamic loading which cause vibrations at or near a resonance condition (Shen, 2002).

Damping

Damping is the dissipation of mechanical energy from a system while subjected to cyclic loading (Lazan, 1959 and Ungar 2001). Damping materials are designed to maximize the energy dissipation in a system. Most damping materials must be combined with structural elements to be useful in engineering applications. When combined in this manner the damping material is generally called a 'damping treatment' (Ungar, 2001). These treatments can be used to avoid premature failure by reducing the displacement amplitude of oscillations at resonance, which reduces the cyclic stresses. A system with relatively no damping will have a larger displacement amplitude at resonance than one with damping (**Figure 1**) (Baz, 2001). In the figure, frequency is along the horizontal axis and vibration amplitude is along the vertical axis. The zero damping curve in the figure will theoretically extend to infinity. Damping is generally found to be one of the most structure-sensitive properties that can be measured (Lazan, 1968). There are two major categories of damping behavior; elastic and inelastic. For a material to be "perfectly elastic" its stress-strain curve must be linear and no rate or time dependence is

present. "Inelasticity" is simply any deviation from the "perfectly elastic" condition. There are several different types of damping mechanisms to include: dynamic hysteresis, static hysteresis, plastic strain damping, and internal friction. For reasons discussed later in this chapter internal friction is the mechanism of concern for this study. The effect of such test conditions as stress amplitude, frequency, and temperature can be significant and must therefore be well understood and documented. All testing was done at room temperature. The effects of stress amplitude and frequency are presented in **Chapter IV**.

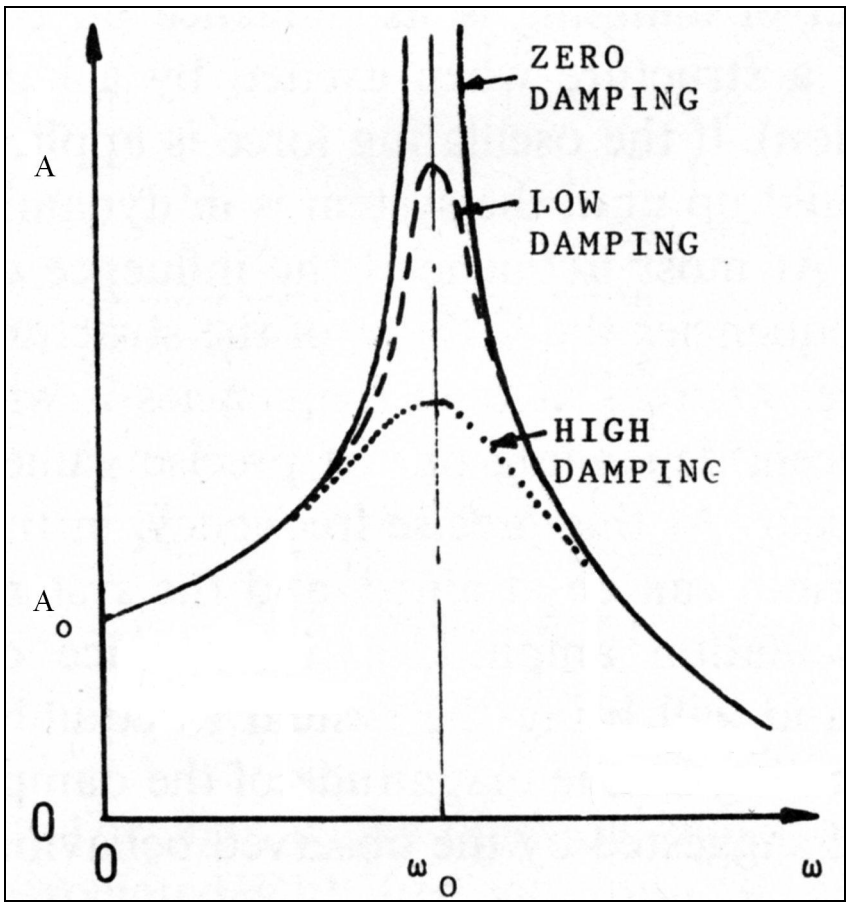

Figure 1. Effect of Damping

There are two main approaches to damping design: passive and active. Active damping techniques incorporate the control of sensors and actuators and are generally used for low frequency excitations. The most common active dampers are made of piezoelectric films bonded to the specimen. Passive damping techniques include the application of damping coatings. Viscoelastic coatings are generally more effective against high frequency excitations, but are typically effective for only small frequency ranges because of the significant variation of the damping material properties with temperature and frequency (Baz, 2001). Hard coatings do not generally suffer from these constraints. The propulsion community, in its quest for a solution to the high cycle fatigue problem, has focused its efforts on passive damping, due to its simplicity of application and effectiveness at high frequency. Some hybrid approaches also exist; which are combinations of active and passive methods and can provide control over broader frequency ranges. (Baz, 2001)

Damping Treatments

Surface damping coatings are often used to solve resonant noise and vibration problems associated with structures of small cross-sectional area, such as beams, plates, or turbine engine airfoils. These coatings can be easily applied and provide high damping over wide temperature and frequency ranges (Nashif, 1985). Traditionally the materials used have been viscoelastic polymeric plastics or elastomers. A viscoelastic material has the properties of both viscous (energy dissipating) and elastic (energy storing) materials. The damping arises from relaxation and recovery of the polymer network after

it has been deformed, and a strong dependence exists between frequency effects and temperature effects because of the direct relationship between material temperature and molecular motion. By proper tailoring, polymeric materials can be manufactured to possess a wide variety of damping, strength, durability, creep resistance, thermal stability, and other desirable properties, over selected temperature and frequency ranges (Nashif, 1985).

High-damping metal alloys have better damping properties than common metals but do not provide the same level of damping that viscoelastic materials do. However, viscoelastic materials are generally effective only for a small temperature range while the high-damping metal alloys can be effective over a greater temperature range (Ungar, 2001). These high damping alloys are not usually the best adapted to practical construction purposes, since the gain in damping is often at the expense of stiffness, strength, durability, corrosion resistance, cost, machinability, or long term stability (Nashif, 1985). In aircraft engines, even a small amount of damping can have a pronounced effect, and damping over an extended temperature range is crucial. Over the past few years the propulsion community has shifted focus from viscoelastic damping materials back to metallic or hard coatings.

The usefulness of hard coatings as dampers has been known to engineers since the early 1960's. The damping mechanism was initially assumed to be friction between the particles; which was recently supported experimentally (Green, 2002, Shipton, 2003, and Patsias, 2003). These coatings generally behave in a non-linear strain-dependent manner. Of particular interest is the air plasma sprayed oxide ceramic coating known as Magnesium Aluminate Spinel (mag spinel), $MgO+Al_2O_3$.

Mag Spinel

The value of mag spinel is that it has a higher damping capacity than other ceramic materials (Shipton, 2003). Magnesium aluminate spinel ($MgO+Al_2O_3$) is an aggregate consisting of 25 to 28% MgO, and small amounts of other oxides (e.g. CaO, SiO_2, Ma_2O, Fe_2O_3) and 71 to 74% Al_2O_3. The density of powders provided for use in erosion/corrosion control is typically given as 3.3 gm/cm^3 (Torvik 2002). Its properties make it useful for erosion resistance against gas streams at elevated temperature; hence, its interest for use in gas turbine engines. Torvik, et al. have reported that mag spinel provides enough damping to be of interest to the propulsion community (Torvik, 2002).

Application of Mag Spinel

The two most common methods for applying hard coatings are air plasma spraying and physical vapor deposition. The mag spinel for this research was applied by air plasma spraying. Air plasma spray offers advantages in cost, lower application temperatures, and fewer limitations on component size (Patsias, 2001). Plasma spraying provides a denser, stronger coating than most other spray processes. The high temperature of the plasma allows materials with high melting points to be applied as a coating that cannot be applied by any other means (APS Materials, 2004).

Plasma spraying is the process of applying a coating to a substrate material by injecting the coating in a powder form into a high temperature plasma gas and spraying it at high velocity onto the target substrate. The plasma gas (typically air, argon, nitrogen,

hydrogen, or helium) converts the powder to a molten state. As the spray impacts the substrate, it cools very quickly, forming a bond with the surface (**Figure 2**) (APS Materials, 2004). When the spray chamber contains the common atmosphere, the process is known as air plasma spraying, which is the most common form of plasma spraying. Occasionally, the atmosphere can provide undesirable contaminants to the coating so the chamber is filled with an inert gas at low pressure. This process is called vacuum spraying (APS Materials, 2004).

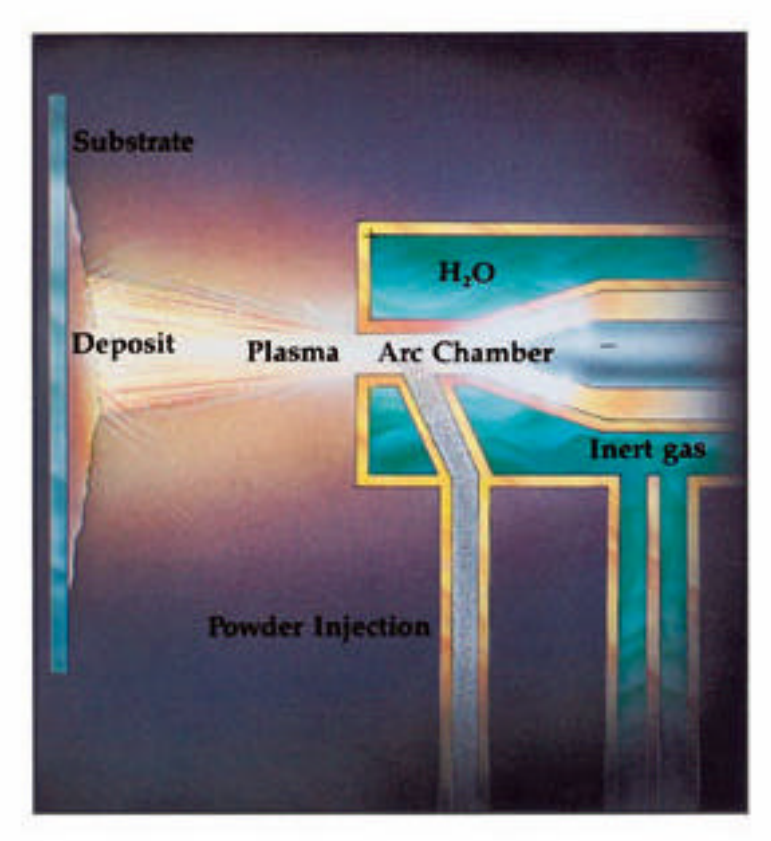

Figure 2. Schematic of Arc Plasma Spray Process (APS Materials, 2004)

The thermal sprayed mag spinel has a more refined defect structure than most other thermal sprayed oxide coatings. The microstructure is similar to a massive array of parallel plates with an aspect ratio typical of any thermally sprayed oxide ceramic. The best performing coatings are those applied with a high power plasma, a fine powder, and a 90^{o} angle. (Shipton, 2003)

Objective of Thesis

The objective of this investigation is to determine the effect on damping of a square titanium plate by the application of a mag spinel hard coating. Ti-6Al-4V was chosen as the plate material for this investigation because of its extensive use in aircraft fan and compressor blades. The aspect ratio of the plates approximates the low aspect ratio blades found in military gas turbine fans. The effect of the coating will be evaluated at the 2^{nd} bending mode (mode 3) and the two stripe, or chordwise bending, mode (mode 4). A three dimensional representation of the first five mode shapes taken from laser vibrometry tests is shown in **Figure 3**.

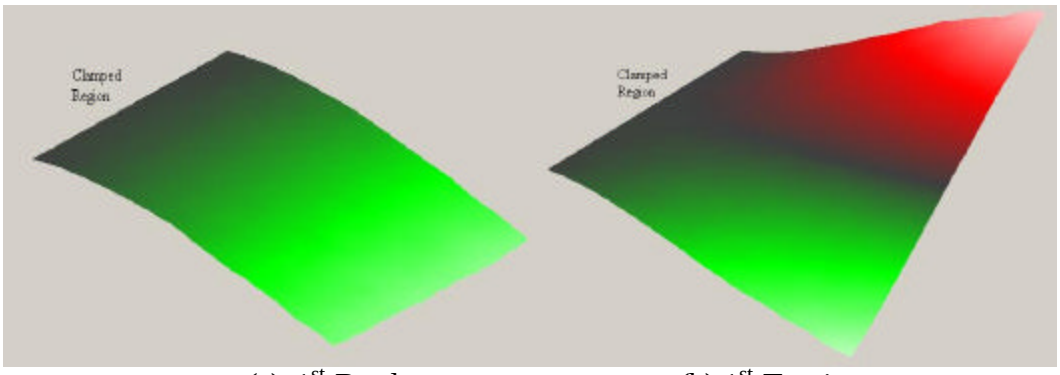

(a) 1st Bend (b) 1st Torsion

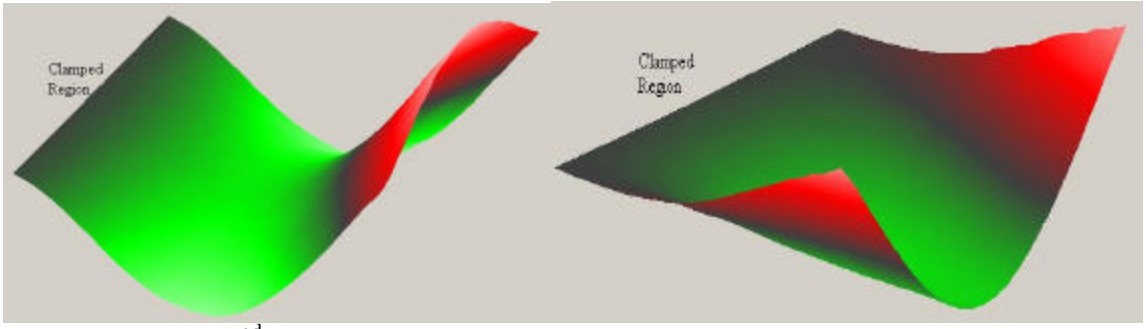

(c) 2nd Bend (d) Chordwise

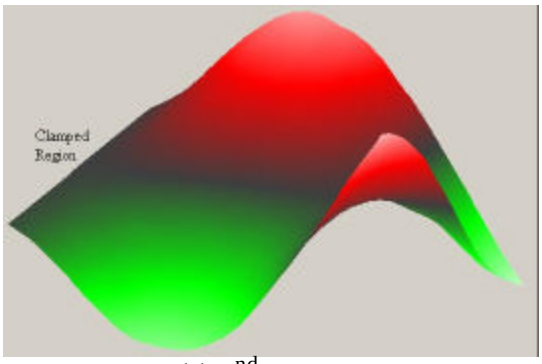

(e) 2nd Torsion

Figure 3. First Five Plate Modes

Related Work

Several approaches to reducing turbine blade vibrations have been to introduce additional damping from blade dampers. Dry friction dampers, which include blade-to-ground, blade-to-blade, and shroud dampers are the most common in use today. However, the gain in damping from dry friction dampers is negligible for high frequency vibration. This has motivated recent research of high frequency dampers. (Shen, 2002)

Some experiments for reducing vibratory stresses on rotating blades have been done by inserting patches of viscoelastic damping materials into milled cavities of the airfoil, which is then sealed with a cover sheet to maintain structural integrity and airfoil shape (Kielb, 2000). This approach is limited by the temperature constraints of the viscoelastic damping treatment and the manufacturability and durability of the milled airfoils (Shen, 2002).

Torvik, et al. (2002) examined the damping effect of mag spinel on Hastalloy X, a nickel-based alloy commonly found in aircraft engines, and found that the coating provided sufficient damping to be effective in reducing vibration amplitudes in aircraft engines. They observed that the response functions were not symmetric about the resonance frequency, and the resonance frequency decreased as the amplitude of the applied force was increased, indicating stiffness non-linearity, or softening. This was also observed by Shen (2002). The amount of energy dissipated by the coating was shown to be strain dependent. They further concluded that over the first four bending modes, the level of damping obtained was independent of frequency. (Ivansic, 2003)

Current Approach

This investigation compares the response of titanium plates before and after a mag spinel coating was applied to each side. The material and aspect ratio were chosen to approximate the low aspect ratio blades found in military gas turbine compressors. The plates were tested with a cantilevered boundary condition for modes three and four. This simulated the cantilevered condition of operational turbine blades and two of the more common mode shape families. The excitation was applied through the base. The specimens used for this study were 4-1/2 in. x 7 in. x 1/8 in. Ti-6Al-4V plates. The effective test area was 4-1/2 in. x 4-1/2 in. with a 2 in. clamped region and a 1/2 in. tail behind the clamp to help when removing the specimen from the fixture (**Figure 4**).

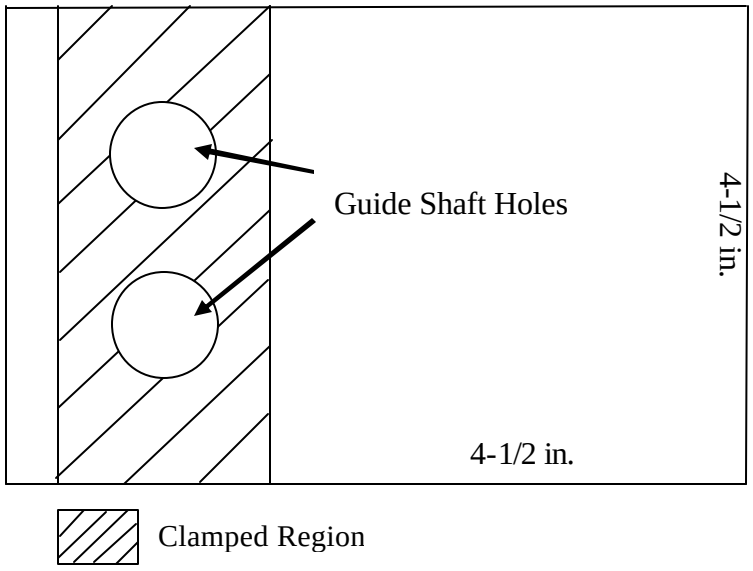

Figure 4. Plate Geometry

For this research a two piece fixture was designed based on prior Turbine Engine Fatigue Facility (TEFF) experience to increase repeatability. Previous designs could not easily prevent the specimens from shifting in an in-plane direction while under load (Ivansic, 2003). This design, which sandwiches the plate between two steel blocks, has eliminated the tendency for the plates to shift by adding two guide shafts through the clamped area of the plate. **Figure 5** shows the plate mounted on the bottom portion of the fixture with the two guide shafts through the clamped region. The top piece slides over the guide shafts and rests on the plate. Four bolts, one through each guide shaft and one beyond both ends of the plate are used to provide the clamping force on the plate. These shafts also eliminated the variability of the effective plate geometry (4-1/2 in. x 4-1/2 in.) from one setup to the next. Without the guide shafts, it would have been necessary for the researcher to measure the test area before each experiment. A slight difference could influence the repeatability of the experiments. The guide shafts eliminated that problem and it can be seen from results presented in **Chapter IV** that repeatability was excellent.

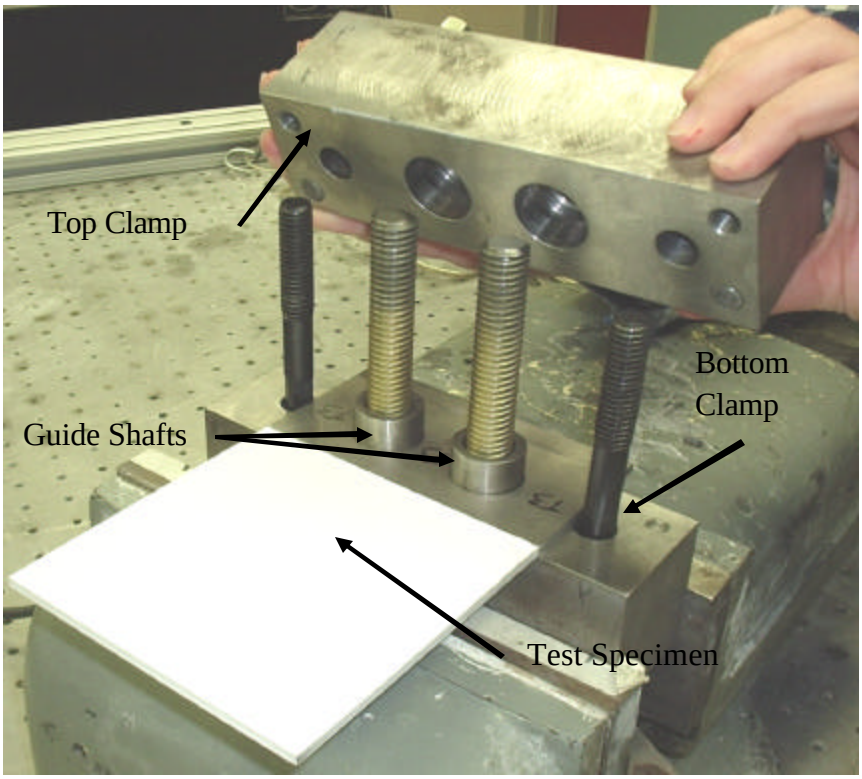

Figure 5. Test Fixture

The mag spinel coating was applied to the test area on both sides of the plate by air plasma spray. All damping tests were conducted at room temperature. Damping was characterized by a series of sine sweeps for each of three plates before and after the mag spinel was applied. The excitation load was increased for each successive sweep. The "half-power bandwidth" method was used to determine the level of damping for each sine sweep and comparisons were made between the coated and uncoated configurations. Test specimens were characterized by frequency, mode shape, damping, and stress pattern. Testing was conducted at the Turbine Engine Fatigue Facility, AFRL/PRTS, Wright-Patterson AFB, OH.

A scanning laser vibrometer measured the frequency for each mode and the displacement contour of the plate. These contours were compared with FEM models, which were used to determine the stress ratio of the stress at the strain gage location (discussed in **Chapter III**) to the maximum stress for the two resonant modes under consideration. Stress and strain are related through Hooke's Law.

$$s = Ee \tag{1}$$

where

s = stress
E = Young's modulus
e = strain

FEM was used to determine the resonant frequencies, mode shapes, and stress ratios for the uncoated plates. Sine sweeps with strain gages attached were used to develop the strain/displacement relationship by comparing the peak laser vibrometer response to the peak strain gage response. Since strain is proportional to displacement for the levels reached in this research, it was necessary to convert the velocity measurements to displacement. Because strain gages will add some damping to the system, the strain/displacement relationship had to be established before the strain gages were removed and the damping could be measured for the uncoated and coated conditions. Damping ratios, for several strains up to a maximum of 500 micro-strain, were determined by conducting sine sweeps on a 6,000 lb electro-dynamic shaker and

measuring the plate's dynamic response with a single point laser vibrometer. The purpose of this research was to focus on the damping characteristics of mag spinel at low strains; therefore 500 micro-strain was chosen as the upper limit. The same titanium plates were compared before and after the mag spinel coating was applied.

II: Prediction Methods

Two methods were used to predict the natural frequencies and mode shapes of the uncoated titanium plates: analytic calculation and finite element modeling. The mathematical calculations were used to validate the FEM.

Approximate Analytic Calculations for Natural Modes of Plates

When a system is subjected to an oscillatory load, vibration occurs. The displacement of the system from the vibration is related to the frequency and strength of the applied load. The amplitude of the displacement will reach peaks at points along the frequency bandwidth known as the natural frequencies. Classical Plate Theory can be used to derive the natural frequencies.

Leissa cites Young for the derivation of the natural frequency equation for a square plate in the clamped-free-free-free condition. In his derivation of the following equation he used the products of beam functions and the Rayleigh method to obtain the natural frequencies (Leissa, 1969). The nominal geometry was used for comparison to experimental values.

$$w_n = \frac{C}{a^2\sqrt{\frac{rt}{D}}} \tag{2}$$

$$\mathrm{D} = \frac{Et^3}{12\left(1-v^2\right)} \tag{3}$$

(Leissa, 1969)

where

w_n = natural frequency
C = modal constant
first five modes:
$C_1 = 3.494$
$C_2 = 8.547$
$C_3 = 21.44$
$C_4 = 27.46$
$C_5 = 31.17$
a = plate length
r = mass density
t = plate thickness
D = flexural rigidity
E = Young's modulus
v = Poisson's ratio

This method gives natural frequency solutions in terms of radians/sec. To convert to Hertz (cycles/sec) use the following equation:

$$f_n = \frac{w_n}{2p} \tag{4}$$

The results for the given modes of interest are presented in **Table 1**.

Table 1. Resonant Frequency Calculations

	Mode 3 (Hz)	Mode 4 (Hz)
Leissa	1257	1610

The shape of the displacement pattern at a natural frequency is called the mode shape. The total motion at any point of the system is the sum of the motions resulting from the vibration of the respective modes. A completely undamped system excited at a natural frequency will continue to oscillate at that frequency. Such a condition is called resonance and if allowed to continue the vibration amplitudes will intensify until the system fails. However, there is always some degree of damping, which not only reduces the vibration amplitude but results in the superposition of all modes at each natural frequency with varying degrees of intensity. If damping is negligible then the intensity of the primary mode approaches unity and the others approach zero. If the only damping is a result of the plate's material properties and the geometry is simple, the modes will closely approximate the undamped natural modes (Soedel, 1993). The research presented here follows that assumption.

There are always nodal points, lines, or surfaces in each of the normal modes of vibration of any system. For the fundamental mode, which corresponds to the lowest natural frequency, the supported or fixed points of the system usually are the only nodal points; for other modes, there are additional nodes. In the modes of vibration corresponding to the higher natural frequencies of some systems, the nodes often assume complicated patterns. In certain problems involving forced vibrations, it may be necessary to know what the nodal patterns are, since a particular mode usually will not be excited by a force acting at a nodal point (Harris, 1996). Mode shapes, as defined by the nodal lines, for the first five modes of a cantilevered square plate are shown in **Figure 6** (Leissa, 1969).

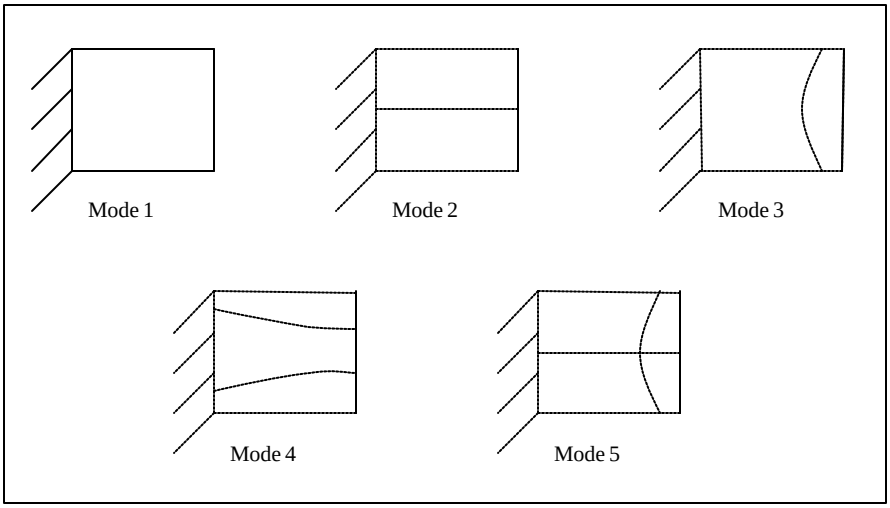

Figure 6. Nodal Lines for Cantilevered Square Plate

Finite Element Models

Finite element modeling was performed using NASTRAN version 2001.0.1 to determine the natural frequencies of the uncoated plates. The nominal plate dimensions of 4 1/2 in. x 4 1/2 in x 1/8 in. were used. Three different mesh densities consisting of 256, 529, and 900 QUAD4 elements, were used to satisfy convergence of the finite model to a continuous system. At each mesh density a lumped mass and consistent mass matrix were used to obtain a bound for the natural frequencies. The lumped mass matrix formulation results in a lower bound on the actual natural frequency and the consistent mass matrix formulation results in an upper bound on the actual natural frequency. The solution algorithm used the Lanczos method to solve the eigenvalue (natural frequency) problem. For a detailed discussion of this solution method see Cook, 2002. For this geometry, all the nodes along one edge of the plate were constrained in all six degrees of

freedom to represent a cantilevered condition and all other nodes were unconstrained. The material properties were obtained from MIL-HDBK-5CD-ROM, May 1997 for Ti-6Al-4V (Young's Modulus = 1.6*10^7, Poissan's Ratio = .31, and Yield Stress = 126 ksi). As the mesh density was increased, the frequency results converged to a single value; see **Table 2** for mode 3 frequencies and **Table 3** for mode 4 frequencies. A comparison to the analytic predictions verified the accuracy of the finite element model. A 256 element model and Young's equation, have very good agreement (**Table 4**). As the number of elements used in the model increases, agreement with the prediction improved. All percent differences in this paper were calculated using **Equation 5**.

$$\% \text{ Diff} = \frac{HighValue - LowValue}{HighValue} * 100\% \tag{5}$$

Table 2. FEM Calculations for Mode 3

# of Elements	Lumped (Hz)	Consistent (Hz)	% Difference
256	1230.7	1244.8	1.13
529	1235.1	1242	0.56
900	1236.8	1240.8	0.32

Table 3. FEM Calculations for Mode 4

# of Elements	Lumped (Hz)	Consistent (Hz)	% Difference
256	1562.6	1587.6	1.57
529	1573	1585.2	0.77
900	1576.9	1584.1	0.45

Table 4. Comparison of FEM to Mathematical Predictions

	FEM Lumped (256 Elements)	Young Prediction	% Difference
Mode 3	1230.7	1257	2.1
Mode 4	1562.6	1610	2.9

The displacement and stress solutions were normalized to a maximum value of unity. This means that the actual stresses and displacements were unknown from the model, but the ratio of the displacement or stress at one point, usually the maximum location, to any other point on the plate is known. The second location is usually where the strain gage is placed. Using this ratio, the maximum stress will be known during experiments, even if the strain gage is not located at the point of maximum stress. Hooke's law (**Equation 1**) was used to relate the stresses to strains. **Figure 7** shows the plate out-of-plane displacement and relative stresses for mode 3. **Figure 8** shows the plate out-of-plane displacement and relative stresses for mode 4.

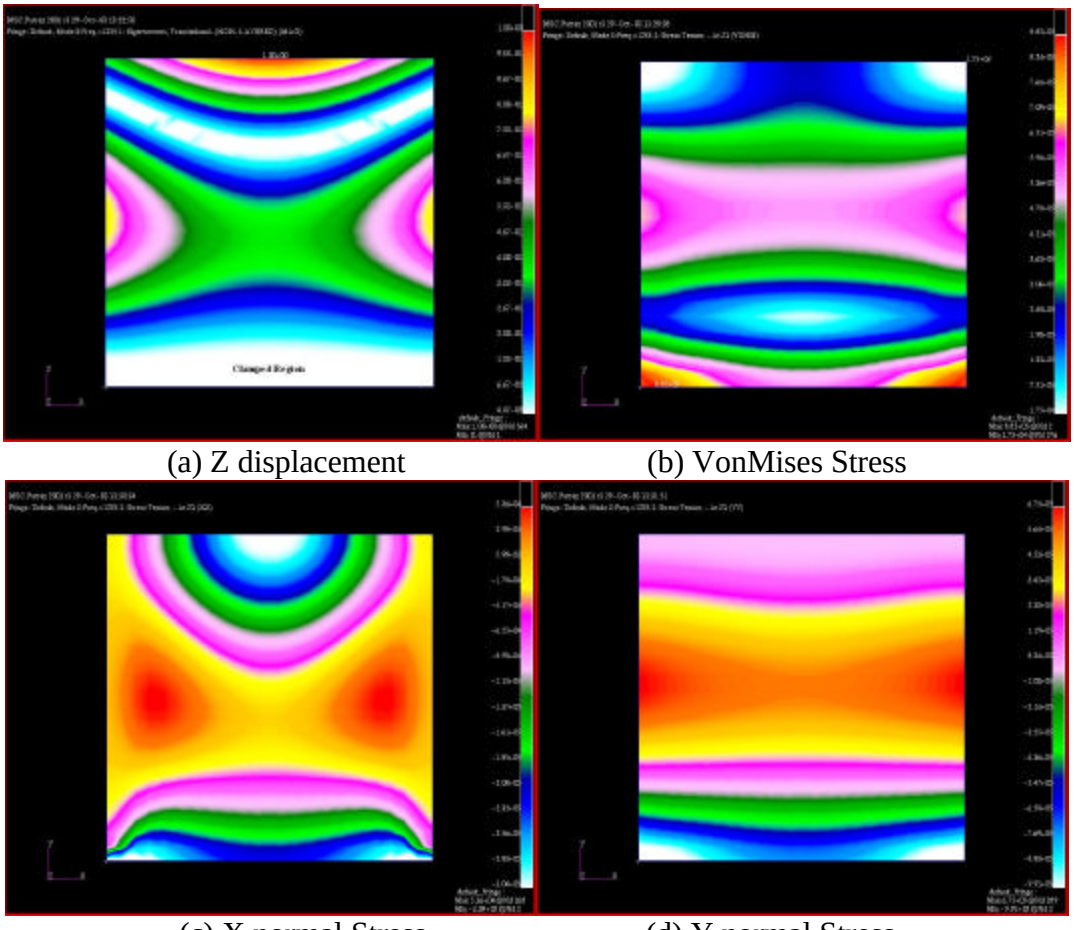

(a) Z displacement (b) VonMises Stress

(c) X normal Stress (d) Y normal Stress

Figure 7. Mode 3 Displacement and Stresses

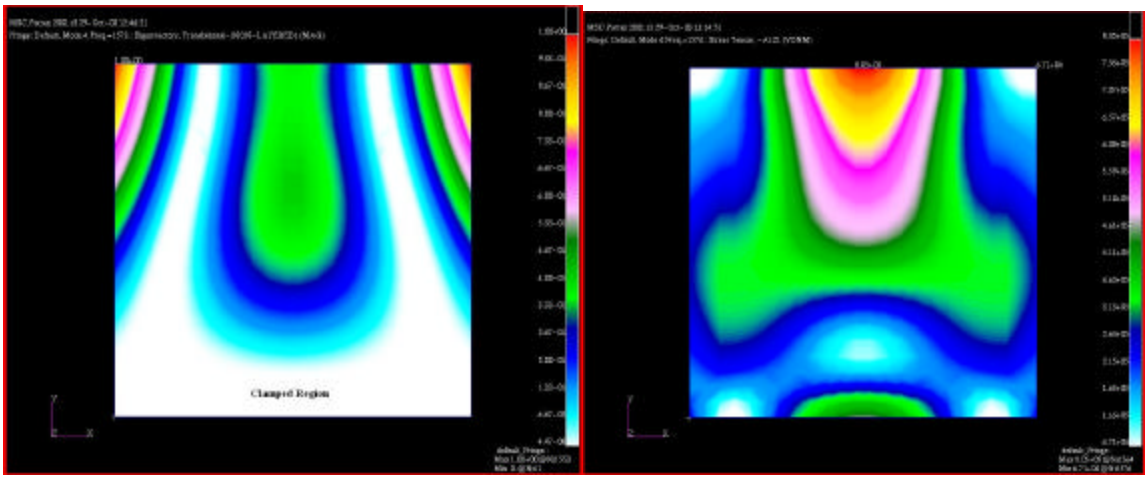

(a) Z displacement (b) VonMises Stress

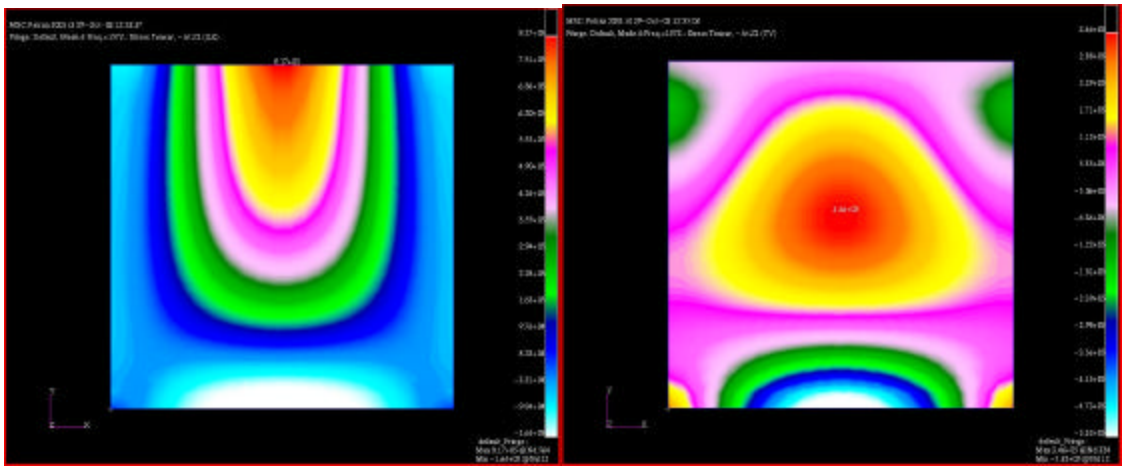

(c) X normal Stress (d) Y normal Stress

Figure 8. Mode 4 Displacement and Stresses

A second model, with 2025 elements, was used to provide an exact node by node match with the scanning laser vibrometer grid. This would verify the accuracy of the finite element model which was used to establish the ratio of the strain at the strain gage location to the maximum strain. This model was also used to determine the location of the single point laser vibrometer during shaker tests.

III: Test Setup and Procedures

This chapter discusses equipment used and the procedures established to obtain test data. These include the test fixture, electro-dynamic shaker, and scanning laser vibrometer. The data collected is presented in Chapter IV, Results and Discussion.

Test Fixture

Essential to collecting accurate and repeatable data is the fixture or clamping device used to attach the plate to the excitation source. Previous work highlighted the difficulty of maintaining consistent boundary conditions from one data set to the next when using a simple sandwich design (Ivansic, 2003). Once installed, there was a tendency for the plate to shift in an in-plane direction while under load, causing the effective plate geometry to change. Even a slight change in geometry can have a significant effect on the results. The current design eliminated this deficiency by adding two guide shafts through the clamped area of the plate. **Figure 9** shows the plate mounted on the bottom portion of the fixture with the two guide shafts through the clamped region. The top piece slides over the guide shafts and rests on the plate. Four bolts, one through each guide shaft and one beyond both ends of the plate are used to provide the clamping force on the plate. These shafts also eliminated the variability of the effective plate geometry (4-1/2 in. x 4-1/2 in.) from one setup to the next. Without the guide shafts, it would have been necessary for the researcher to measure the test area

before each experiment. A slight difference could influence the repeatability of the experiments. The guide shafts eliminated that problem and it can be seen from results presented in **Chapter IV** that repeatability was excellent.

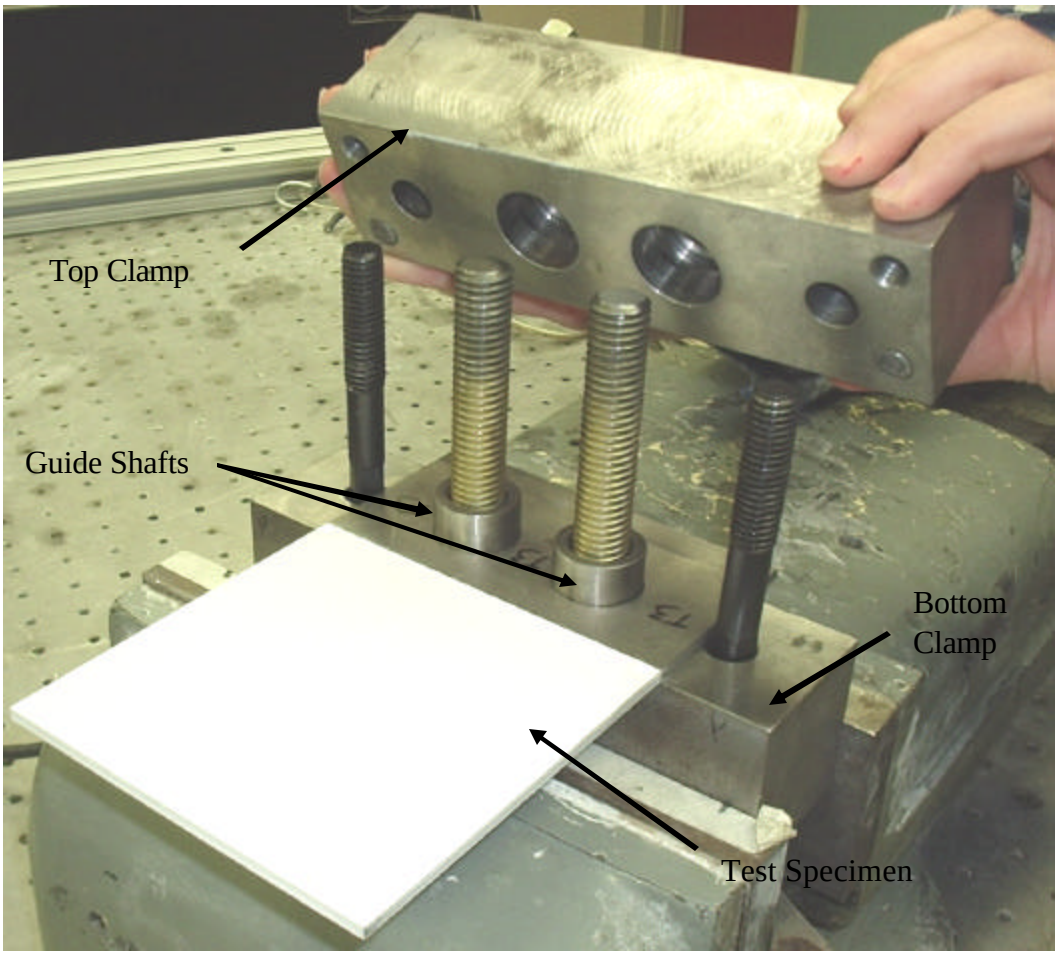

Figure 9. Test Fixture

Test Specimens

Uncoated Plates

The specimens used for this study were 4-1/2 in. x 7 in. x 1/8 in. Ti-6Al-4V annealed plates. The effective test area was 4-1/2 in. x 4-1/2 in. with a 2 in. clamped region and a 1/2 in. tail behind the clamp (**Figure 10**). The tail region served two purposes. The first was to provide a full diameter of material between the shaft holes and the edge of the plate. The second was to have a gripping surface to help remove the snug fitting plate from the clamp. Three plates were obtained from the same sheet of titanium and given a number from T1 to T3. The individual plates were cut from the sheet using a high powered water jet cutting system, which derives its efficiency and power by pressurizing water at up to 55,000 psi and focusing it through a nozzle as small as .003 in. in diameter. Traveling at speeds up to 3 times the speed of sound the water stream cuts with negligible heat added and exerts little vertical or lateral force. Therefore, no internal stresses were added to the plates. The plates used for this research were cut in the same orientation.

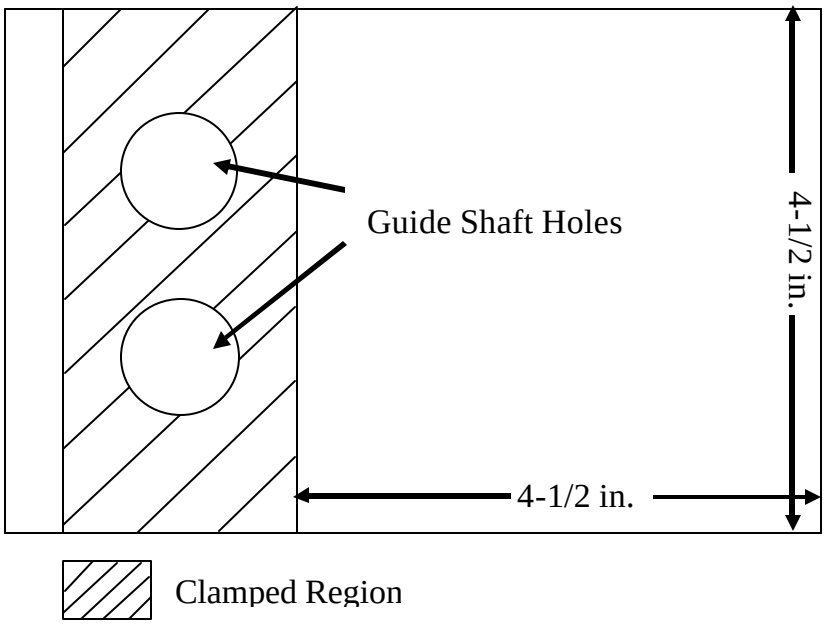

Figure 10. Titanium Plate

Length measurements of the short sides for each plate were made using a Starrett hardened stainless caliper. The long side measurements were made using a Products Engineering 12 inch tempered ruler. Plate thicknesses were measured using a Mitutoyo SR44 micrometer. Each plate was weighed using an Acculab L series balance. Using the measurement averages, summarized in **Table 5**, the titanium density was determined from **Equation 6.**

Table 5. Uncoated Plate Measurements

Uncoated Plates	Average Length (in)	Average Width (in)	Average Thickness (in)	Average Weight(grams)
T1	7	4.501	.126	271.2
T2	7	4.503	.127	274
T3	7	4.503	.127	274.5

$$\rho = \frac{m}{V} \tag{6}$$

$$\rho = .159 \text{ lbf/in}^3 \tag{7}$$

where

ρ = density
m = mass
V = volume

This density is in very close agreement with the MIL-HDBK-5CD-ROM, May 1997 published density of .160 lbf/in^3.

Coated Plates

The mag spinel coatings were applied by APS Materials, Dayton, OH. A coating of .01 in. was applied to both sides of plates T1 through T3. The coating was applied only to the 4 1/2 in. x 4 1/2 in. test surface. Each plate thickness was measured in the same manner used for the uncoated plates. The target thickness was .145 in. All measurements were within .003 in of the target. **Table 6** provides a summary of the coated plate measurements. **Figure 11** shows a sample of both the coated and uncoated plate.

Table 6. Coated Plate Measurements

Coated Plates	Average Length (in)	Average Width (in)	Average Thickness (in)
T1	7	4.501	.146
T2	7	4.503	.146
T3	7	4.503	.147

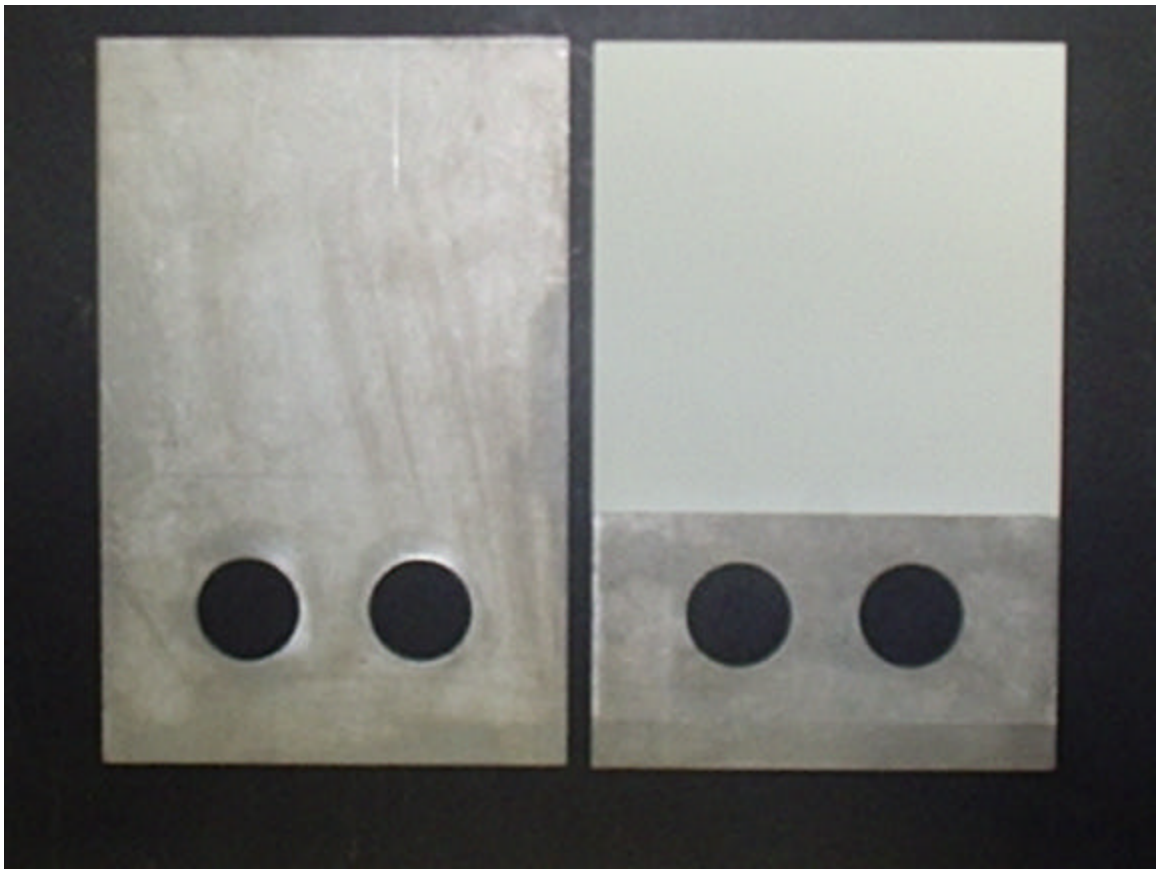

(a) Uncoated (b) Coated

Figure 11. Titanium Plate Specimen

Data Collection

Because of the non-linear characteristics of mag spinel, the standard material characterization techniques cannot be used. The strain-dependent effect must be considered. Previous work showed that when sine-sweep data from various strains or amplitudes are overlapped, the resonant peaks cannot be connected via a straight line (Ivansic, 2003). It can be seen from **Figure 33 thru Figure 37** in **Chapter IV** that for the uncoated plates the peak resonant frequency is very nearly constant as the load is

increased, but for the coated plates the peak frequency is moving nonlinearly down the frequency spectrum as the load is increased. This is known as strain softening. The strain softening effect requires that the sweep be done from high to low frequency; otherwise the peak may be missed.

Strain Gages

Two strain gages, of type CEA-05-062UW-350, were placed on each plate. Based on the scanning laser vibrometry results, presented in Chapter IV, gage one, for mode 3, was placed on the edge 2 ¼ in. from the tip on the side perpendicular to the clamp and gage two, for mode 4, was placed on the edge 2 ¼ in. from the tip on the free edge parallel to the clamp (**Figure 12**). The effect of the strain gages on frequency response was measured using the scanning laser vibrometer. Because the gages may add damping to the plates and because they cannot be glued to the mag spinel coating without changing its properties, damping measurements were not made with strain gages attached. The strain gages were only used on the uncoated plates to establish the strain/displacement relationship.

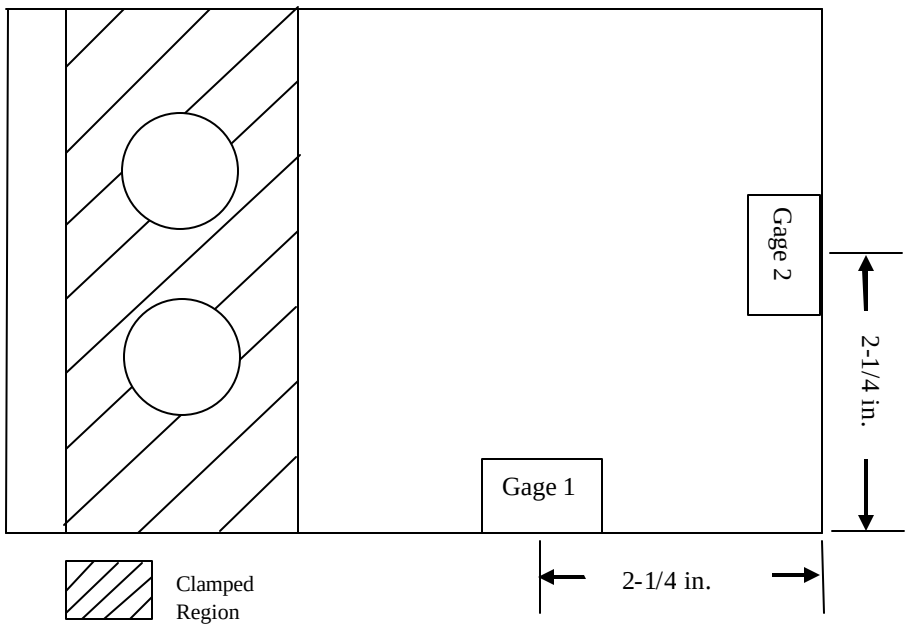

Figure 12. Strain Gage Locations

Modal Characterization

Scanning laser vibrometry was used to identify the mode shapes at each resonant frequency between 0 – 2 kHz. Vibrometry is a non-contact procedure, where a laser is used to map the velocity or displacement of a vibrating specimen at discrete points. The system utilizes the concept of interferometry to measure the velocity or displacement of the vibrating specimen. Interferometry is the optical interference between two coinciding light beams. The two beams for this setup are the reference beam and the reflected beam. The intensity of the coincident beam, a function of the phase difference between the two individual beams, is determined as follows:

$$I(\Delta j) = \frac{I_{max}}{2}(1+\cos(\Delta j)) \quad (8)$$

Where

I = Intensity (W/m^2)
Δj = phase shift

The phase shift is related to the path difference by:

$$\Delta j = 2p\frac{\Delta L}{l} \quad (9)$$

where

ΔL = path difference
l = wavelength of laser

The wavelength (l) and path difference (ΔL) are a function of time if one of the beams is scattered back from the vibrating specimen. The reflected beam also experiences a Doppler shift in its frequency, which is a function of the specimen's velocity. This frequency shift is determined as follows:

$$f_D = 2\frac{|v|}{l} \quad (10)$$

where

f_D = Doppler frequency shift
v = specimen velocity
l = wavelength of laser
(Polytec Laser Doppler Vibrometer User Manual)

The Polytec Laser Doppler Vibrometer system has two parts: the controller (OFV-3001) and the sensor head (OFV-056). Two types of sensor heads are available: single point and scanning laser. The scanning laser is used to find velocities at multiple

points on the specimen, which is required for determining mode shapes. Test parameters are input to the controller which then directs the sensor head. The sensor head generates the laser beam, which is split into the reference beam and the specimen beam. The laser beam is reflected off the test specimen and returned to the sensor head as the reflected beam. It is combined with the reference signal and sent to the controller, which compares the frequencies and phases and calculates the velocities and displacements. The procedure is repeated for as many times as there are grid points on the plate surface. When complete, the velocities of all the grid points are combined to create a velocity map of the surface of the plate as a function of position for each frequency. If the velocities are converted to displacements a mode shape at that resonant frequency is created.

All three plates were tested with each possible configuration: uncoated without strain gages, uncoated with strain gages, and coated. Each plate was held using the mounting fixture designed for the sine sweeps. The torque on the two bolts that pass through the guide shafts was 125 ft-lbs and the torque on the two outer bolts was 100 ft-lbs. The guide shaft bolts were set at a higher torque because they were directly above the plate and provided most of the clamping force. The fixture was then placed in a vise bolted to the table, which was floated to prevent outside vibrations from interfering with the experiment. An air horn placed at the free end corner provided the excitation source. See **Figure 13**. Sweeps were done between 0 – 2 kHz, which captured the first five resonant modes and displacement shapes. These shapes can be compared directly to the FEM modal results. The controller was set to take a data point at every 312.5 mHz, which provides a very high resolution output.

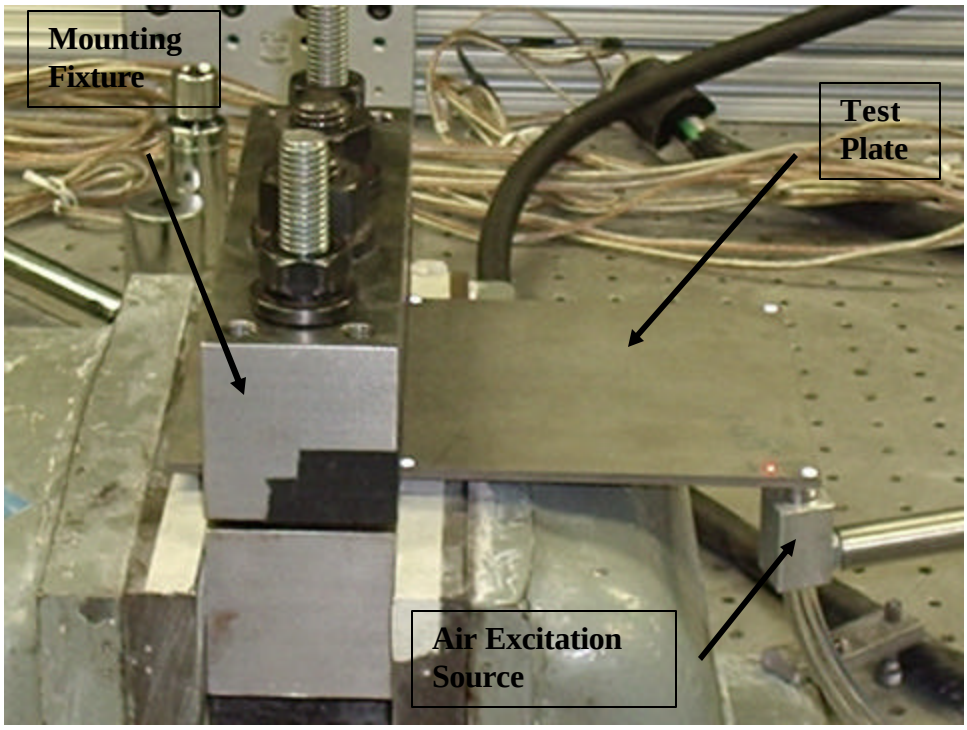

Figure 13. Laser Vibrometry Setup

Strain-Velocity-Displacement Calibration

The strain/velocity relationship was determined for the 2nd bend mode (mode 3) and the chordwise bend mode (mode 4) for all three plates using the 18,000 lb. shaker and verified on the 6,000 lb shaker. The verification was necessary because equipment failure on the 18,000 shaker made it necessary to complete the tests on the 6,000 lb shaker.

Each plate was clamped between two mounting blocks, which were bolted horizontally to the shaker (**Figure 14**). A laser, mounted to a rigid support, was used to measure the plate velocity at a single point. The target point was near one of the free corners opposite the clamped section, 0.1 in. from the free edge and 0.7 in. from the side

(**Figure 15**). The laser controller was not configured to take displacement measurements; therefore velocities were measured and converted to displacements. The velocity for maximum strain at this position for both modes was such that the laser controller would not have to be changed between mode testing. An accelerometer was placed at the base of the shaker to record the input load. It is acceptable to equate a change in acceleration as the equivalent change in applied force because the mass of the system is not changing and force changes linearly with acceleration. VibrationVIEW software, version 4.0.17, was used to control the data acquisition. The resonant frequency for each mode, determined from the modal characterization test, was swept through at a rate of 5 Hz/min. The peaks from the laser and the appropriate strain gage establish the strain/velocity relationship at that excitation load. This process was repeated up to twenty times for each plate as the load was increased to create a complete strain/velocity curve. The strain/velocity relationship was determined for each mode and plate. Since strain is a function of displacement, the velocity measurements were converted to displacements. Maximum displacement is correlated using the following relationship:

$$d = \frac{v}{w} \tag{11}$$

where

d = displacement
v = velocity
w = frequency (radians/sec)

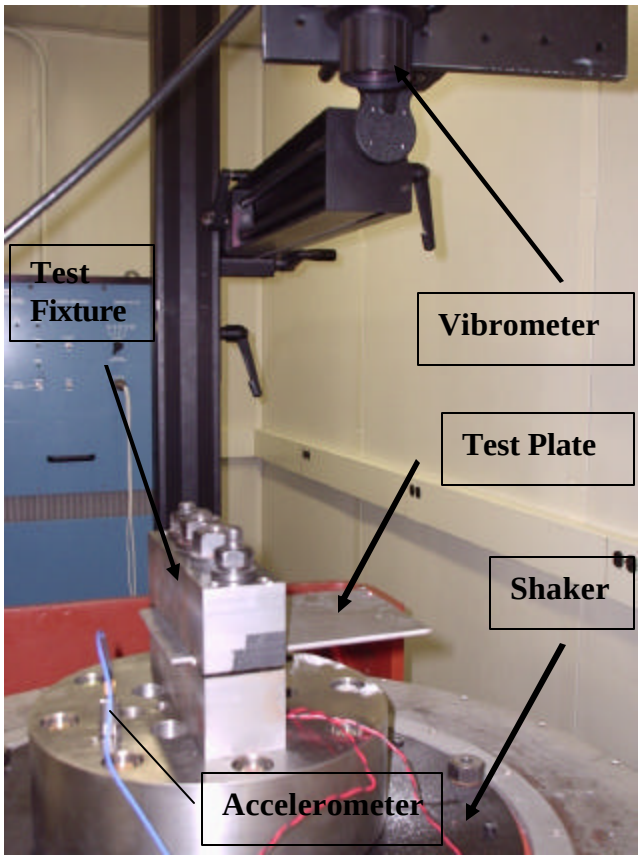

Figure 14. Shaker Table Setup

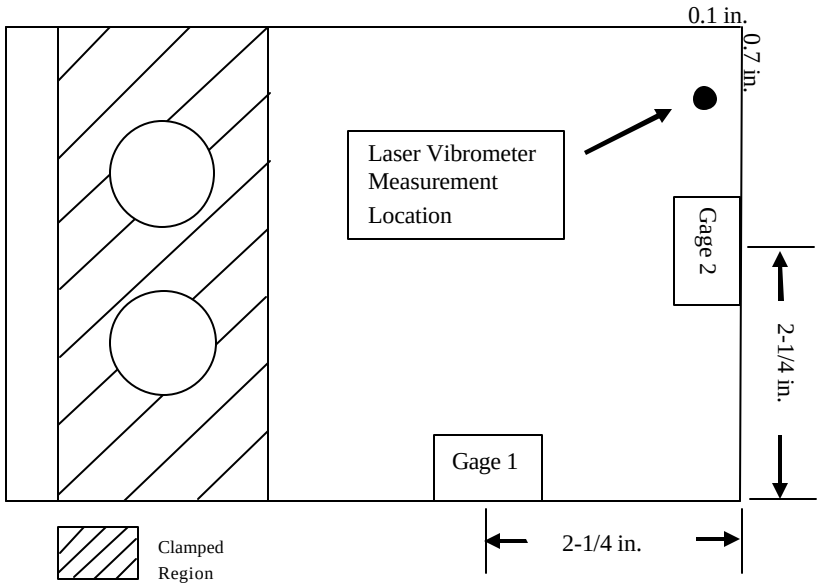

Figure 15. Laser Vibrometer Measurement Location

These curves represent the baseline curves for comparison to the coated plate. Since strain gages were not applied directly to the mag spinel, velocity was the only measurement available. An equivalent displacement from the coated plates results in the same strain at the plate coating interface. Since the coating increases the damping of the plate, it is expected that a greater applied load will be required to produce the same displacement as for the uncoated plate.

Damping Characterization

Sine sweeps were used to determine the resonant frequencies and level of damping as a function of the maximum strain. The sweeps were conducted on a 6,000 lb shaker using the VWIN software, version 4.74. Each plate was clamped between the two mounting blocks, which were bolted to the shaker (**Figure 14**). An accelerometer was placed at the base of the shaker to record the input acceleration. The addition of strain gages may influence the damping of the system, therefore; it was necessary to measure damping with the strain gages removed. The damping levels of the uncoated plates without strain gages were established to provide a baseline for determining the damping levels provided by the mag spinel coating. A laser, mounted to a rigid support, was used to measure the plate velocity at a single point. The target point was near one of the free corners opposite the clamped section, 0.1 in. from the free edge and 0.7 in. from the side (**Figure 15**). Velocities were measured at this location for both modes – 2^{nd} bend and chordwise bend – and converted to strain using the strain/displacement curve already established.

The frequency range for the sine sweeps was broad enough to capture response levels of 70% of the peak value. This provides sufficient data to perform the "half-power bandwidth" calculations, discussed later in this section. Each sweep was done at 5 Hz/min to ensure the peak was not missed. If the sweeps are made to quickly then the response does not have enough time to rise to the true peak amplitude. Six to ten different input accelerations representing a range of 10 – 100 maximum strain and another six to eight representing a range of 100 – 500 maximum strain were tested. The VWIN software takes the excitation signal and the plate response signal and conducts a fast Fourier transform to convert the data to the frequency domain. The output is an amplitude (velocity) versus frequency graph, where each peak represents a resonant frequency and mode.

Damping was determined by the "half-power bandwidth" calculation. The half-power is calculated by measuring the bandwidth of the frequency curve $1/\sqrt{2}$ (or approximately 3dB) down from the resonant peak (**Figure 16**) (Meirovitch, 1986).

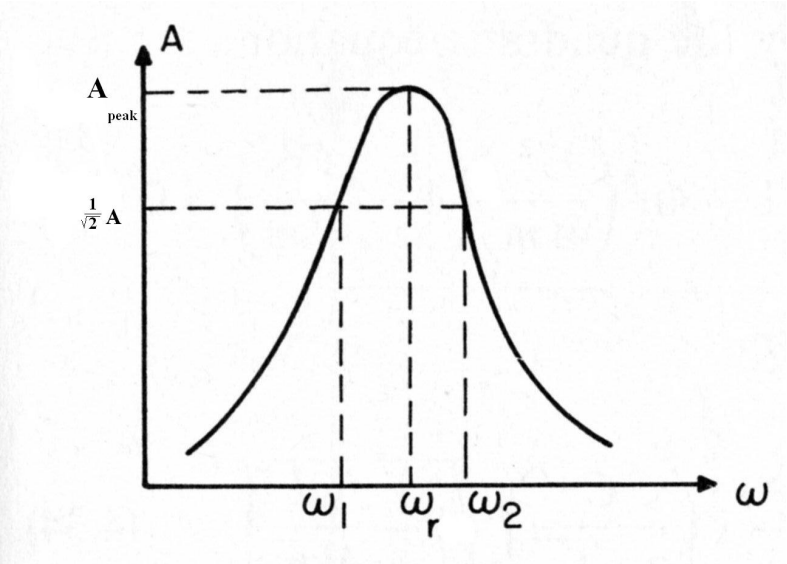

Figure 16. Half-power Bandwidth

The damping ratio, in percent, is then found using the following equation:

$$z = \frac{\Delta w}{2w_r} \tag{12}$$

where

z = damping ratio
Δw = bandwidth $(w_2 - w_1)$
w_r = resonant frequency

A parameter commonly used in the damping community is the quality factor (Q). The quality factor was developed by electrical engineers as a measure of the clarity of an electrical signal. The quality factor and damping ratio are inversely proportional.

$$Q = \frac{1}{2z} \tag{13}$$

(Meirovitch, 1986)

The VWIN software has the capability of determining the Quality factor by this method. It can be seen from this equation that as damping (z) increases, Q decreases. Therefore, a good damping material will dissipate more energy and have a lower Q value.

Another measure of damping is observed through the system loss factor (Nashif, 1985).

$$h = \frac{v_2 - v_1}{v_r} \tag{14}$$

where

h = system loss factor
w_r = resonant frequency
w_1 = frequency to the left of w_r where amplitude is $\frac{1}{\sqrt{2}} A_{peak}$
w_2 = frequency to the right of w_r where amplitude is $\frac{1}{\sqrt{2}} A_{peak}$

As damping increases so does the system loss factor. The relationship between $\Delta w / w_r$ and h is linear only for small ?, as shown in **Figure 17** (Nashif, 1985**).** The loss factors for this research do not go above 0.01.

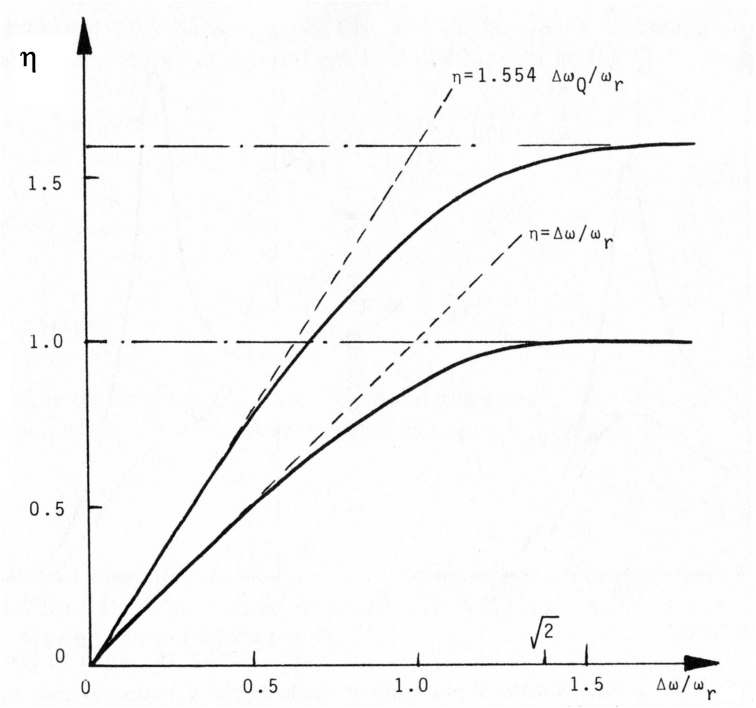

Figure 17. Nonlinearity of h

When comparing **Equation 12, 13,** and **14** the following relationship is observed.

$$h = 2z = \frac{1}{Q} \tag{15}$$

IV: Results and Discussion

Resonant Frequencies

Resonant Frequencies were experimentally determined from sine sweeps and laser vibrometry for both the uncoated and coated plates. The resonant frequencies were determined from the peaks on a frequency response curve. Theoretical predictions were also made using Classical Plate Theory and finite element modeling.

Comparison to Theoretical Predictions

Comparisons of the resonant frequencies between theoretical predictions and experimental results could only be made with the uncoated plates. If a good correlation exists between the theoretical and experimental results, the finite element model can be used as a benchmark for comparison of experimental values. The modes of interest for this research, mode 3 and 4, are compared in **Table 7** and **Table 8** respectively. The finite element model prediction is within 1.5% of the experimental results for mode 3 and within 3.3% for mode 4. Therefore, the finite element model closely approximates reality. The theoretical predictions have even closer agreement. Because the measured frequencies are so very close to the theoretical predictions, it can be assumed the test fixture provided a very rigid boundary condition. A loose fixture would have resulted in measured frequencies much lower than predicted.

Table 7. Comparison of Theoretical to Experimental Mode 3 Natural Frequency for the Uncoated Plates without Strain Gages (Frequencies are in Hz)

MODE 3	Theoretical Prediction (Young)	Finite Element Method	Scanning Laser Vibrometer	Sine Sweep
Plate T1	1257	1244.8	1247.7	1245.8
Plate T2	1257	1244.8	1259.8	1255.0
Plate T3	1257	1244.8	1263.3	1257.1

Table 8. Comparison of Theoretical to Experimental Mode 4 Natural Frequency for the Uncoated Plates without Strain Gages (Frequencies are in Hz)

MODE 4	Theoretical Prediction (Young)	Finite Element Method	Scanning Laser Vibrometer	Sine Sweep
Plate T1	1610	1587.6	1618.1	1614.5
Plate T2	1610	1587.6	1634.8	1632.1
Plate T3	1610	1587.6	1639.4	1635.3

Experimental Resonant Frequencies

All three plate conditions; uncoated without strain gages, uncoated with strain gages, and coated, were tested for frequency response between 0 - 2 kHz for all three plates using the scanning laser vibrometer. Five resonant frequencies can be identified within this range for each plate. Due to limitations of the test equipment the excitation load from the air horn was not measured. Therefore, just the location of the peak frequencies shown in **Figure 18 thru Figure 20** are compared for the different plate configurations and not the amplitudes. Resultant strain levels do not exceed 2 micro-strain for either mode 3 or 4. Configuration effects and repeatability were compared by repeating sine sweeps for the uncoated plates, with and without strain gages, and again when the plates were coated. It can be seen from **Table 9 thru Table 14** that repeatability was excellent, with no more than a 0.3% difference between test runs of the

same plate configuration. The effect on frequency response due the strain gages was another area of interest. It can be seen from **Table 15 thru Table 17** that there was no significant influence to frequency response from the strain gages, with no more than a 1% difference in frequency response with strain gages added. It can also be seen from **Table 18 thru Table 20** that the mag spinel coating caused a small increase in the resonant frequencies, with no more than 5.2% difference. This increase was expected based on the increased plate thickness from the mag spinel coating.

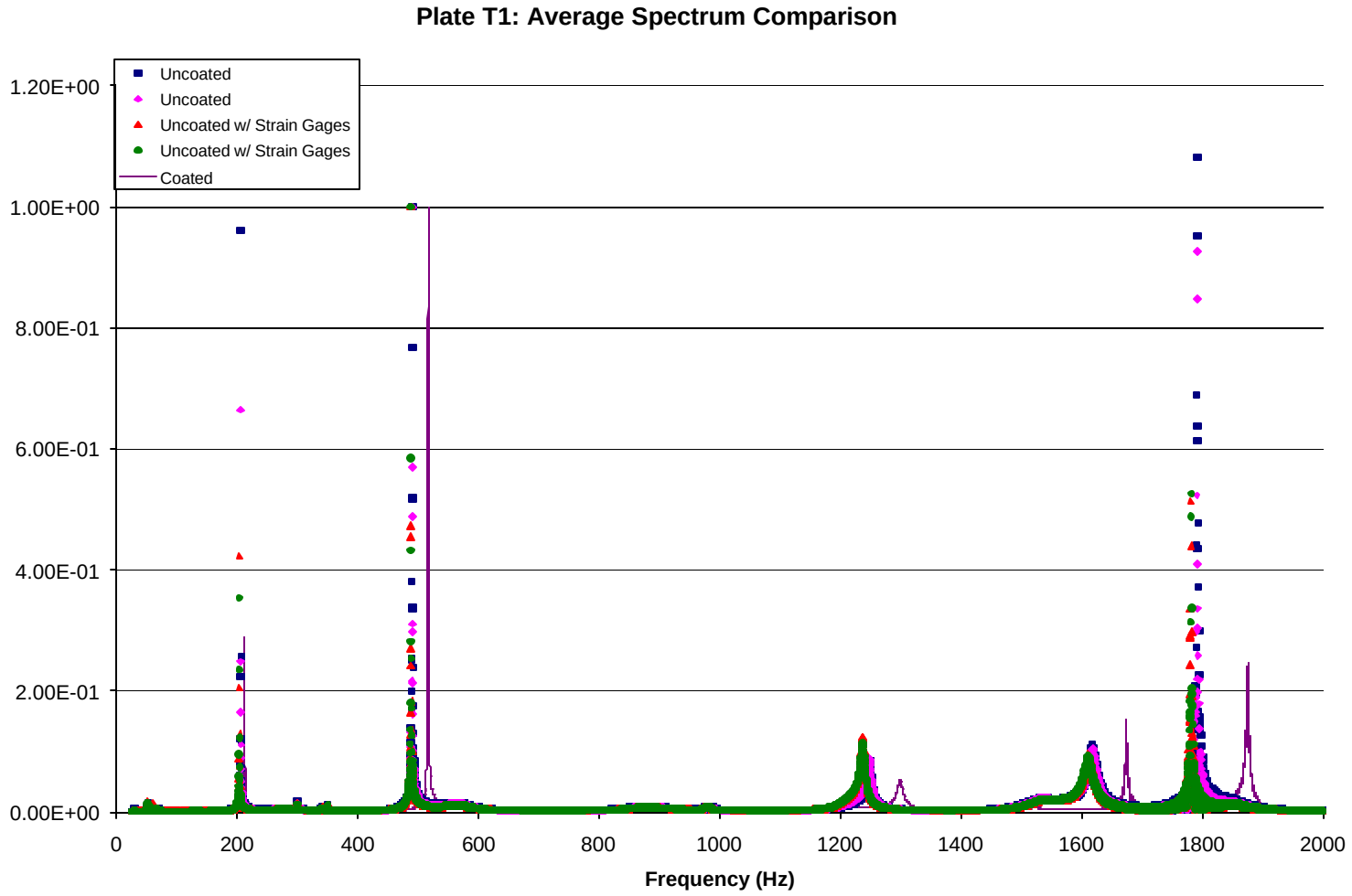

Figure 18. Frequency Response from Laser Vibrometer for Plate T1 (Uncoated with and without Strain Gages and Coated)

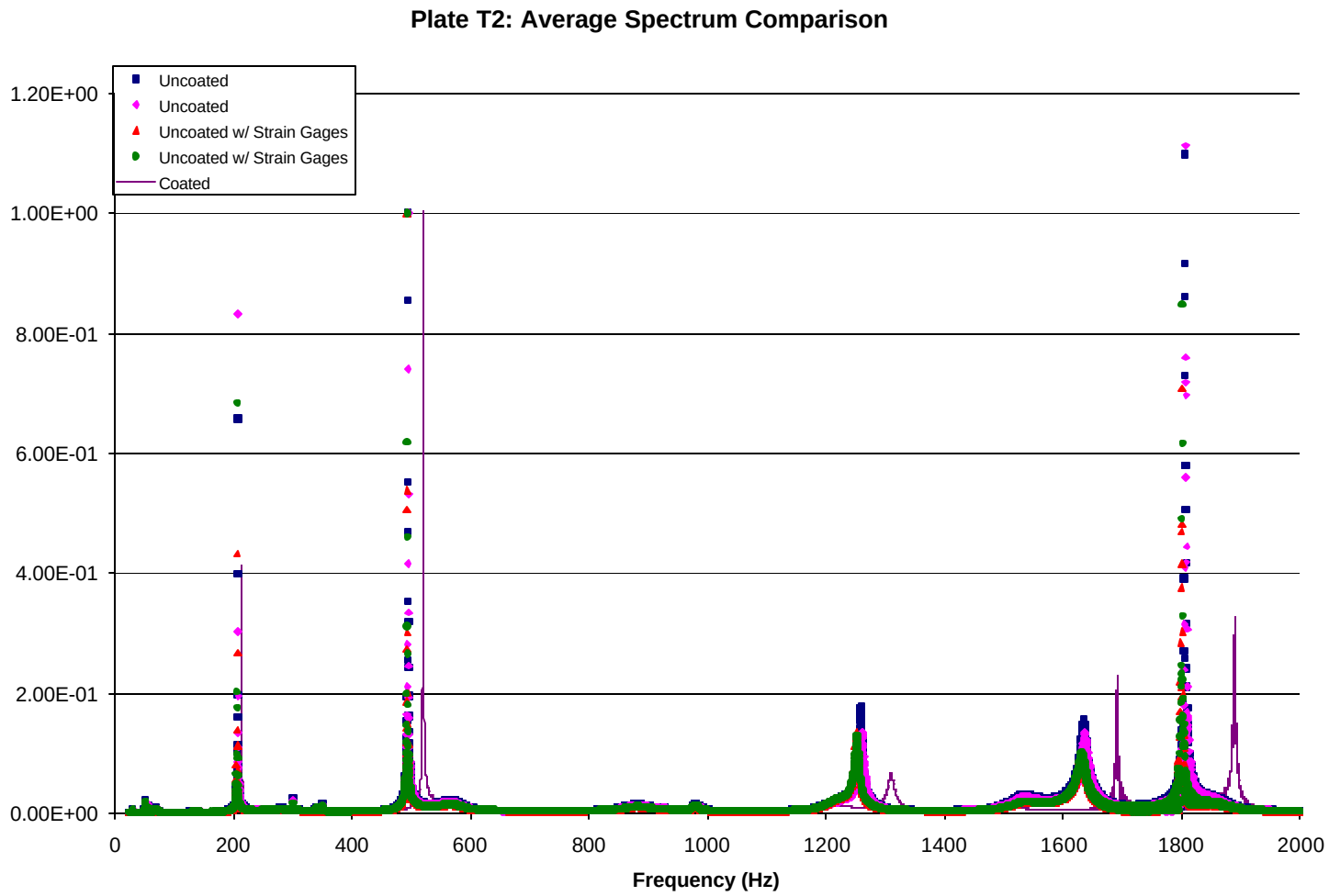

Figure 19. Frequency Response from Laser Vibrometer for Plate T2 (Uncoated with and without Strain Gages and Coated)

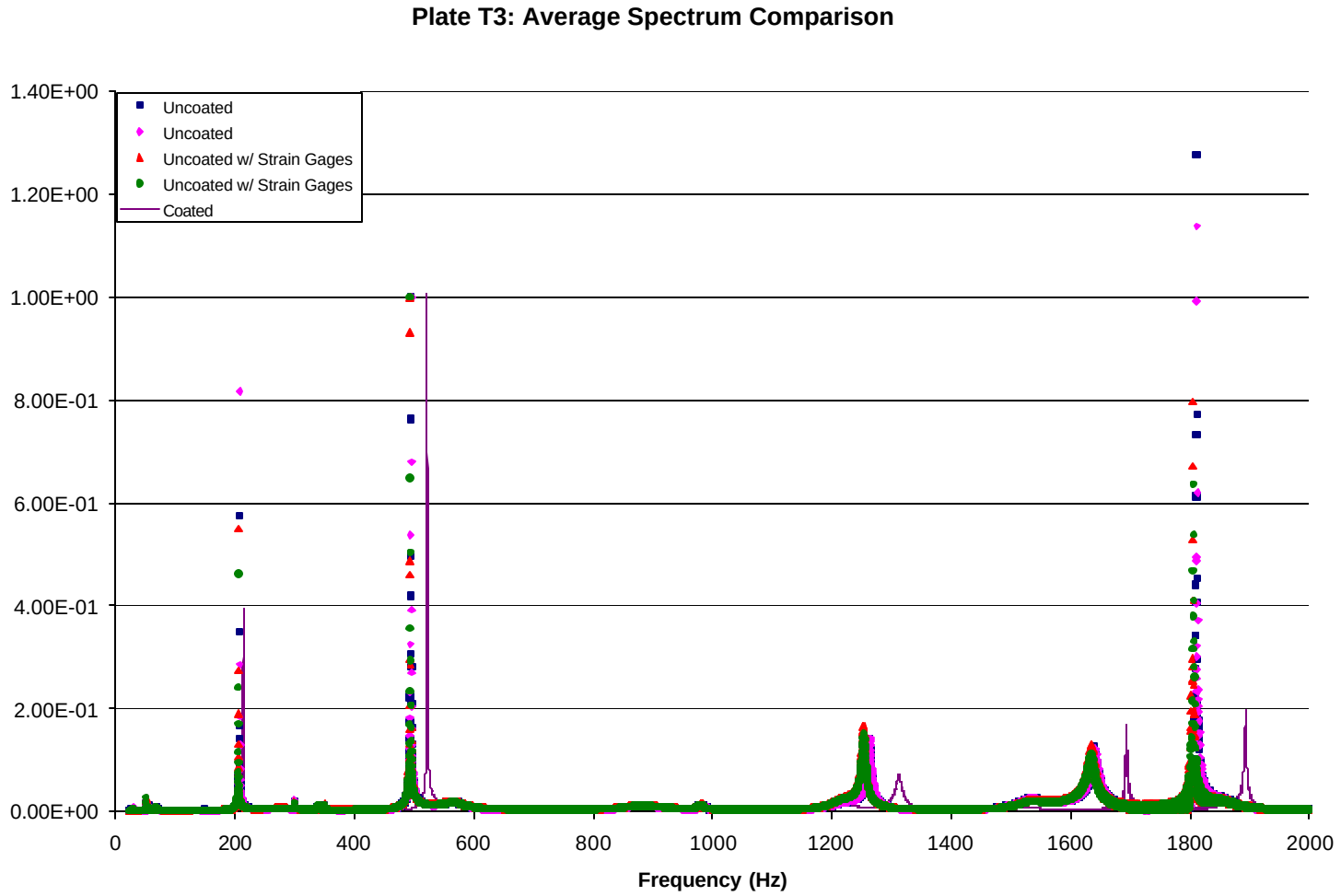

Figure 20. Frequency Response from Laser Vibrometer for Plate T3 (Uncoated with and without Strain Gages and Coated)

Table 9. Resonant Frequency from Laser Vibrometer Test for Plate T1 (Uncoated without Strain Gages) (Frequencies are in Hz)

Plate T1	Uncoated (Run 1)	Uncoated (Run 2)	Average	% Diff
Mode 1	205.63	205.31	205.47	0.15
Mode 2	490.31	490.00	490.16	0.06
Mode 3	1248.13	1247.19	1247.66	0.08
Mode 4	1618.13	1618.13	1618.13	0.00
Mode 5	1791.56	1790.94	1791.25	0.03

Table 10. Resonant Frequency from Laser Vibrometer Test for Plate T2 (Uncoated without Strain Gages) (Frequencies are in Hz)

Plate T2	Uncoated (Run 1)	Uncoated (Run 2)	Average	% Diff
Mode 1	207.50	208.13	207.81	-0.30
Mode 2	494.38	494.69	494.53	-0.06
Mode 3	1258.75	1260.94	1259.85	-0.17
Mode 4	1634.06	1635.63	1634.85	-0.10
Mode 5	1805.94	1806.88	1806.41	-0.05

Table 11. Resonant Frequency from Laser Vibrometer Test for Plate T3 (Uncoated without Strain Gages) (Frequencies are in Hz)

Plate T3	Uncoated (Run 1)	Uncoated (Run 2)	Average	% Diff
Mode 1	208.13	208.44	208.28	-0.15
Mode 2	495.00	495.00	495.00	0.00
Mode 3	1262.81	1263.75	1263.28	-0.07
Mode 4	1639.38	1639.38	1639.38	0.00
Mode 5	1810.94	1811.56	1811.25	-0.03

Table 12. Resonant Frequency from Laser Vibrometer Test for Plate T1 (Uncoated with Strain Gages) (Frequencies are in Hz)

Plate T1	Uncoated w/ Strain Gages (Run 1)	Uncoated w/ Strain Gages (Run 2)	Average	% Diff
Mode 1	203.44	203.44	203.44	0.00
Mode 2	487.81	488.13	487.97	-0.06
Mode 3	1237.19	1237.19	1237.19	0.00
Mode 4	1611.25	1611.25	1611.25	0.00
Mode 5	1780.63	1781.88	1781.26	-0.07

Table 13. Resonant Frequency from Laser Vibrometer Test for Plate T2 (Uncoated with Strain Gages) (Frequencies are in Hz)

Plate T2	Uncoated w/ Strain Gages (Run 1)	Uncoated w/ Strain Gages (Run 2)	Average	% Diff
Mode 1	205.94	206.25	206.09	-0.15
Mode 2	493.13	493.44	493.28	-0.06
Mode 3	1250.94	1251.88	1251.41	-0.08
Mode 4	1631.88	1631.88	1631.88	0.00
Mode 5	1800.00	1800.63	1800.32	-0.04

Table 14. Resonant Frequency from Laser Vibrometer Test for Plate T3 (Uncoated with Strain Gages) (Frequencies are in Hz)

Plate T3	Uncoated w/ Strain Gages (Run 1)	Uncoated w/ Strain Gages (Run 2)	Average	% Diff
Mode 1	206.25	206.25	206.25	0.00
Mode 2	493.44	494.06	493.75	-0.13
Mode 3	1253.13	1254.06	1253.60	-0.07
Mode 4	1635.63	1634.06	1634.85	0.10
Mode 5	1804.06	1805.31	1804.69	-0.07

Table 15. Comparison of Resonant Frequencies from Laser Vibrometer for Plate T1: Uncoated with and without Strain Gages (Frequencies are in Hz)

Plate T1	Uncoated Average	Uncoated w/ Strain Gages Average	% Diff of Averages
Mode 1	205.47	203.44	0.99
Mode 2	490.16	487.97	0.45
Mode 3	1247.66	1237.19	0.84
Mode 4	1618.13	1611.25	0.43
Mode 5	1791.25	1781.26	0.56

Table 16. Comparison of Resonant Frequencies from Laser Vibrometer for Plate T2: Uncoated with and without Strain Gages (Frequencies are in Hz)

Plate T2	Uncoated Average	Uncoated w/ Strain Gages Average	% Diff of Averages
Mode 1	207.81	206.09	0.83
Mode 2	494.53	493.28	0.25
Mode 3	1259.85	1251.41	0.67
Mode 4	1634.85	1631.88	0.18
Mode 5	1806.41	1800.32	0.34

Table 17. Comparison of Resonant Frequencies from Laser Vibrometer for Plate T3: Uncoated with and without Strain Gages (Frequencies are in Hz)

Plate T3	Uncoated Average	Uncoated w/ Strain Gages Average	% Diff of Averages
Mode 1	208.28	206.25	0.98
Mode 2	495.00	493.75	0.25
Mode 3	1263.28	1253.60	0.77
Mode 4	1639.38	1634.85	0.28
Mode 5	1811.25	1804.69	0.36

Table 18. Comparison of Uncoated Resonant Frequencies to Coated Resonant Frequencies from Laser Vibrometer for Plate T1 (Frequencies are in Hz)

Plate T1	Uncoated Average	Coated	% Diff of Uncoated Avg. and Coated
Mode 1	205.47	211.88	3.02
Mode 2	490.16	516.25	5.05
Mode 3	1247.66	1298.44	3.91
Mode 4	1618.13	1674.38	3.36
Mode 5	1791.25	1875.00	4.47

Table 19. Comparison of Uncoated Resonant Frequencies to Coated Resonant Frequencies from Laser Vibrometer for Plate T2 (Frequencies are in Hz)

Plate T2	Uncoated Average	Coated	% Diff of Uncoated Avg. and Coated
Mode 1	207.81	213.75	2.78
Mode 2	494.53	520.00	4.90
Mode 3	1259.85	1308.75	3.74
Mode 4	1634.85	1690.63	3.30
Mode 5	1806.41	1888.75	4.36

Table 20. Comparison of Uncoated Resonant Frequencies to Coated Resonant Frequencies from Laser Vibrometer for Plate T3 (Frequencies are in Hz)

Plate T3	Uncoated Average	Coated	% Diff of Uncoated Avg. and Coated
Mode 1	208.28	214.38	2.84
Mode 2	495.00	522.19	5.21
Mode 3	1263.28	1312.50	3.75
Mode 4	1639.38	1693.44	3.19
Mode 5	1811.25	1892.81	4.31

Mode Shapes

Scanning laser vibrometry yields not only the resonance frequencies, but also the mode shape at each resonant frequency. A three-dimensional representation of the first five mode shapes taken from laser vibrometry was shown in **Figure 3** of Chapter I. Results from the previous section revealed that the frequency response was virtually unaffected by the addition of strain gages and only a slight increase was observed when the mag spinel was applied. Before the strain/displacement relationship obtained from the uncoated plates with strain gages could be applied to the uncoated plates without strain gages and the coated plates, the mode shape, and hence the displacement pattern, had to be verified as the same for all three plate configurations. The comparison between the laser vibrometer data and the finite element model for plate T1, shown in **Figure 21 and Figure 22**, reveal that the mode shape is unaltered by the removal of strain gages or the addition of mag spinel. Only data for one plate is presented here, but the shapes are the same for all plates and configurations. (In **Figure 22**, missing data is shown as a discontinuity). See Appendix A: Scanning Laser Vibrometer Mode Shapes for mode shape results for all test configurations.

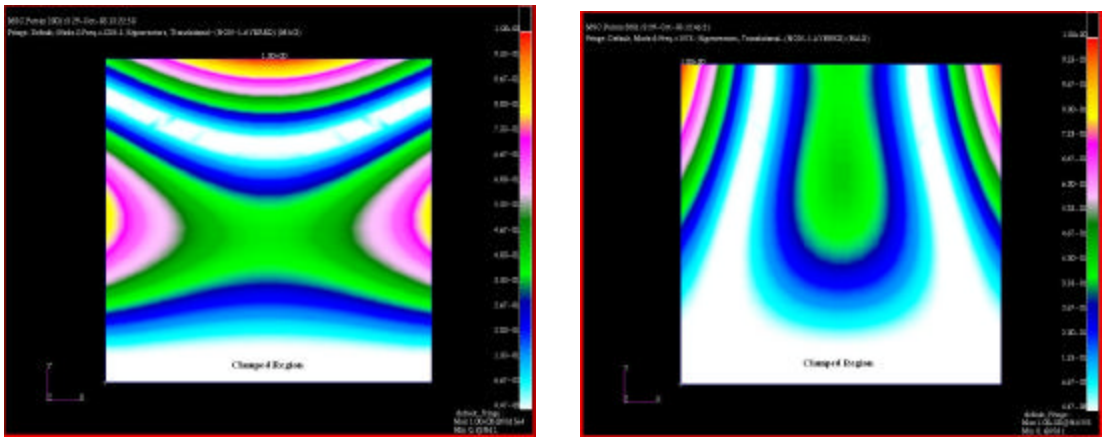

(a) Mode 3 (b) Mode 4

Figure 21. FEM Solutions: Out-of-Plane Displacement

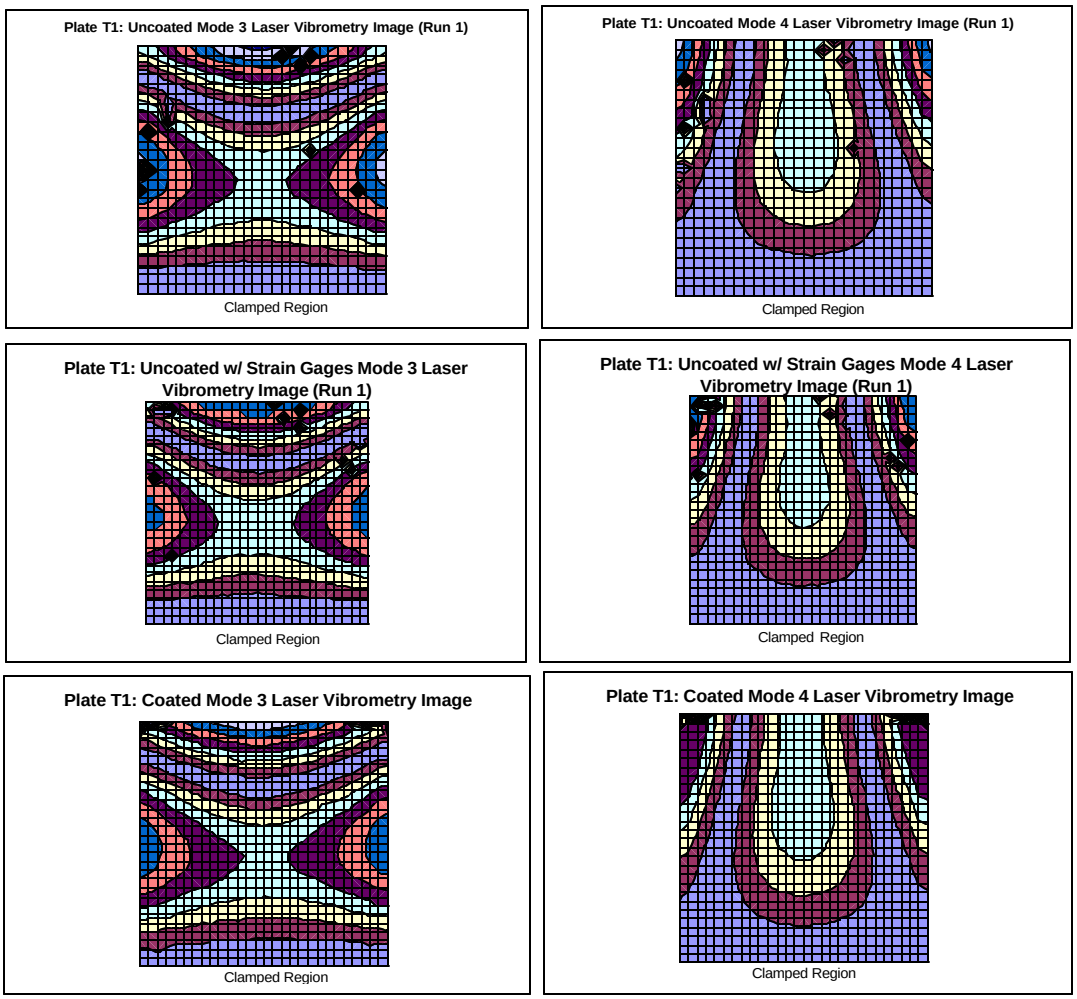

Figure 22. Laser Vibrometer Results: Out-of-Plane Displacement

Since the overall mode shapes were the same for all plate configurations, the next step was to conduct a more detailed mode shape comparison. This was done by plotting a section of the laser vibrometry data from the edge perpendicular to the clamp for mode 3 and the free edge for mode 4 and comparing them to the finite element model. The mesh density of the finite model was such that each node was matched to a scan point from the laser vibrometer. The results from the finite model and the laser vibrometry tests were normalized to a maximum displacement of unity and are presented in **Figure 23 thru Figure 28** for all three plates. The test data for the plate configurations and finite model are virtually identical.

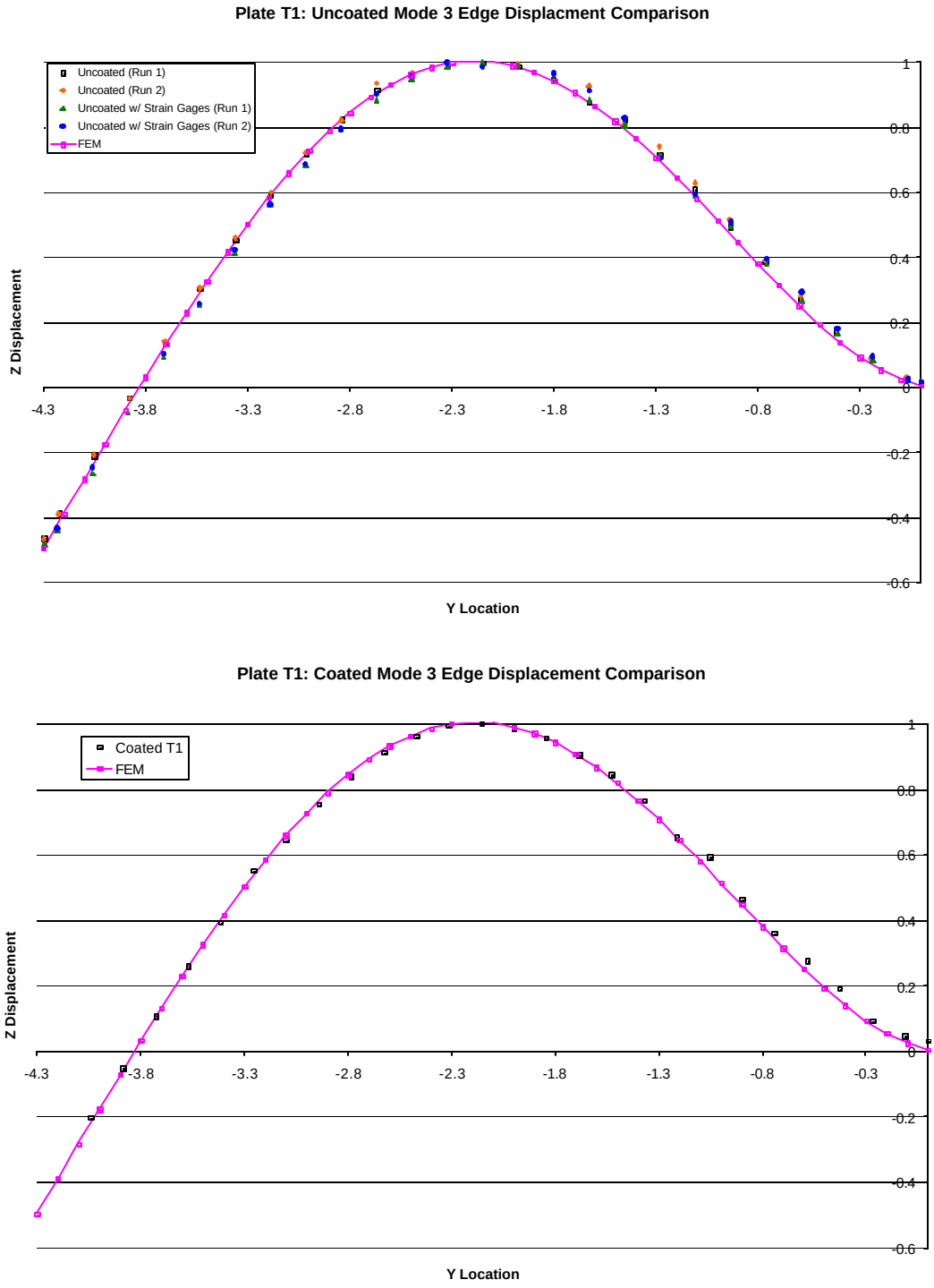

Figure 23. Plate T1: Mode 3 Section Comparison

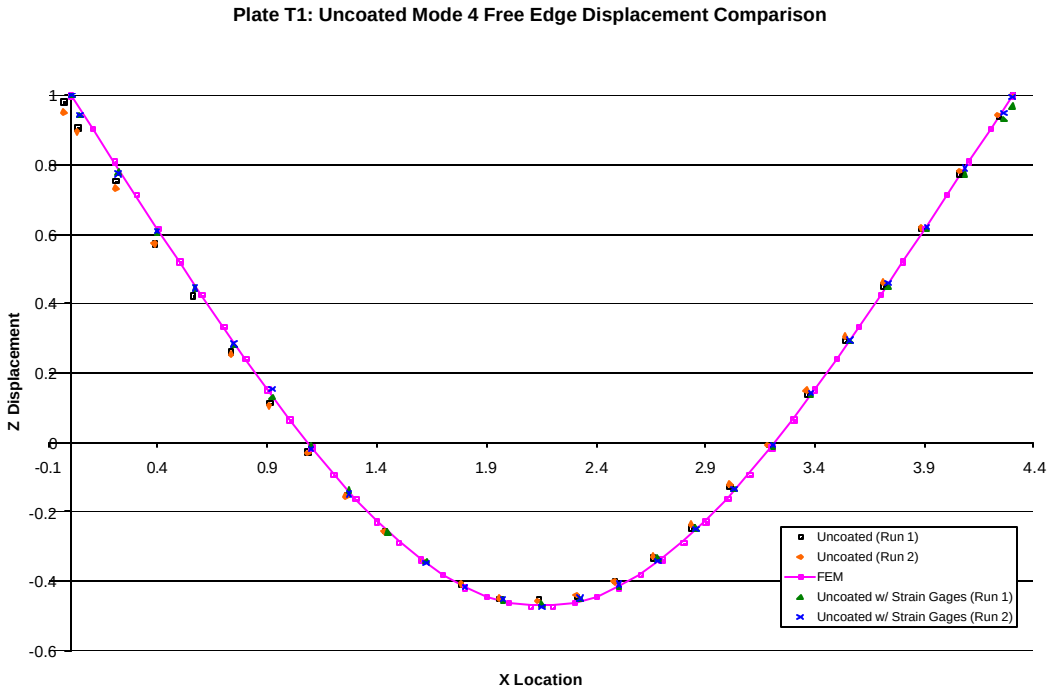

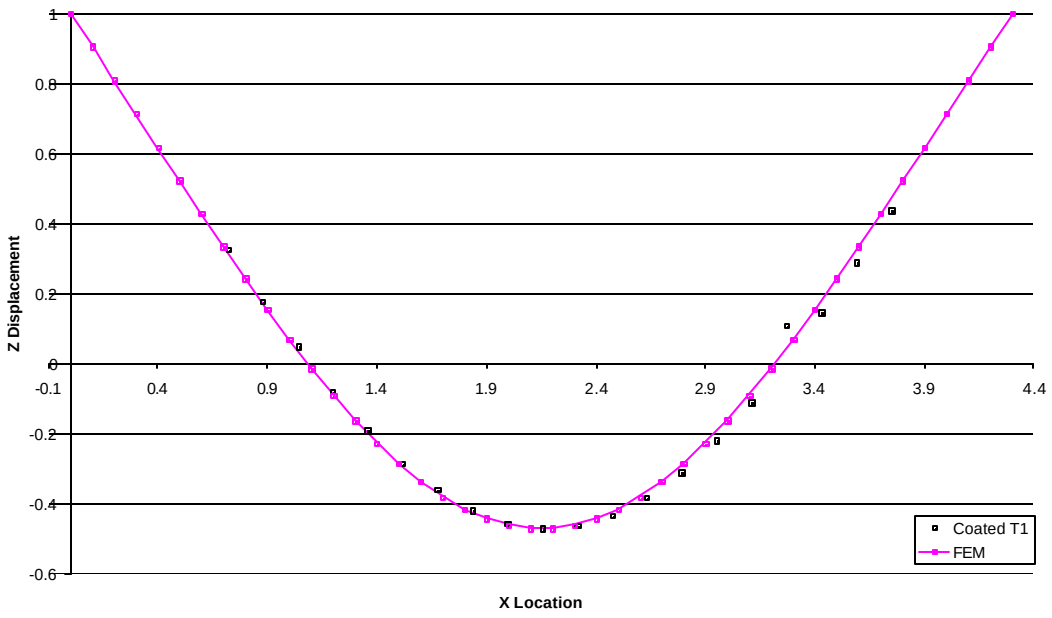

Figure 24. Plate T1: Mode 4 Section Comparison

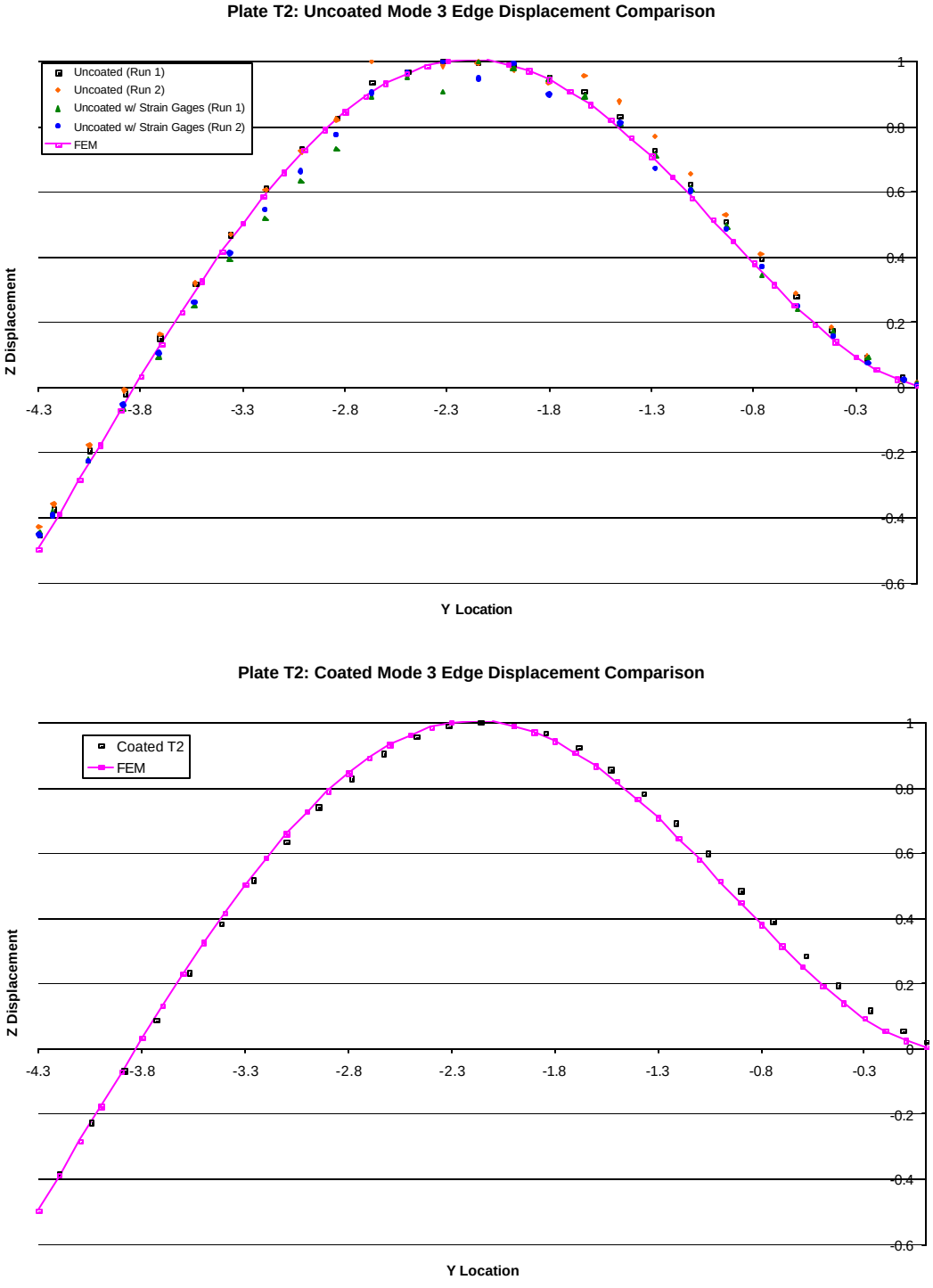

Figure 25. Plate T2: Mode 3 Section Comparison

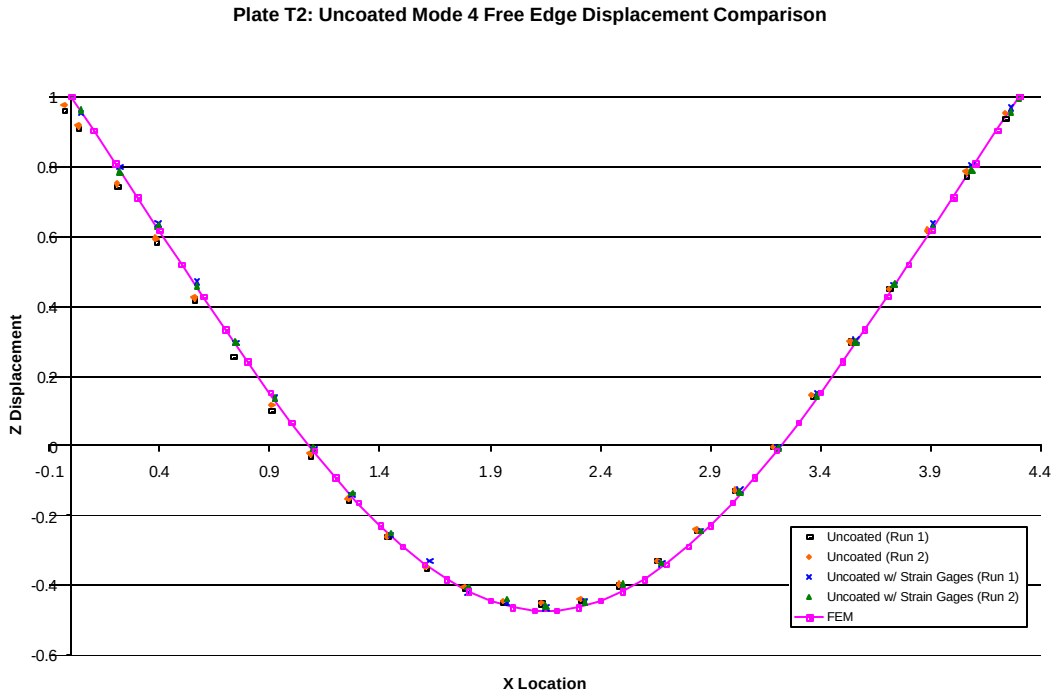

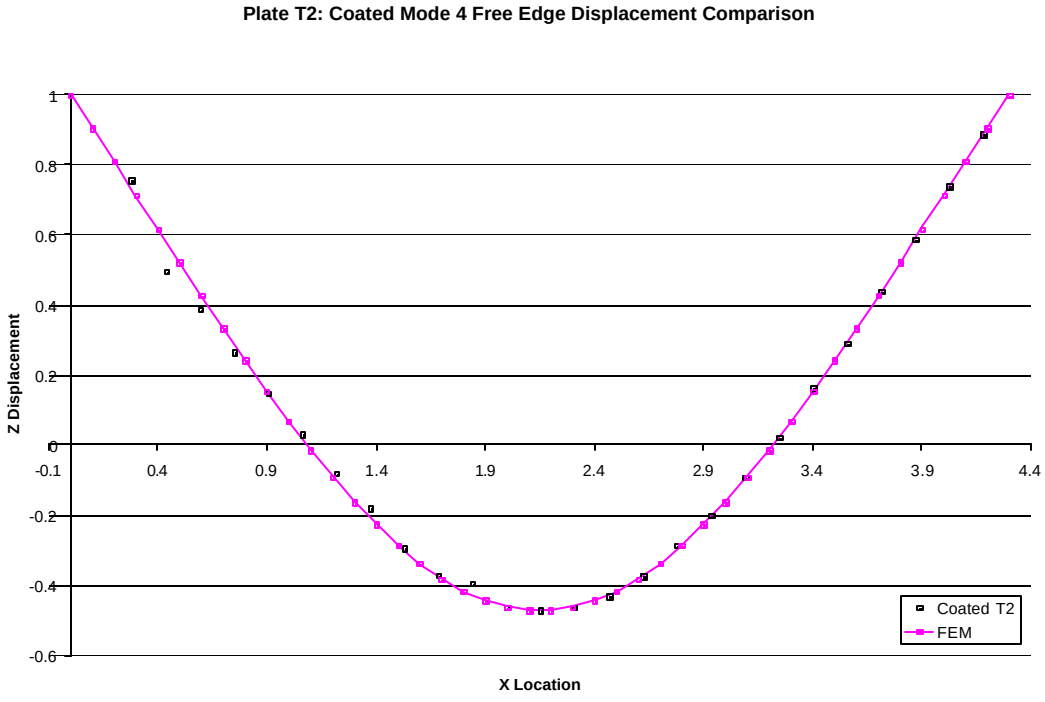

Figure 26. Plate T2: Mode 4 Section Comparison

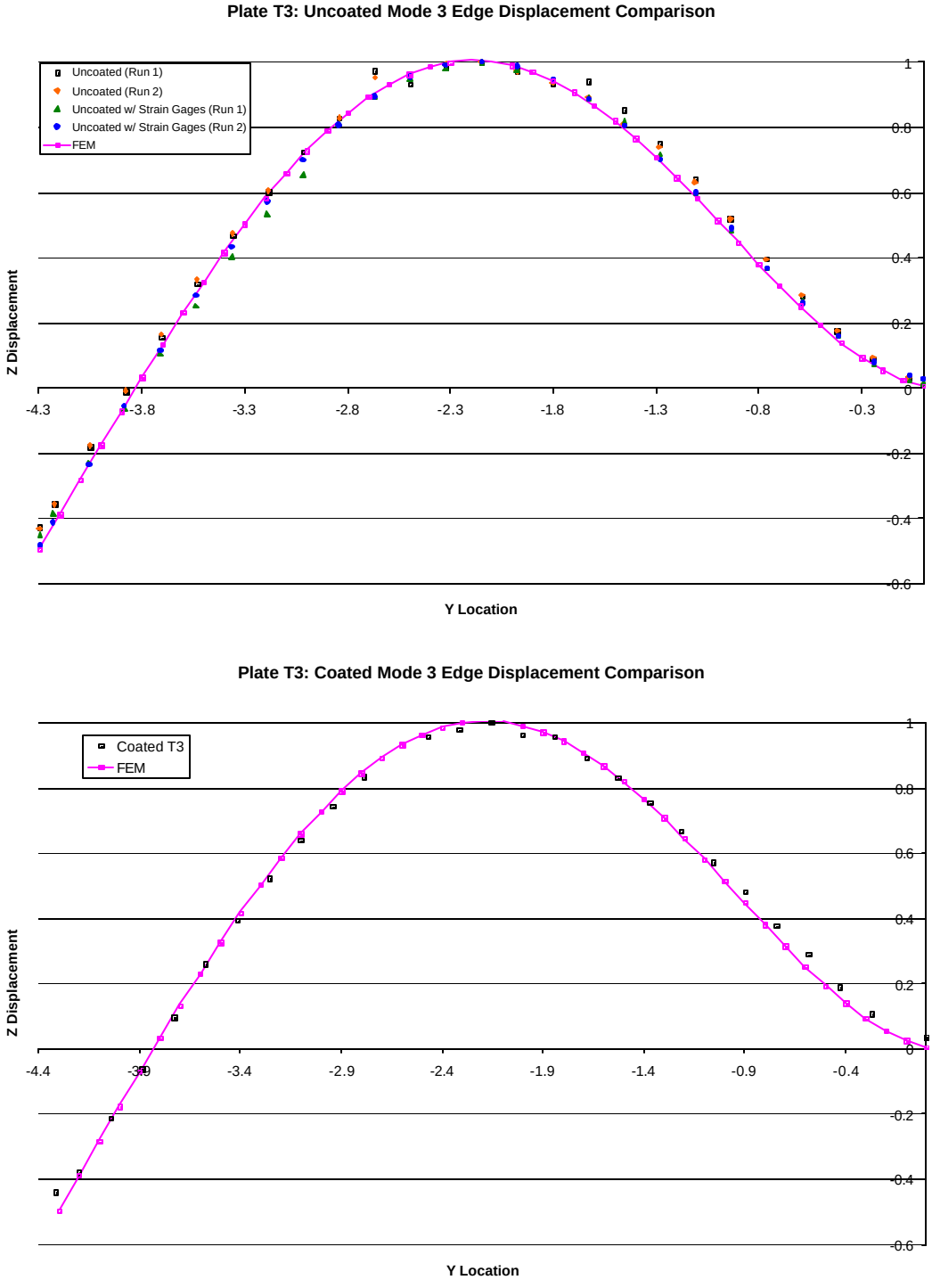

Figure 27. Plate T3: Mode 3 Section Comparison

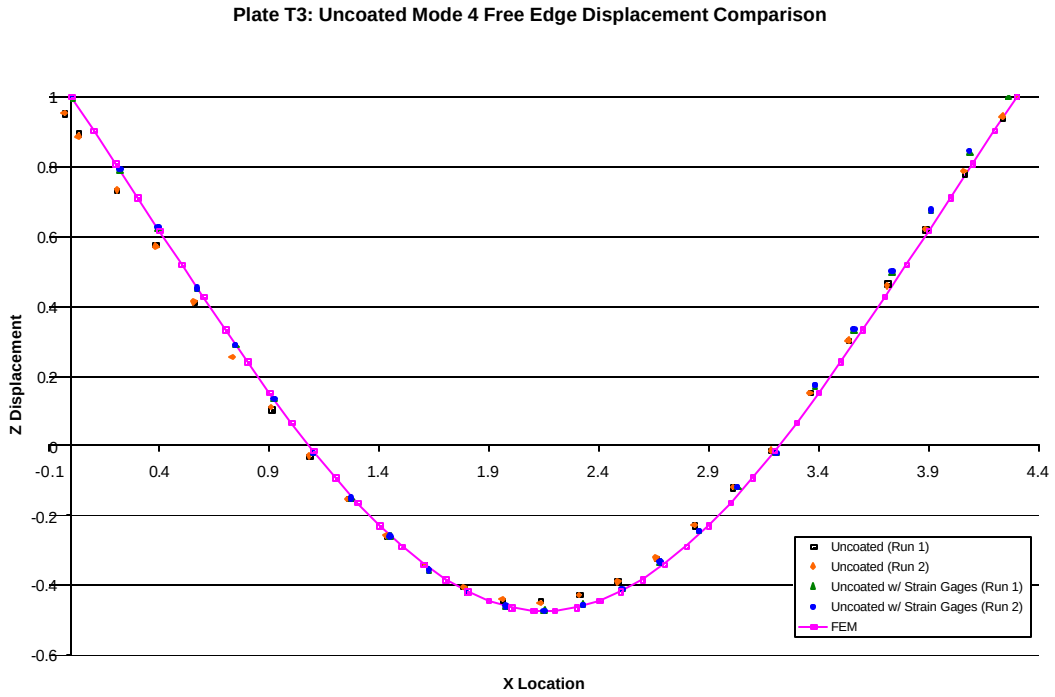

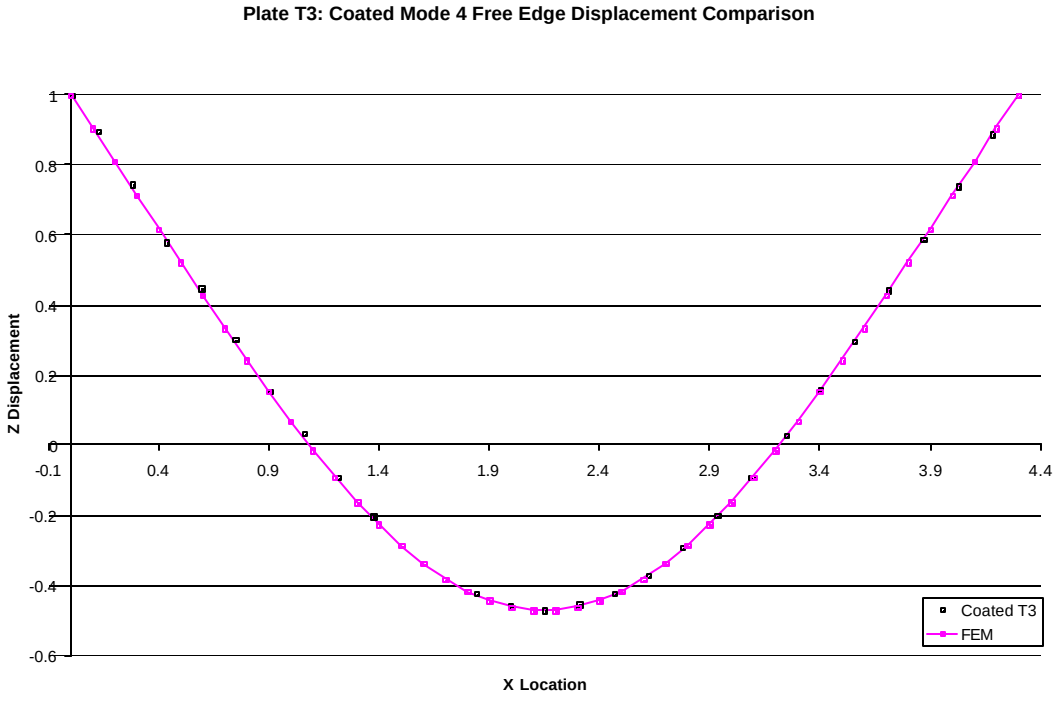

Figure 28. Plate T3: Mode 4 Section Comparison

Because the finite model was validated with test results, the ratio of the strain at the strain gage to the maximum strain could be established. For mode 3 the strain gage was placed at the point of maximum displacement which was 2 ¼ in. from the tip on the edge perpendicular to the clamp. The ratio of strain at this location to the point of maximum strain (at the clamped edge) is .6583. For mode 4 the strain gage was placed at the center of the free edge, 2 ¼ in. from the tip. See **Figure 12** in **Chapter I**. This is the maximum strain point for mode 4. This validation also allowed the strain/displacement relationship to be applied to all the plate configurations.

Strain/Displacement Relationship

Establishing the strain/displacement relationship with the single-point laser vibrometer was necessary because damping measurements were to be conducted on the plates without strain gages. However, comparisons of damping based on strain rather than velocity were desired. Because strain gages would not be attached to the mag spinel coating they should also not be included in the baseline uncoated damping measurements. To determine this relationship the velocity and strain at resonance were measured for each mode by conducting up to twenty slow (5 Hz/min) sine sweeps, with an increased excitation load for each sweep. The details of the test setup are discussed in **Chapter III**. 500 micro-strain was the upper limit for this research. Since strain is proportional to displacement and not velocity, the velocity measurements had to be converted to displacements. As indicated previously, this is done by dividing the velocity at peak resonance by the peak resonance frequency. Because there is very little shift in the

resonant frequency from low to high load for the uncoated plate this step may seem unimportant. However, the strain softening effect of the mag spinel coating causes a noticeable shift in resonant frequency as excitation loads are increased and thus the frequency influence is more pronounced. The strain/displacement relationship for each plate can be seen in **Figure 29 thru Figure 31**. Strains for both modes are reported at the maximum strain location. Error bars are plotted to show the level of agreement each data point is with the trendline. The equations of the trendlines are used to convert displacements to strains.

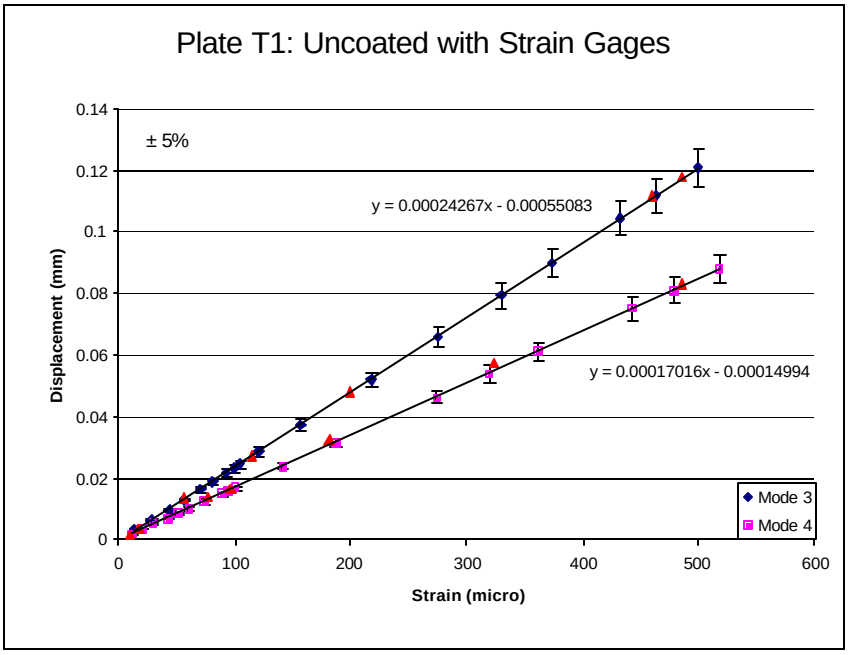

Figure 29. Strain/Displacement Relationship for Plate T1

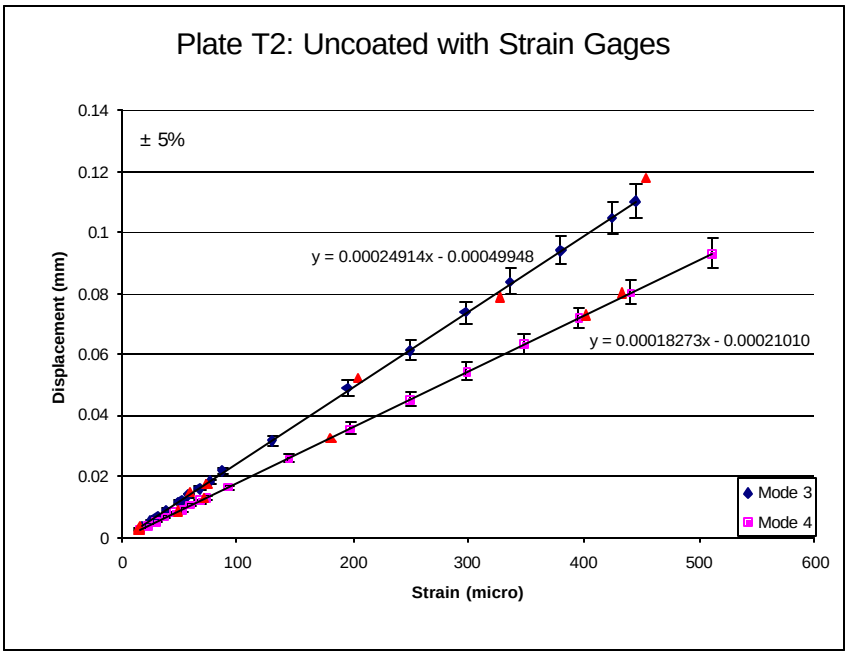

Figure 30. Strain/Displacement Relationship for Plate T2

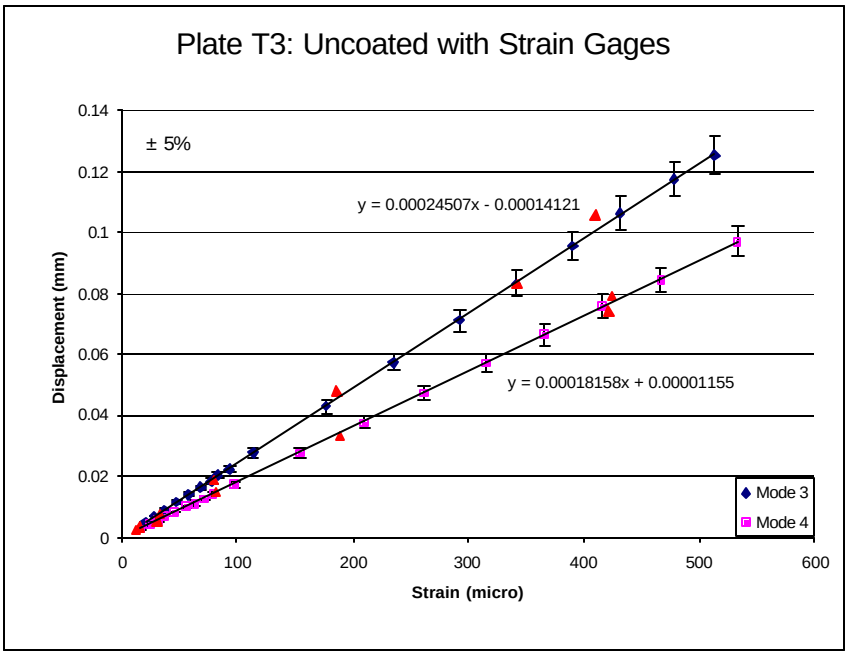

Figure 31. Strain/Displacement Relationship for Plate T3

Damping

Damping characterization was conducted by a series of sine sweeps on the uncoated and coated plate configurations. The sweeps were made using a 6,000 lb shaker. Results of the sweeps are shown in **Figure 32 thru Figure 37**. The non-linearity is immediately apparent when comparing the uncoated sweeps to the coated sweeps. The peaks for each sweep were fairly frequency stable as the load increased for the uncoated plates, but the peaks for the coated plates decreased by as much as 25 Hz as the load was increased. This phenomenon is known as strain softening. The small frequency decrease, less than 5 Hz, for the uncoated plates may be attributed to a less than perfect boundary condition at the fixture. For a perfectly linear system with a perfect boundary condition the peaks would occur at the same frequency for all loads. Another observation is the increased load needed for the coated plate to produce a sweep with an equivalent velocity to the uncoated plate. This is a legitimate method for quantifying Q, but it says nothing about the strain levels and is therefore not used in this report.

As was expected, the mag spinel coating caused an increase in damping; even at very low strain levels. The non-linear relationship between Q and strain is plotted in **Figure 38 thru Figure 40**. A best fit curve was applied to the experimental results and error bars of 5% were added to each data point to provide a perspective of how well the data fits the trendline (there is no correlation to any predicted precision of the measurements). The Q's show a rapid decrease, increased damping, up to about 100 micro-strain for both modes. The decreasing trend continues beyond 100 micro-strain for mode 3 but it levels off for mode 4. From the best fit curves the predicted improvement

in damping over the uncoated plates were calculated for selected strains. The results are presented in **Table 21 thru Table 23** for the individual plates. The average increase in damping across all three plates is presented in **Table 24**. **Appendix B** contains the experimental data for each point used to generate the curves in **Figure 38 to Figure 40**. Mode 4 was tested first for each plate, with the first sweep at the high strain point and the last sweep at the low strain point. The same process was then repeated for mode 3. Repeat strain points for both modes were measured in the same manner (high strain to low strain) and taken after the sweeps for both modes were complete.

At 10 micro-strain the difference in Q for mode 3 is 16% and for mode 4 is 63%. At 100 micro-strain the difference in Q for mode 3 is 25% and for mode 4 is 76%. At 500 micro-strain the difference in Q for mode 3 is 31% and for mode 4 is 82%.

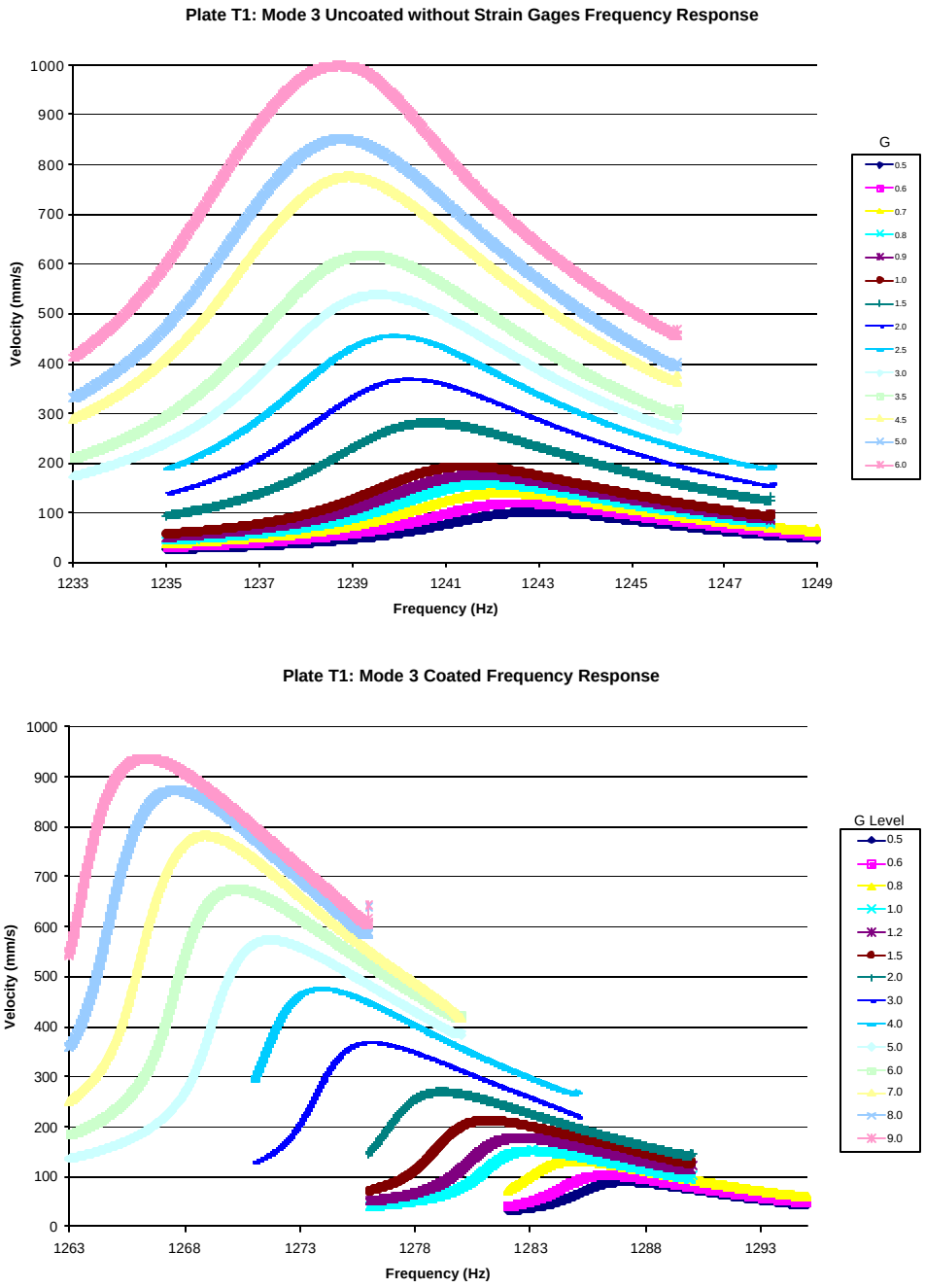

Figure 32. Sine Sweeps for Plate T1: Mode 3 Uncoated and Coated

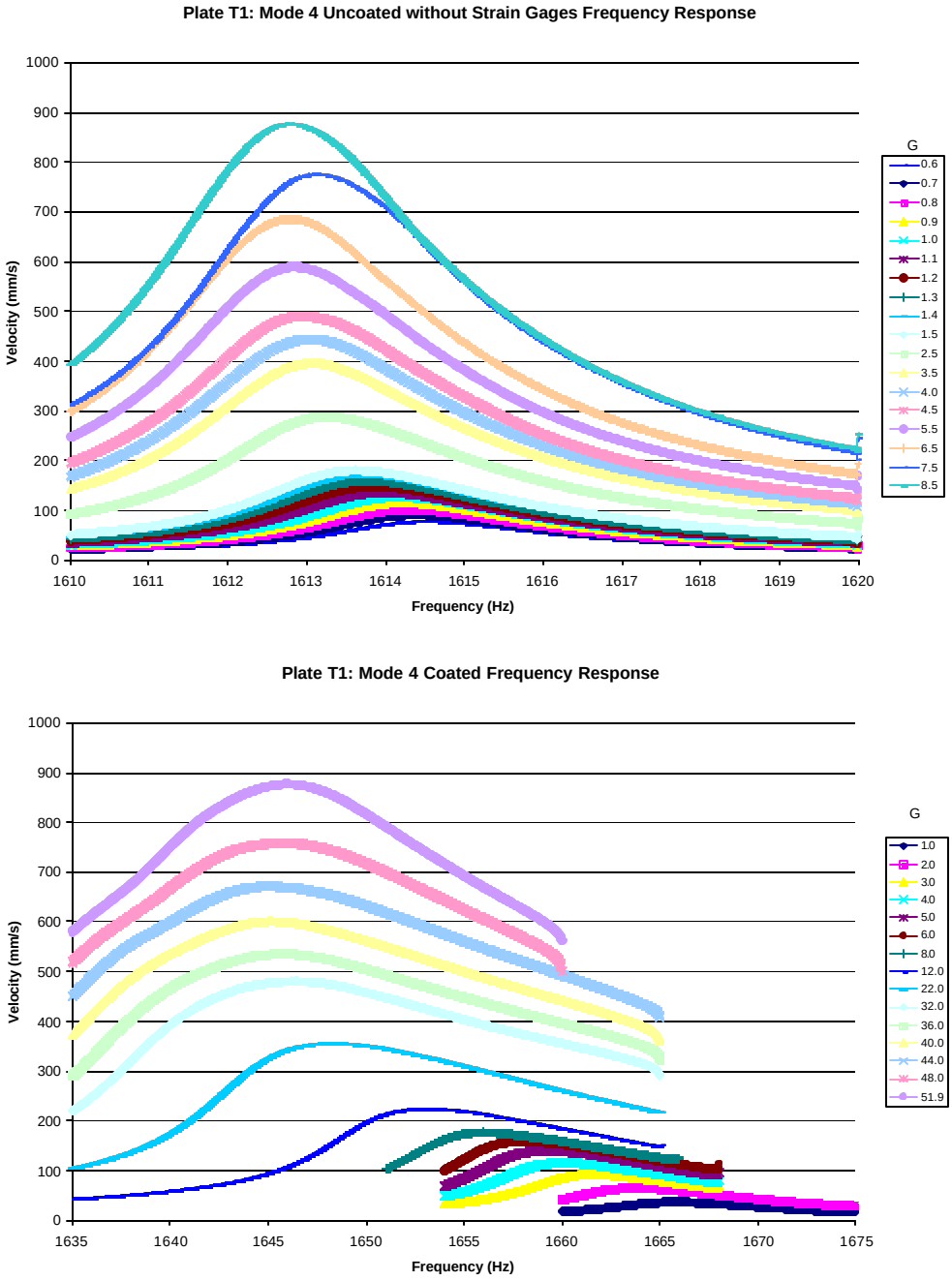

Figure 33. Sine Sweeps for Plate T1: Mode 4 Uncoated and Coated

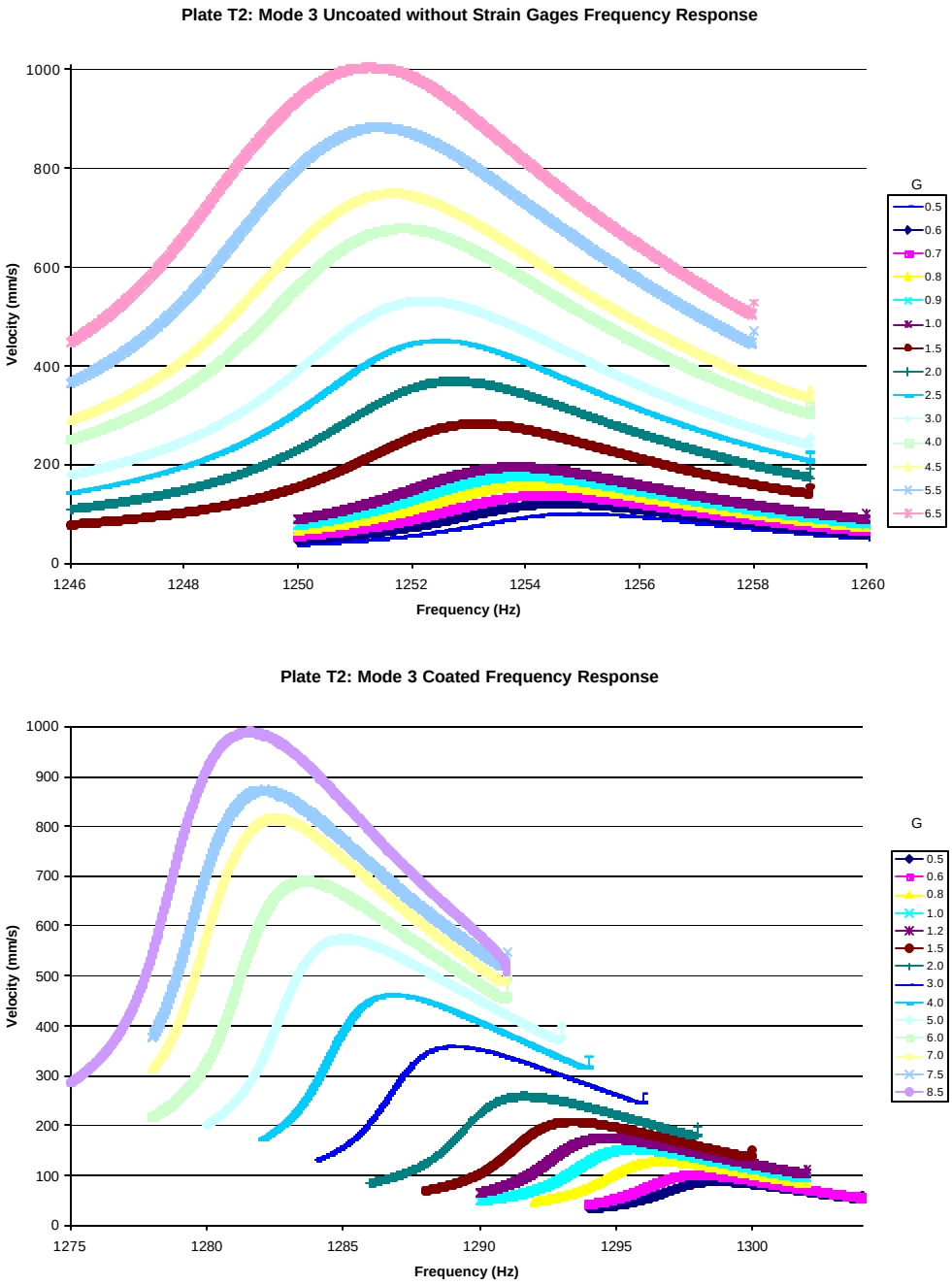

Figure 34. Sine Sweeps for Plate T2: Mode 3 Uncoated and Coated

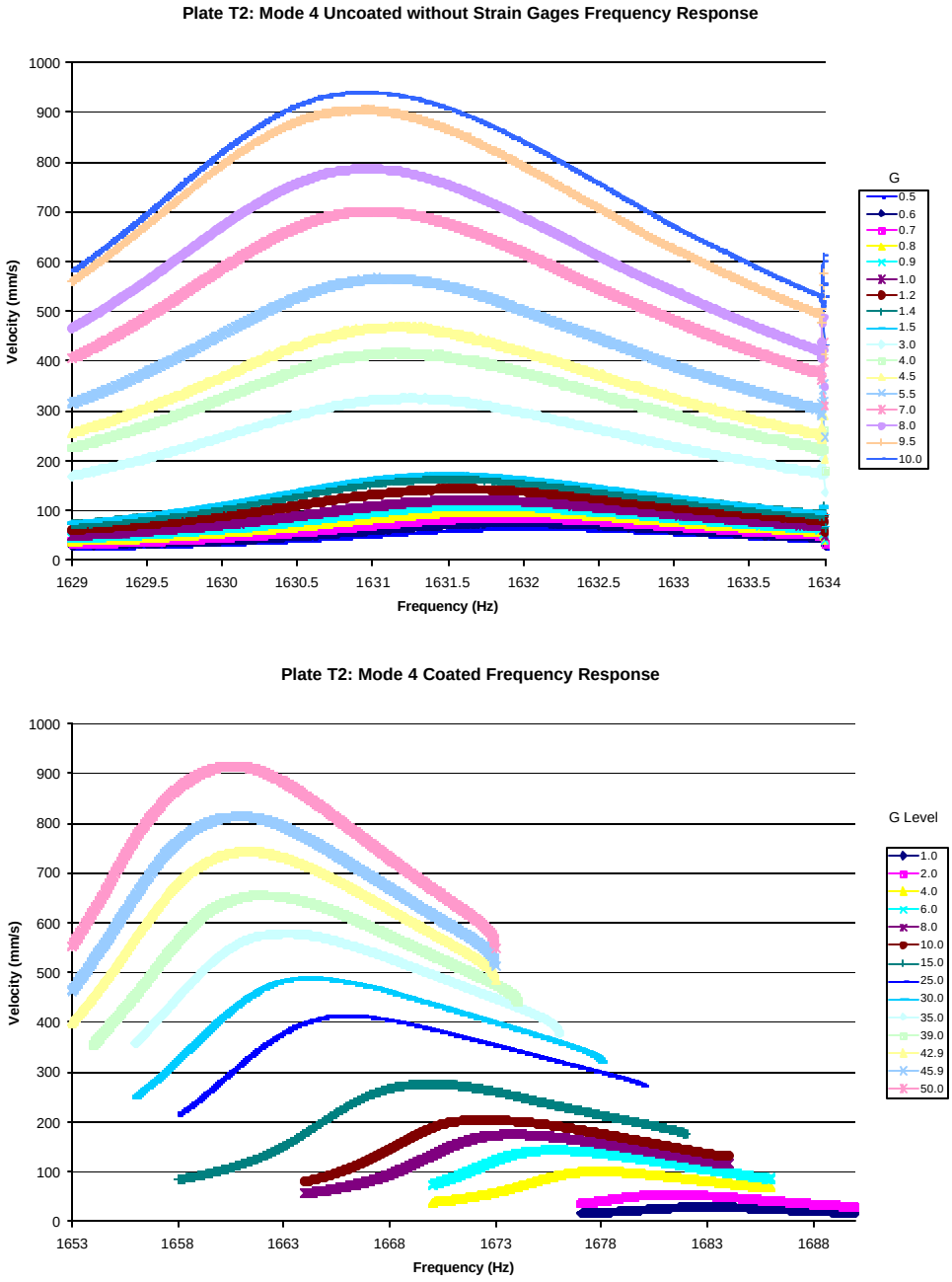

Figure 35. Sine Sweeps for Plate T2: Mode 4 Uncoated and Coated

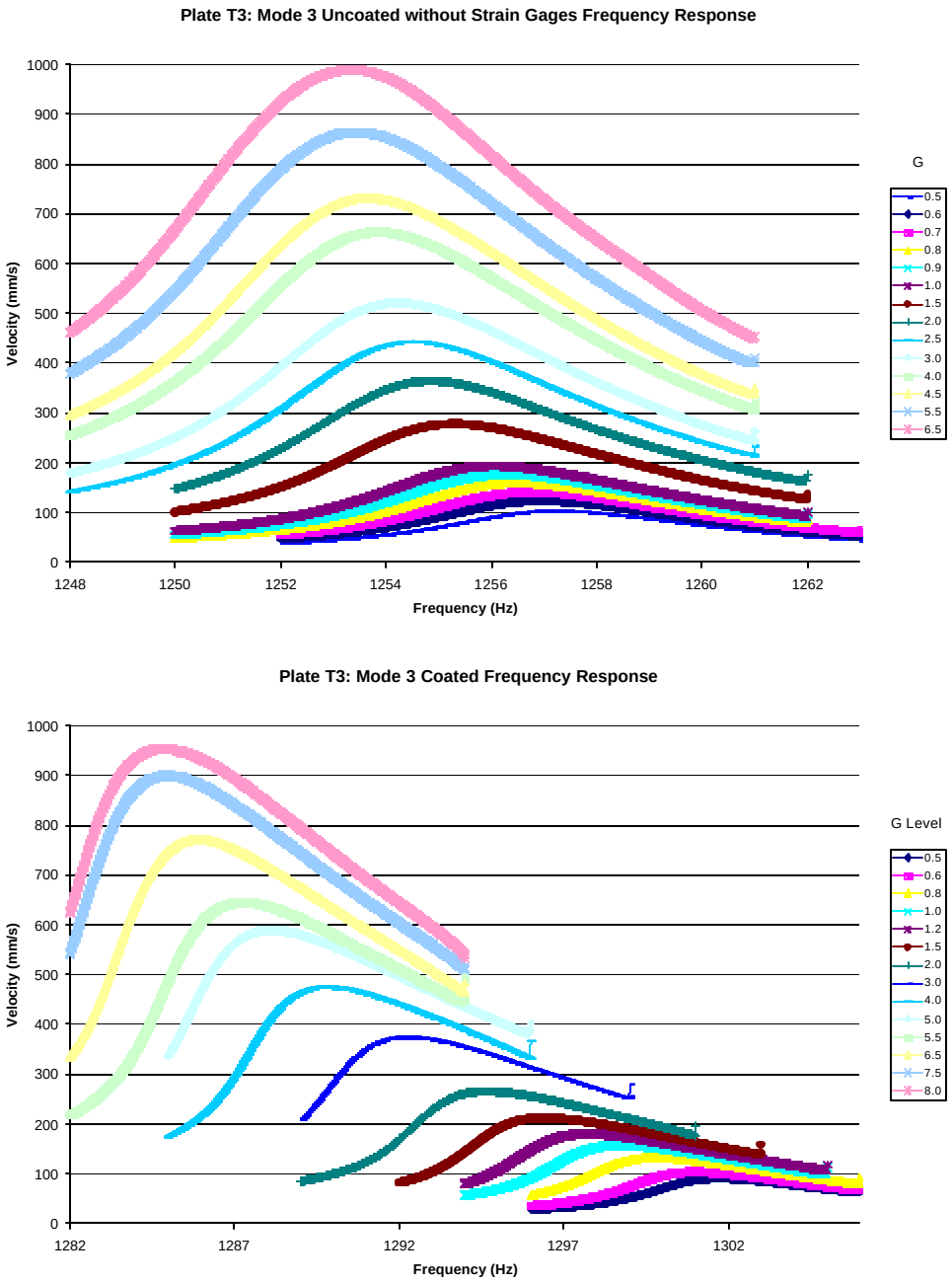

Figure 36. Sine Sweeps for Plate T3: Mode 3 Uncoated and Coated

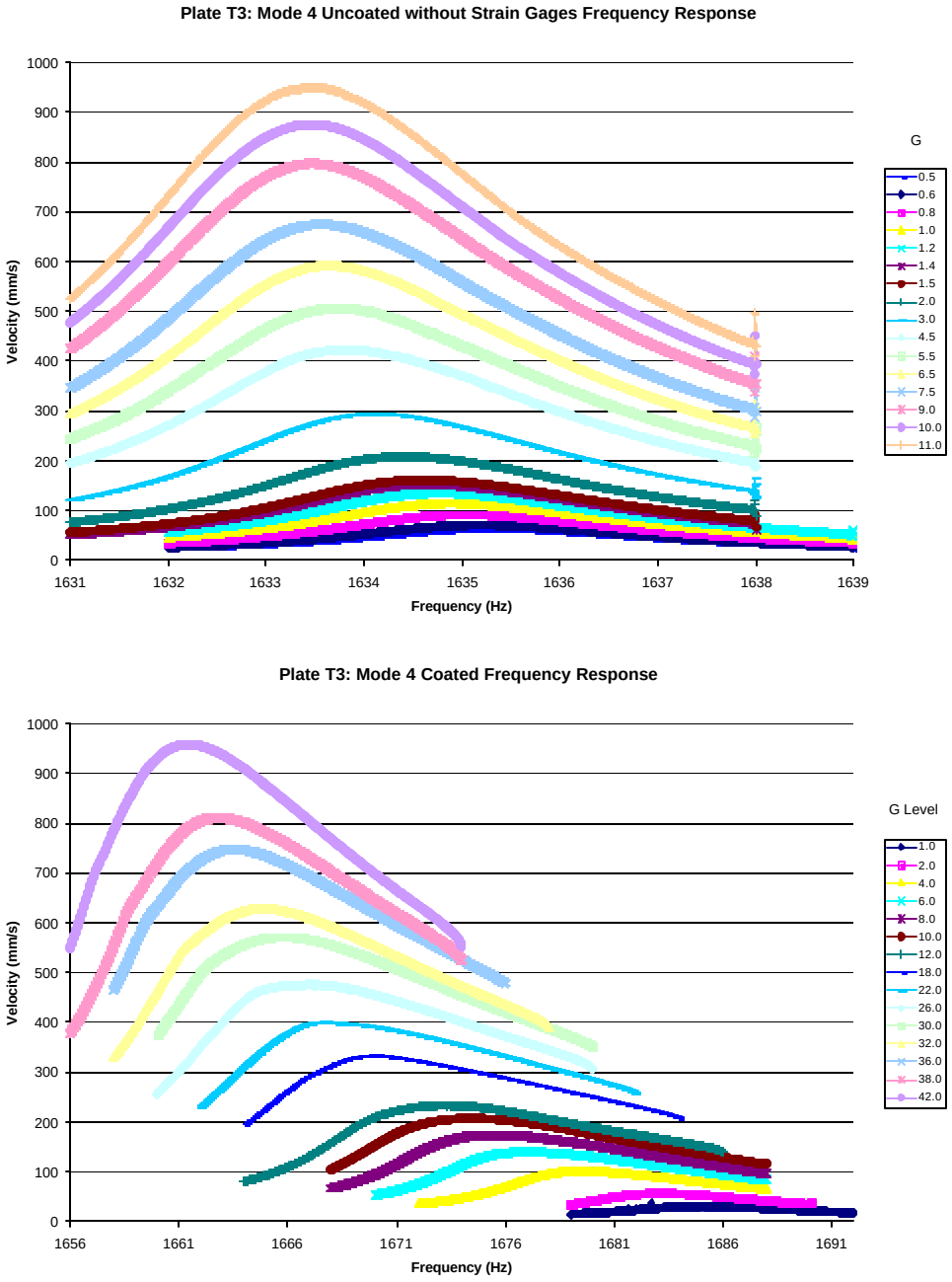

Figure 37. Sine Sweeps for Plate T3: Mode 4 Uncoated and Coated

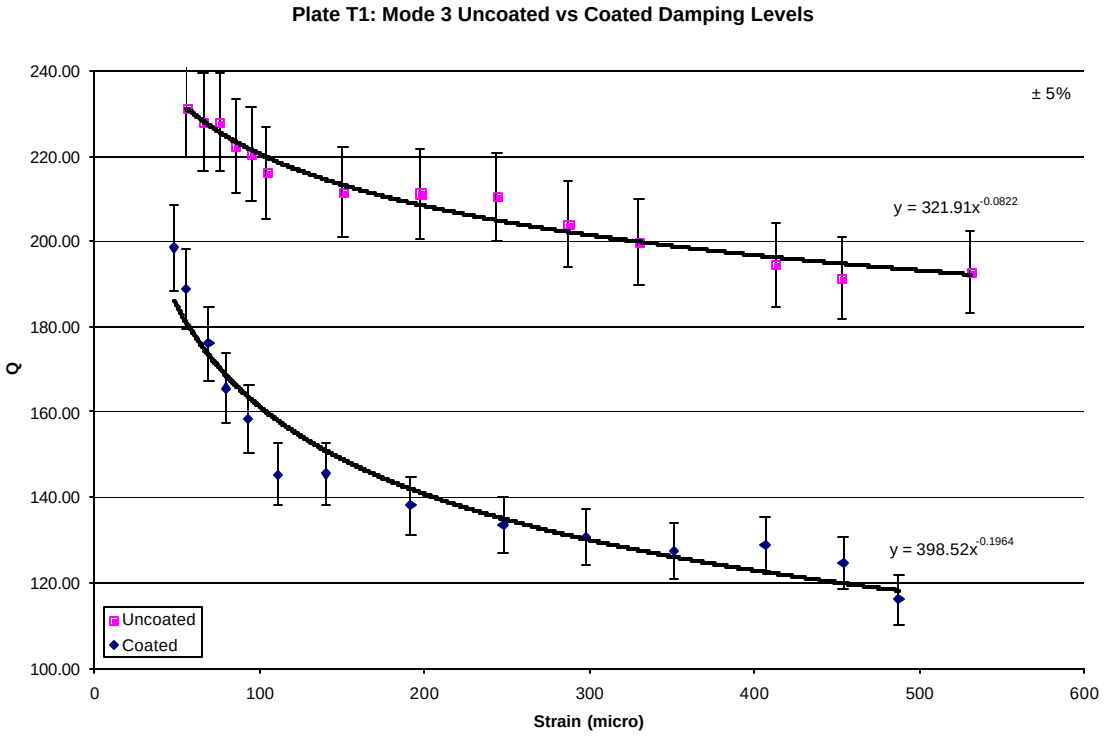

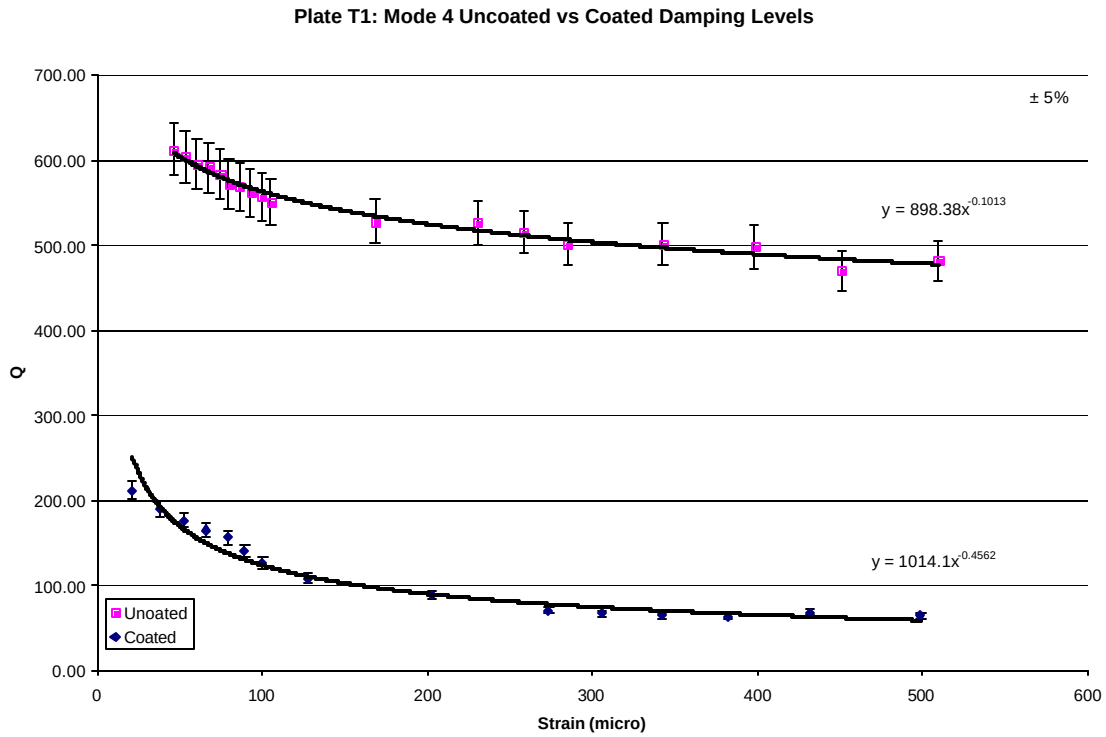

Figure 38. Q-Strain Relationship for Plate T1: Uncoated and Coated

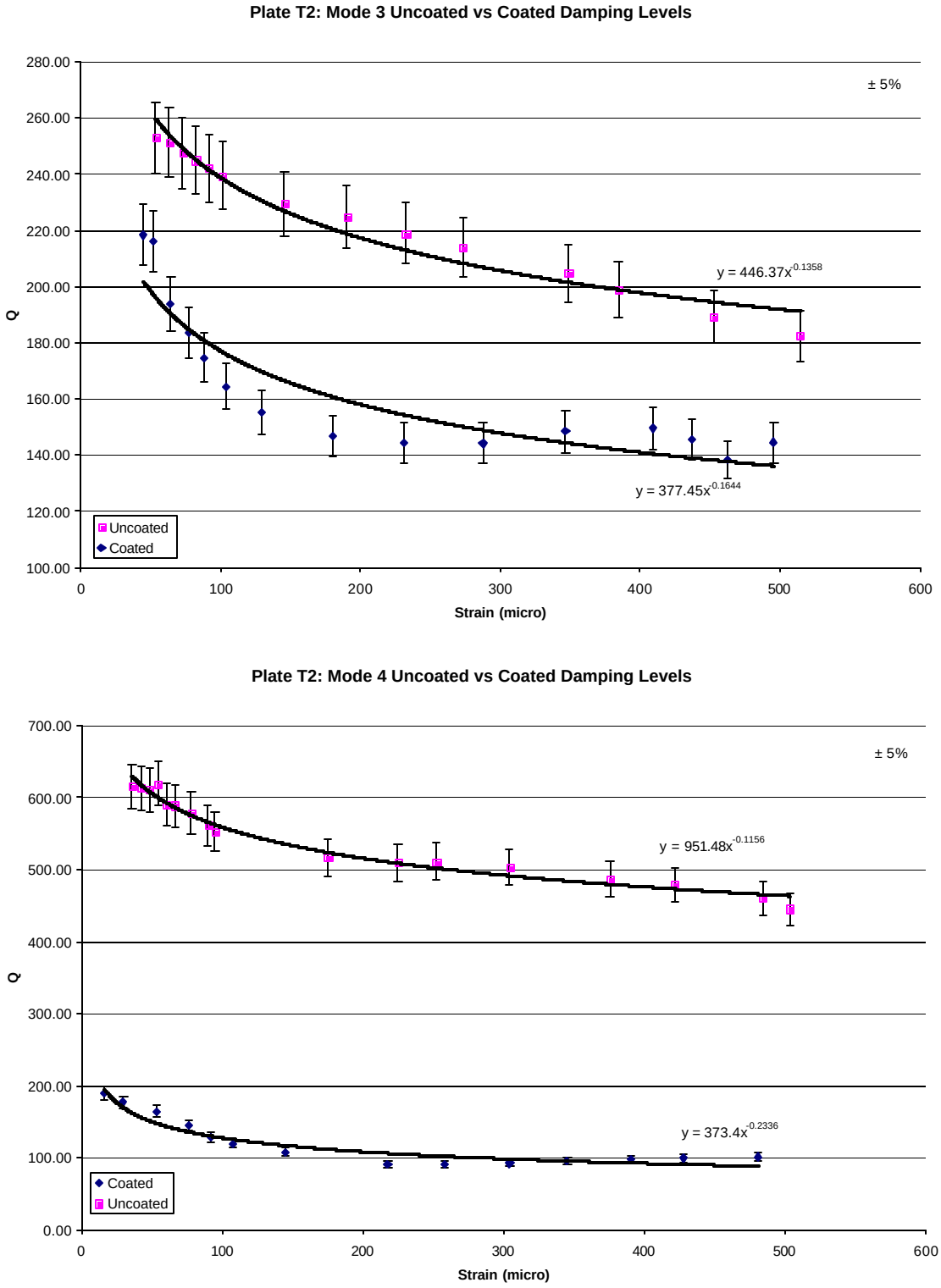

Figure 39. Q-Strain Relationship for Plate T2: Uncoated and Coated

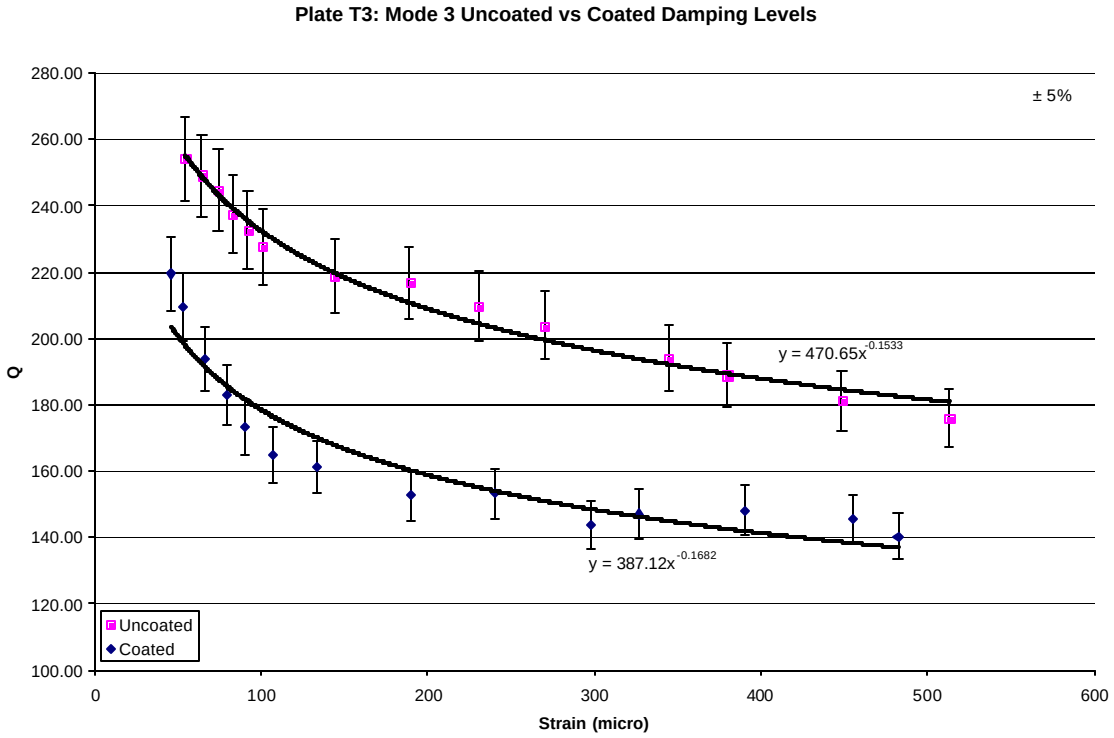

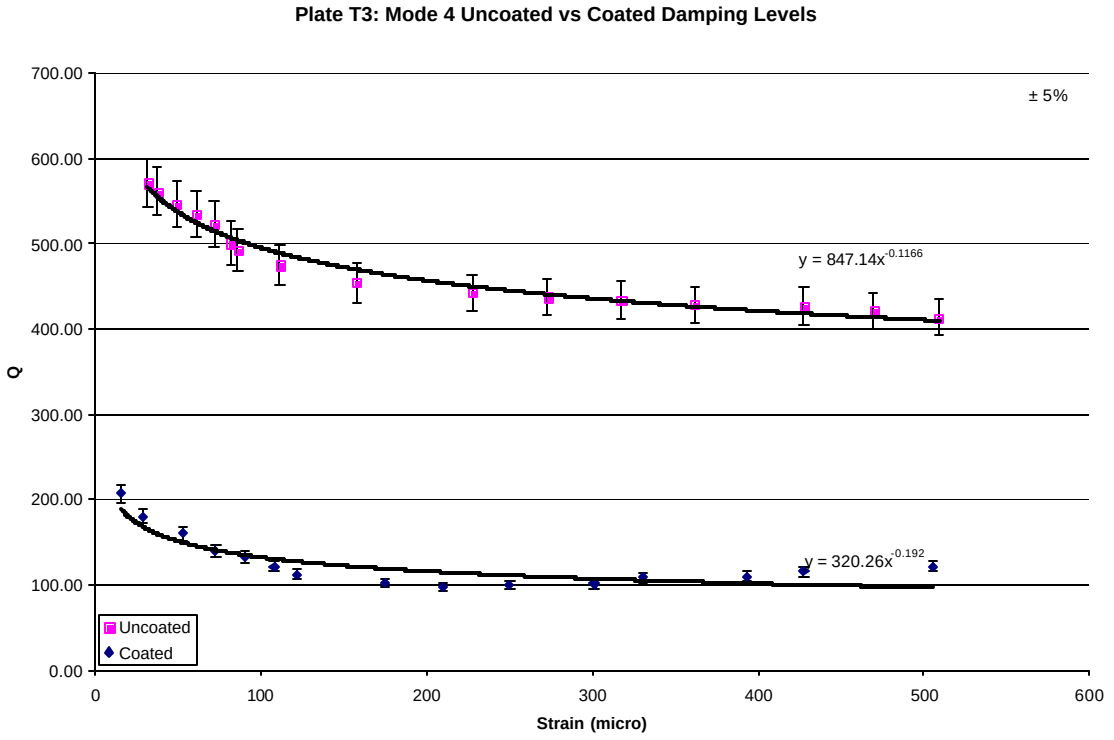

Figure 40. Q-Strain Relationship for Plate T3: Uncoated and Coated

Table 21. Uncoated versus Coated Q Comparison at Different Strains for Plate T1

Plate T1	Mode 3	Mode 3	Mode 3	Mode 4	Mode 4	Mode 4
Strain	Uncoated Q	Coated Q	% Diff	Uncoated Q	Coated Q	% Diff
10	266.40	253.54	4.83	711.48	354.68	50.15
20	251.65	221.27	12.07	663.23	258.53	61.02
30	243.40	204.34	16.05	636.54	214.87	66.24
40	237.71	193.11	18.76	618.26	188.44	69.52
50	233.39	184.83	20.81	604.44	170.20	71.84
60	229.92	178.33	22.44	593.38	156.62	73.61
70	227.02	173.01	23.79	584.19	145.98	75.01
80	224.54	168.53	24.94	576.34	137.36	76.17
90	222.38	164.68	25.95	569.50	130.17	77.14
100	220.46	161.31	26.83	563.46	124.06	77.98
150	213.24	148.96	30.14	540.78	103.11	80.93
200	208.25	140.78	32.40	525.25	90.43	82.78
250	204.47	134.74	34.10	513.51	81.68	84.09
300	201.43	130.00	35.46	504.11	75.16	85.09
350	198.89	126.12	36.59	496.30	70.05	85.88
400	196.72	122.86	37.55	489.63	65.91	86.54
450	194.82	120.05	38.38	483.83	62.47	87.09
500	193.14	117.59	39.12	478.69	59.53	87.56

Table 22. Uncoated versus Coated Q Comparison at Different Strains for Plate T2

Plate T2	Mode 3	Mode 3	Mode 3	Mode 4	Mode 4	Mode 4
Strain	Uncoated Q	Coated Q	% Diff	Uncoated Q	Coated Q	% Diff
10	326.51	258.50	20.83	729.12	218.06	70.09
20	297.18	230.66	22.38	672.98	185.46	72.44
30	281.26	215.78	23.28	642.16	168.70	73.73
40	270.48	205.82	23.91	621.16	157.74	74.61
50	262.41	198.40	24.39	605.34	149.73	75.27
60	255.99	192.54	24.78	592.71	143.48	75.79
70	250.69	187.73	25.12	582.25	138.41	76.23
80	246.18	183.65	25.40	573.33	134.16	76.60
90	242.28	180.13	25.65	565.57	130.52	76.92
100	238.83	177.04	25.88	558.73	127.34	77.21
150	226.04	165.62	26.73	533.14	115.83	78.27
200	217.38	157.97	27.33	515.70	108.31	79.00
250	210.89	152.28	27.79	502.57	102.81	79.54
300	205.73	147.78	28.17	492.09	98.52	79.98
350	201.47	144.08	28.48	483.40	95.03	80.34
400	197.85	140.96	28.76	475.99	92.12	80.65
450	194.71	138.25	29.00	469.56	89.62	80.91
500	191.94	135.88	29.21	463.87	87.44	81.15

Table 23. Uncoated versus Coated Q Comparison at Different Strains for Plate T3

Plate T3	Mode 3	Mode 3	Mode 3	Mode 4	Mode 4	Mode 4
Strain	Uncoated Q	Coated Q	% Diff	Uncoated Q	Coated Q	% Diff
10	330.67	262.81	20.52	647.67	205.83	68.22
20	297.34	233.89	21.34	597.39	180.18	69.84
30	279.42	218.47	21.81	569.80	166.68	70.75
40	267.36	208.15	22.15	551.00	157.73	71.37
50	258.37	200.48	22.41	536.85	151.11	71.85
60	251.25	194.43	22.62	525.56	145.91	72.24
70	245.38	189.45	22.79	516.20	141.66	72.56
80	240.41	185.24	22.95	508.22	138.07	72.83
90	236.11	181.61	23.08	501.29	134.99	73.07
100	232.33	178.42	23.20	495.17	132.28	73.29
150	218.32	166.66	23.66	472.31	122.38	74.09
200	208.91	158.79	23.99	456.73	115.80	74.65
250	201.88	152.94	24.24	445.00	110.94	75.07
300	196.32	148.32	24.45	435.64	107.13	75.41
350	191.73	144.52	24.62	427.87	104.00	75.69
400	187.85	141.31	24.77	421.26	101.37	75.94
450	184.48	138.54	24.90	415.52	99.10	76.15
500	181.53	136.11	25.02	410.45	97.12	76.34

Table 24. Average Uncoated versus Average Coated Q Comparison at Different Strains

	Mode 3	Mode 3	Mode 3	Mode 4	Mode 4	Mode 4
Strain	Average Uncoated Q	Average Coated Q	% Diff	Average Uncoated Q	Average Coated Q	% Diff
10	307.86	258.28	16.10	696.09	259.52	62.72
20	282.05	228.61	18.95	644.53	208.06	67.72
30	268.02	212.86	20.58	616.17	183.42	70.23
40	258.52	202.36	21.72	596.81	167.97	71.86
50	251.39	194.57	22.60	582.21	157.01	73.03
60	245.72	188.43	23.31	570.55	148.67	73.94
70	241.03	183.40	23.91	560.88	142.02	74.68
80	237.05	179.14	24.43	552.63	136.53	75.29
90	233.59	175.47	24.88	545.46	131.89	75.82
100	230.54	172.25	25.28	539.12	127.90	76.28
150	219.20	160.41	26.82	515.41	113.77	77.93
200	211.51	152.51	27.90	499.23	104.84	79.00
250	205.75	146.65	28.72	487.03	98.47	79.78
300	201.16	142.03	29.39	477.28	93.60	80.39
350	197.36	138.24	29.96	469.19	89.70	80.88
400	194.14	135.04	30.44	462.30	86.47	81.30
450	191.34	132.28	30.87	456.30	83.73	81.65
500	188.87	129.86	31.25	451.00	81.36	81.96

V: Conclusions and Recommendations

Conclusions

The clamp design used for this research showed excellent repeatability during the scanning laser vibrometer tests. This is partially because the excitation source provided by the air horn was very small. Repeatability became an issue when sine sweeps were conducted at much higher input loads on the shakers. Higher mode 3 stresses at the fixture than mode 4 made experimental results more difficult to repeat for mode 3. Through trial and error, it was discovered that adding jack screws to the rear of the clamp made the data repeatable. The jack screws were threaded through the top clamp and impinged on the top surface of the bottom clamp. This caused the front edge of the clamps to grip the plate tighter and prevented any back and forth vibration in the clamp.

Test results revealed that the resonant frequencies varied by less than 5% when the mag spinel coating was applied and that the mode shapes were unaffected. These measurements were made using the scanning laser vibrometer with an air horn used as the excitation source. The equipment used was not capable of quantifying the actual input force; however, it was very small compared to the levels used for the sine sweep tests. It was assumed for this research that the mode shape was unaltered by the mag spinel at the higher strain levels. By making this assumption the strain/displacement relationship could be used at all strain levels.

Strain softening was seen in the frequency response when the mag spinel was applied. The peaks for each sweep were fairly stable as the load was increased for the uncoated plates, but the peaks for the coated plates decreased by as much as 25 Hz as the load increased. The small frequency decrease, less than 5 Hz, for the uncoated plates may be attributed to a less than perfect boundary condition at the fixture. For a perfectly linear system with a perfect boundary condition the peaks would occur at the same frequency for all loads.

As was expected, the mag spinel coating caused an increase in damping; even at very low strain levels. For all three plates, damping appears to be a function of mode shape. The Q's show a rapid decrease, increased damping, up to about 100 micro-strain for both modes. The decreasing trend continues beyond 100 micro-strain for mode 3 but it levels off for mode 4.

The average increase in damping at 10 micro-strain for mode 3 is 16% and for mode 4 is 63%. At 100 micro-strain the average increase in damping for mode 3 is 25% and for mode 4 is 76%. At 500 micro-strain the average increase in damping for mode 3 is 31% and for mode 4 is 82%.

Recommendations

The width to length ratio of the clamp used for this research was 3.5. By increasing the width and bringing the ratio closer to 1, this researcher feels that the clamp will be more stable and clamping effects will be less likely to creep into the experimental results.

At this time it is uncertain how valid the strain/displacement curves are at higher strain levels than provided by the air horn. Future work should determine the effect of mag spinel on the mode shapes and strains at high strains.

Only one coating thickness was used in this research. The damping sensitivity to thicker and thinner coats should be evaluated. This research should also be repeated at temperatures characteristic of fan, compressor, and turbine blades, since that is the ultimate purpose of this research and the Air Force's interest in damping treatments in general.

Appendix A: Scanning Laser Vibrometer Mode Shapes

Plate T1

Plate T1: Uncoated Mode 3 Laser Vibrometry Image (Run 1)

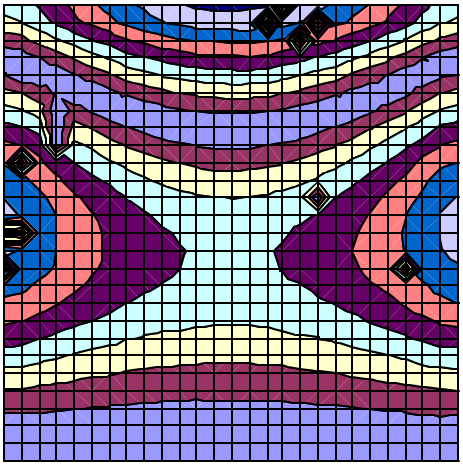

Clamped Region

Plate T1: Uncoated Mode 4 Laser Vibrometry Image (Run 1)

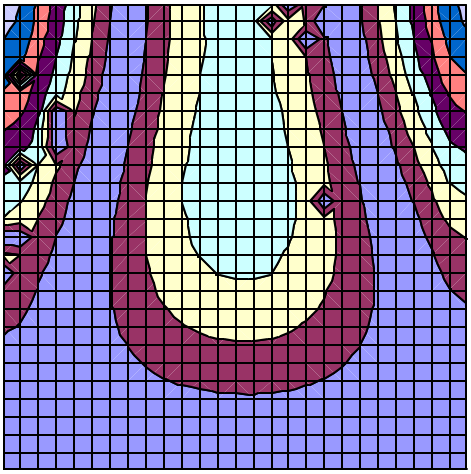

Clamped Region

Plate T1: Uncoated Mode 3 Laser Vibrometry Image (Run 2)

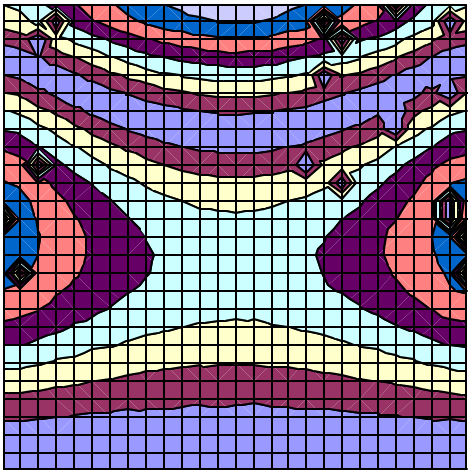

Clamped Region

Plate T1: Uncoated Mode 4 Laser Vibrometry Image (Run 2)

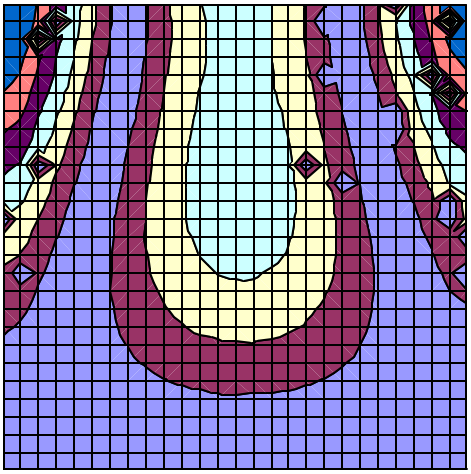

Clamped Region

Plate T1: Uncoated w/ Strain Gages Mode 3 Laser Vibrometry Image (Run 1)

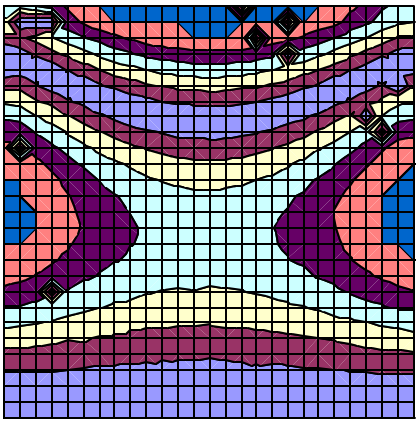

Clamped Region

Plate T1: Uncoated w/ Strain Gages Mode 4 Laser Vibrometry Image (Run 1)

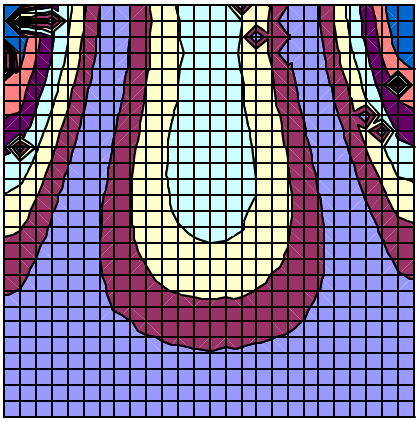

Clamped Region

Plate T1: Uncoated w/ Strain Gages Mode 3 Laser Vibrometry Image (Run 2)

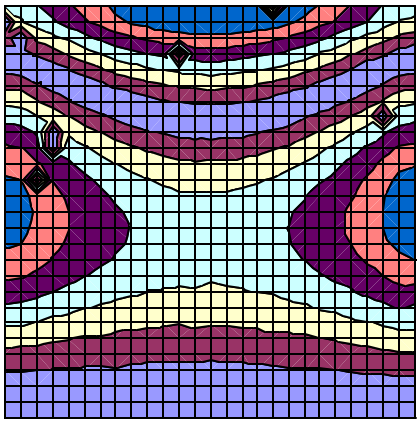

Clamped Region

Plate T1: Uncoated w/ Strain Gages Mode 4 Laser Vibrometry Image (Run 2)

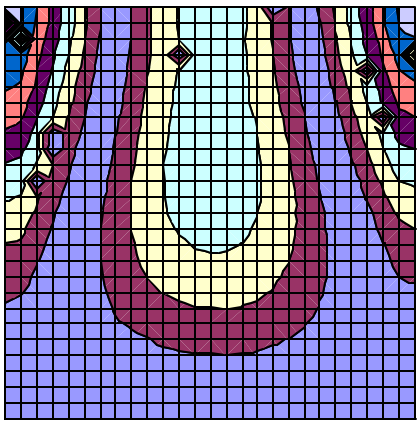

Clamped Region

Plate T1: Coated Mode 3 Laser Vibrometry Image

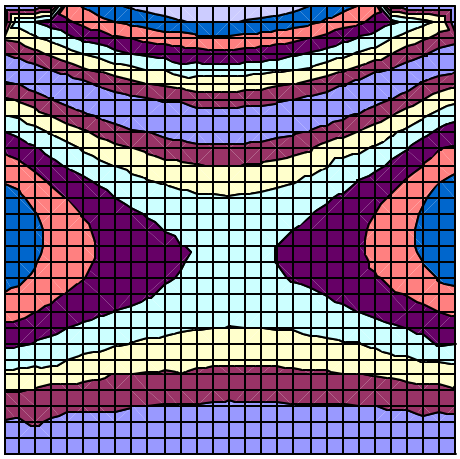

Clamped Region

Plate T1: Coated Mode 4 Laser Vibrometry Image

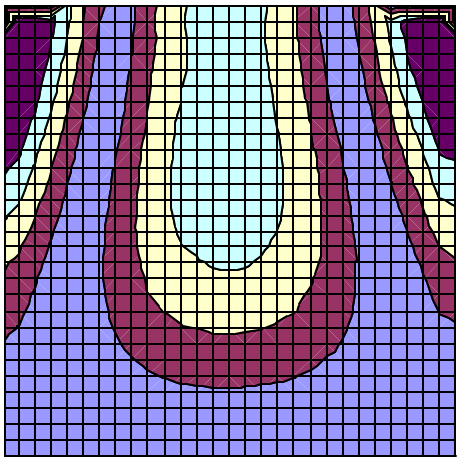

Clamped Region

Plate T2

Plate T2: Uncoated Mode 3 Laser Vibrometry Image (Run 1)

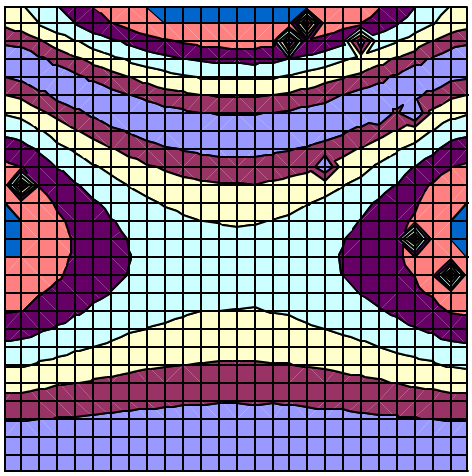

Clamped Region

Plate T2: Uncoated Mode 4 Laser Vibrometry Image (Run 1)

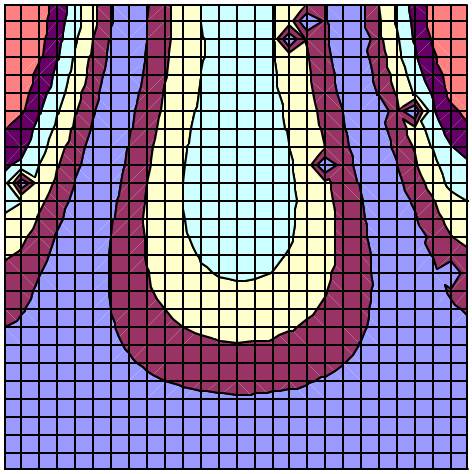

Clamped Region

Plate T2: Uncoated Mode 3 Laser Vibrometry Image (Run 2)

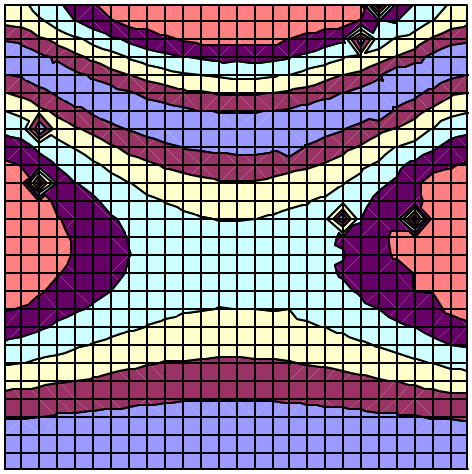

Clamped Region

Plate T2: Uncoated Mode 4 Laser Vibrometry Image (Run 2)

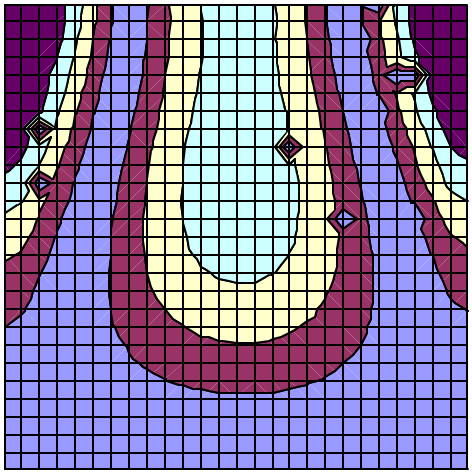

Clamped Region

Plate T2: Uncoated w/ Strain Gages Mode 3 Laser Vibrometry Image (Run1)

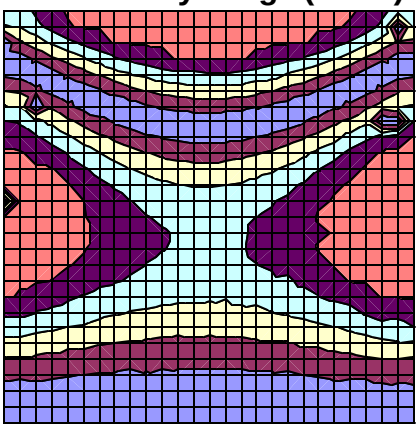

Clamped Region

Plate T2: Uncoated w/ Strain Gages Mode 4 Laser Vibrometry Image (Run 1)

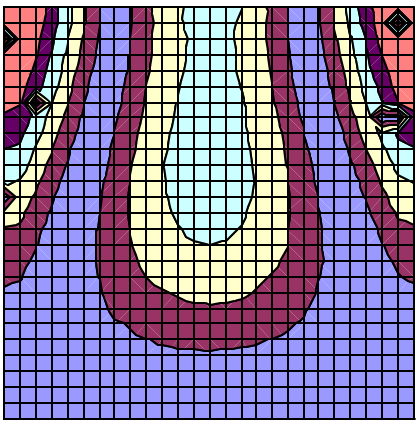

Clamped Region

Plate T2: Uncoated w/ Strain Gages Mode 3 Laser Vibrometry Image (Run 2)

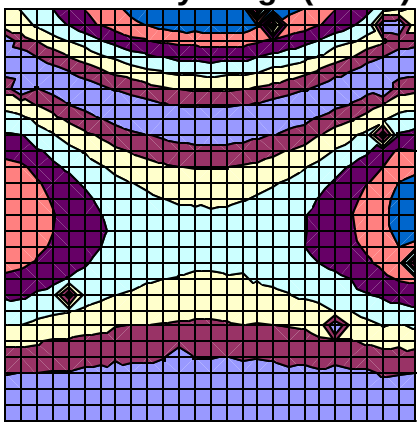

Clamped Region

Plate T2: Uncoated w/ Strain Gages Mode 4 Laser Vibrometry Image (Run 2)

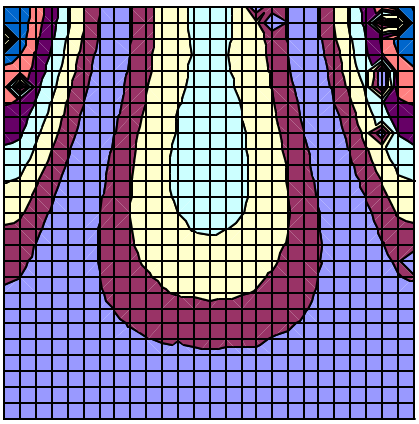

Clamped Region

Plate T2: Coated Mode 3 Laser Vibrometry Image

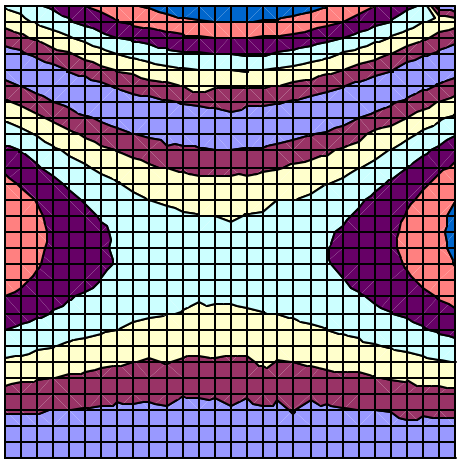

Clamped Region

Plate T2: Coated Mode 4 Laser Vibrometry Image

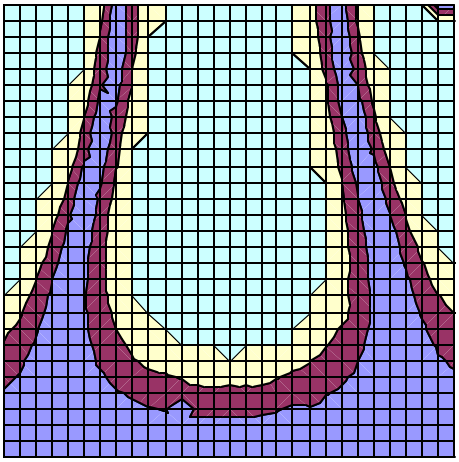

Clamped Region

Plate T3

Plate T3: Uncoated Mode 3 Laser Vibrometry Image (Run 1)

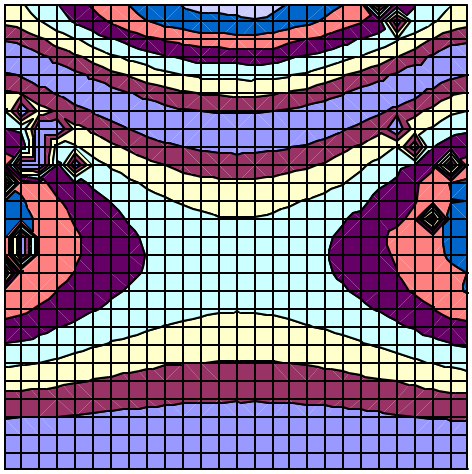

Clamped Region

Plate T3: Uncoated Mode 4 Laser Vibrometry Image (Run 1)

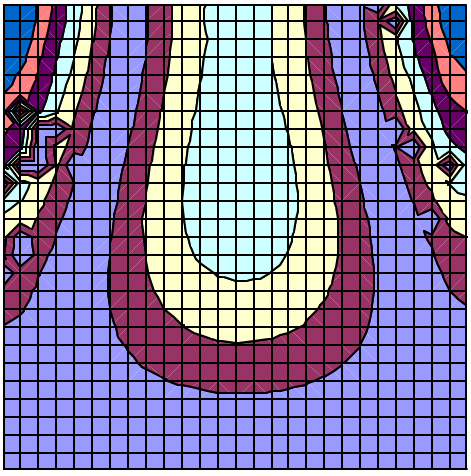

Clamped Region

Plate T3: Uncoated Mode 3 Laser Vibrometry Image (Run 2)

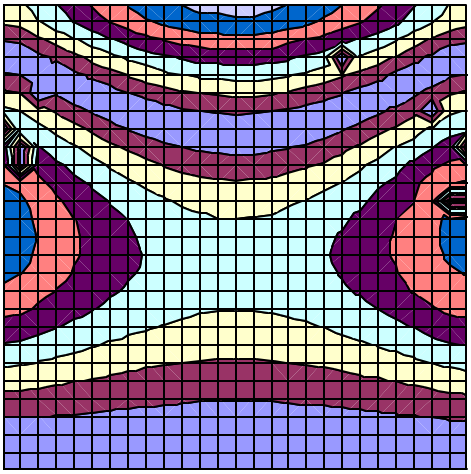

Clamped Region

Plate T3: Uncoated Mode 4 Laser Vibrometry Image (Run 2)

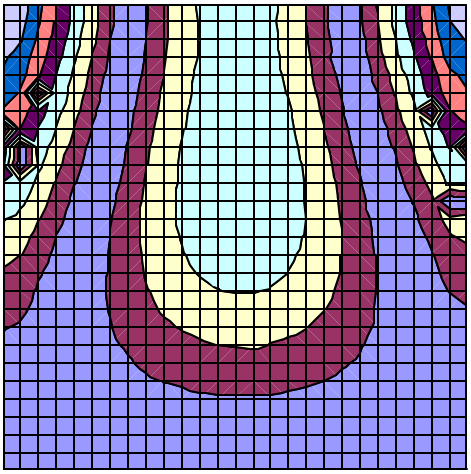

Clamped Region

Plate T3: Uncoated w/ Strain Gages Mode 3 Laser Vibrometry Image (Run 1)

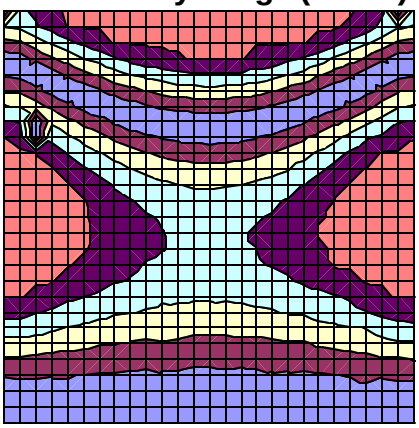

Clamped Region

Plate T3: Uncoated w/ Strain Gages Mode 4 Laser Vibrometry Image (Run 1)

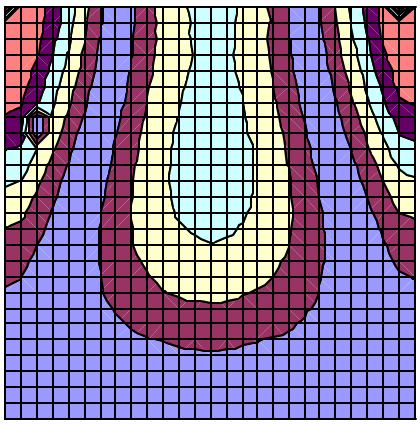

Clamped Region

Plate T3: Uncoated w/ Strain Gages Mode 3 Laser Vibrometry Image (Run 2)

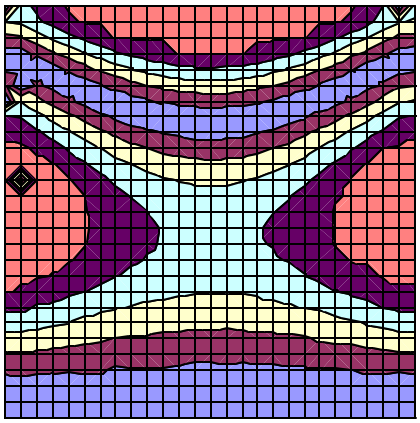

Clamped Region

Plate T3: Uncoated w/ Strain Gages Mode 4 Laser Vibrometry Image (Run 2)

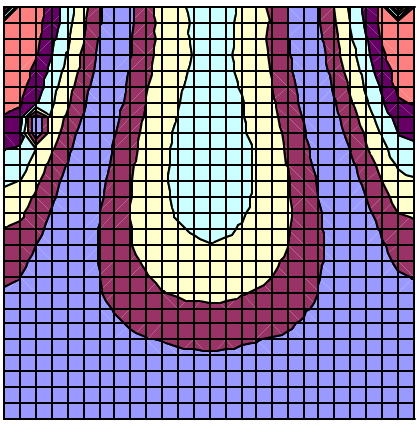

Clamped Region

Plate T3: Coated Mode 3 Laser Vibrometry Image

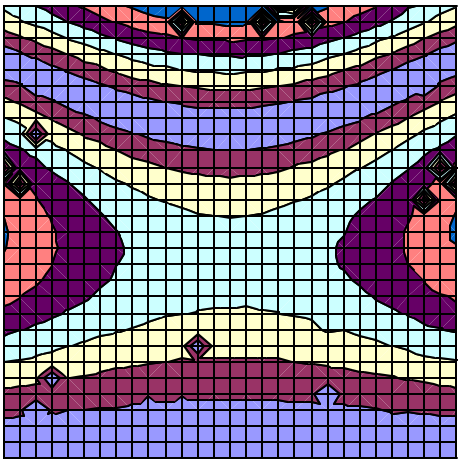

Clamped Region

Plate T3: Coated Mode 4 Laser Vibrometry Image

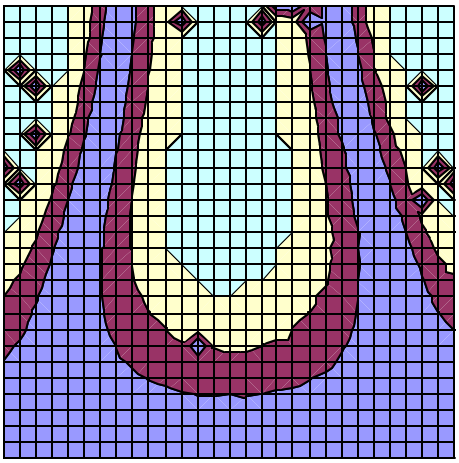

Clamped Region

Appendix B: Experimental Data for Uncoated and Coated Plate Sine Sweeps

Plate T1

Uncoated Mode 3

	Peak	Peak	Peak	Max	
accel (g)	Velocity	Frequency	Displacement	Strain	Q
0.5	102	1243	0.01306	56.09	231.20
0.6	120.6	1242.5	0.01545	65.93	227.90
0.7	139.9	1242.2	0.01792	76.13	227.90
0.8	158	1241.9	0.02025	85.71	222.40
0.9	175.8	1241.8	0.02253	95.12	220.40
1	193	1241.4	0.02474	104.23	216.20
1.5	280.8	1240.7	0.03602	150.70	211.70
2	369	1240.1	0.04736	197.42	211.30
2.5	456.7	1239.9	0.05862	243.84	210.40
3	538.4	1239.5	0.06913	287.15	204.00
3.5	619.3	1239.3	0.07953	330.01	199.80
4.5	775.7	1239	0.09964	412.88	194.50
5	851.3	1238.8	0.10937	452.97	191.30
6	998.4	1238.7	0.12828	530.89	192.70
0.5	108.7	1245.8	0.01389	59.49	267.30
1	198.8	1244.6	0.02542	107.03	225.20
6.5	993	1239.5	0.12750	527.69	170.50

Uncoated Mode 4

	Peak	Peak	Peak	Max	
accel (g)	Velocity	Frequency	Displacement	Strain	Q
0.6	78.1	1614.5	0.00770	46.13	612.85
0.7	90.4	1614.4	0.00891	53.26	605.10
0.8	102.8	1614.3	0.01014	60.44	595.80
0.9	115	1614.2	0.01134	67.52	592.11
1	127.2	1614.2	0.01254	74.59	585.00
1.1	136	1613.9	0.01341	79.70	572.80
1.2	147.3	1613.9	0.01453	86.25	569.40
1.3	158.8	1613.8	0.01566	92.92	562.70
1.4	170.2	1613.7	0.01679	99.53	557.80
1.5	180.2	1613.6	0.01777	105.33	551.42
2.5	289	1613.3	0.02851	168.43	528.70
3.5	396.4	1613.1	0.03911	230.73	527.20
4	444	1613	0.04381	258.34	515.95
4.5	490.5	1613	0.04840	285.31	502.50
5.5	589.7	1612.9	0.05819	342.85	501.20
6.5	685.2	1612.8	0.06762	398.26	498.60
7.5	776.5	1613	0.07662	451.15	470.80
8.5	877.4	1612.8	0.08658	509.72	482.40
0.6	78.6	1614.6	0.00775	46.41	599.60
1.4	174.9	1614	0.01725	102.24	562.80
8.5	906	1613	0.08940	526.24	481.30

Coated Mode 3

accel (g)	Peak Velocity	Peak Frequency	Peak Displacement	Max Strain	Q
0.5	90.2	1287.2	0.01115	48.23	198.50
0.6	103.8	1286.2	0.01284	55.20	188.90
0.8	131.6	1284.9	0.01630	69.44	176.00
1	152	1283.4	0.01885	79.95	165.60
1.2	178.4	1282.5	0.02214	93.50	158.50
1.5	212.3	1281.2	0.02637	110.95	145.30
2	269.5	1279.1	0.03353	140.45	145.50
3	368.7	1275.9	0.04599	191.79	138.10
4	476.7	1273.9	0.05956	247.69	133.40
5	573.3	1271.7	0.07175	297.94	130.60
6	676.2	1270.2	0.08473	351.42	127.40
7	782.1	1268.9	0.09810	406.51	129.00
8	872.5	1267.6	0.10955	453.70	124.60
9	937	1266.3	0.11777	487.57	116.10
0.5	88.51	1287.1	0.01094	47.37	191.80
1.2	174.4	1282.5	0.02164	91.46	156.60
9	1002	1268.4	0.12573	520.37	124.40

Coated Mode 4

accel (g)	Peak Velocity	Peak Frequency	Peak Displacement	Max Strain	Q
1	36.2	1665.8	0.00346	21.21	212.40
2	66	1663.8	0.00631	37.98	190.70
3	91.65	1661.6	0.00878	52.47	176.80
4	115	1660.2	0.01102	65.67	165.70
5	139.2	1659.2	0.01335	79.35	156.80
6	156.7	1658	0.01504	89.28	141.60
8	176	1656	0.01692	100.29	127.10
12	224	1653.1	0.02157	127.62	108.80
22	356	1648.3	0.03437	202.89	89.20
32	480	1646.5	0.04640	273.55	70.80
36	536.7	1645.9	0.05190	305.87	67.30
40	600.3	1645.4	0.05807	342.12	65.00
44	670.9	1645.1	0.06491	382.32	63.80
48	759	1645.9	0.07339	432.20	68.70
52	876.7	1646.1	0.08476	499.03	64.80
1	32.3	1663.9	0.00309	19.04	207.00
8	181.3	1653	0.01746	103.47	136.00
52	796	1636.8	0.07740	455.74	78.00

Plate T2

Uncoated Mode 3

	Peak	Peak	Peak	Max	
accel (g)	Velocity	Frequency	Displacement	Strain	Q
0.5	101.5	1255	0.01287	53.67	253.00
0.6	120.8	1254.7	0.01532	63.51	251.30
0.7	139.3	1254.4	0.01767	72.94	247.50
0.8	157.9	1254.1	0.02004	82.44	245.00
0.9	176.1	1254	0.02235	91.71	242.20
1	194.9	1253.8	0.02474	101.31	239.50
1.5	282.1	1253.1	0.03583	145.82	229.50
2	369.2	1252.7	0.04691	190.28	225.00
2.5	451.9	1252.5	0.05742	232.49	219.00
3	531.6	1252.3	0.06756	273.18	214.00
4	679.6	1251.8	0.08640	348.82	204.90
4.5	749.2	1251.7	0.09526	384.37	199.10
5.5	882.9	1251.4	0.11229	452.71	189.10
6.5	1003.7	1251.3	0.12766	514.42	182.40
0.5	108.4	1255.2	0.01374	57.17	261.40
1	204.1	1254.2	0.02590	105.96	239.50
6.5	1026.9	1251.7	0.13057	526.09	176.70

Uncoated Mode 4

	Peak	Peak	Peak	Max	
accel (g)	Velocity	Frequency	Displacement	Strain	Q
0.5	64.7	1632.1	0.00631	35.68	615.40
0.6	76.5	1632	0.00746	41.98	613.40
0.7	88.1	1631.8	0.00859	48.17	610.50
0.8	99.2	1631.7	0.00968	54.10	619.10
0.9	110.5	1631.8	0.01078	60.13	591.10
1	121.9	1631.7	0.01189	66.22	589.30
1.2	143.7	1631.6	0.01402	77.86	578.80
1.4	165.5	1631.5	0.01614	89.50	562.10
1.5	175.2	1631.5	0.01709	94.68	552.60
3	325.4	1631.3	0.03175	174.89	516.80
4	418.6	1631.1	0.04084	224.68	510.00
4.5	469.7	1631.3	0.04583	251.93	511.30
5.5	567	1631	0.05533	303.94	504.00
7	700.6	1631	0.06837	375.28	486.50
8	786.3	1630.9	0.07673	421.07	479.30
9.5	903.8	1630.9	0.08820	483.83	460.10
10	940.1	1631	0.09174	503.18	445.50
0.5	62.5	1631.7	0.00610	34.51	602.90
1.5	177.1	1631.3	0.01728	95.71	557.20
10	979.6	1630.6	0.09561	524.40	457.30

Coated Mode 3

accel (g)	Peak Velocity	Peak Frequency	Peak Displacement	Max Strain	Q
0.5	87.4	1298.7	0.01071	45.00	218.30
0.6	101.8	1297.9	0.01248	52.11	216.00
0.8	127	1296.7	0.01559	64.57	193.80
1	152.2	1295.6	0.01870	77.05	183.50
1.2	174.4	1294.7	0.02144	88.06	174.70
1.5	206.4	1293.4	0.02540	103.95	164.40
2	257.9	1291.5	0.03178	129.57	155.20
3	359.1	1289	0.04434	179.97	146.60
4	462.4	1286.8	0.05719	231.56	144.40
5	574.5	1285	0.07116	287.61	144.10
6	692.5	1283.5	0.08587	346.67	148.40
7	817	1282.5	0.10139	408.96	149.50
7.5	873.3	1282.1	0.10841	437.13	145.40
8	925.1	1283	0.11476	462.62	138.30
8.5	990.1	1281.6	0.12296	495.52	144.60
0.5	85.1	1297.4	0.01044	43.91	214.80
1.5	202.7	1292.3	0.02496	102.20	163.00
8.5	992.1	1281.4	0.12322	496.60	129.30

Coated Mode 4

accel (g)	Peak Velocity	Peak Frequency	Peak Displacement	Max Strain	Q
1	28.9	1682.9	0.00273	16.11	190.40
2	54.95	1681.1	0.00520	29.62	176.80
4	100.2	1678	0.00950	53.16	164.00
6	143.2	1675.6	0.01360	75.59	144.00
8	174.3	1673.9	0.01657	91.84	128.50
10	204.2	1672.5	0.01943	107.49	119.80
15	275.4	1669.8	0.02625	144.80	108.30
25	413.6	1665.9	0.03951	217.39	91.20
30	489.9	1664.3	0.04685	257.53	90.20
35	578.7	1663.2	0.05538	304.20	92.20
39	656	1662	0.06282	344.93	95.60
43	742.8	1661.4	0.07116	390.56	97.90
46	813.6	1660.9	0.07796	427.81	99.20
50	914.6	1660.7	0.08765	480.83	101.40
1	27.2	1681.5	0.00257	15.24	185.80
10	200.7	1669.8	0.01913	105.84	120.20
50	852.5	1659.4	0.08176	448.61	85.40

Plate T3

Uncoated Mode 3

	Peak	Peak	Peak	Max	
accel (g)	Velocity	Frequency	Displacement	Strain	Q
0.5	103.6	1257.1	0.01312	54.10	254.30
0.6	122.8	1257	0.01555	64.02	249.20
0.7	141.9	1256.9	0.01797	73.89	244.80
0.8	158.9	1256.5	0.02013	82.70	237.40
0.9	176.5	1256.3	0.02236	91.82	232.60
1	193.6	1256	0.02453	100.68	227.60
1.5	277.6	1255.3	0.03520	144.19	218.90
2	363.8	1254.9	0.04614	188.85	216.90
2.5	443.5	1254.5	0.05627	230.17	209.90
3	520.5	1254.3	0.06604	270.07	203.90
4	664.2	1253.9	0.08431	344.58	194.10
4.5	731.7	1253.7	0.09289	379.60	188.90
5.5	864.4	1253.4	0.10976	448.45	181.40
6.5	989.1	1253.4	0.12559	513.06	175.90
0.5	104.7	1257.4	0.01325	54.65	259.20
1	196.4	1256.4	0.02488	102.09	238.50
6.6	977.1	1253.7	0.12404	506.72	172.10

Uncoated Mode 4

	Peak	Peak	Peak	Max	
accel (g)	Velocity	Frequency	Displacement	Strain	Q
0.5	59.4	1635.3	0.00578	31.77	570.90
0.6	70.4	1635.2	0.00685	37.67	561.10
0.8	92.4	1635	0.00899	49.47	546.20
1	113.7	1634.9	0.01107	60.89	534.30
1.2	134.2	1634.8	0.01306	71.89	522.80
1.4	152.5	1634.6	0.01485	81.71	500.70
1.5	160.8	1634.6	0.01566	86.16	492.60
2	207.9	1634.4	0.02024	111.43	474.60
3	294.5	1634.1	0.02868	157.90	454.20
4.5	423.9	1633.8	0.04129	227.35	442.30
5.5	508.6	1633.7	0.04955	272.81	437.30
6.5	591.6	1633.7	0.05763	317.34	433.46
7.5	674.3	1633.5	0.06570	361.75	428.70
9	796.7	1633.5	0.07762	427.43	426.80
10	875.2	1633.5	0.08527	469.55	420.80
11	948.7	1633.4	0.09244	509.02	413.30
0.5	57.8	1635.3	0.00563	30.92	543.30
2	203.8	1634.5	0.01984	109.22	464.00
11	936.4	1633.5	0.09124	502.39	395.40

Coated Mode 3

accel (g)	Peak Velocity	Peak Frequency	Peak Displacement	Max Strain	Q
0.5	90.48	1301.7	0.01106	45.72	219.50
0.6	104.3	1301	0.01276	52.64	209.50
0.8	131.6	1299.8	0.01611	66.33	194.00
1	156.8	1298.7	0.01922	78.99	182.90
1.2	179.5	1297.7	0.02201	90.41	173.30
1.5	211.9	1296.4	0.02601	106.73	164.90
2	265	1294.6	0.03258	133.51	161.20
3	375.8	1292.1	0.04629	189.46	152.70
4	476.1	1289.8	0.05875	240.30	153.20
5	590	1288.1	0.07290	298.04	143.90
5.5	646.7	1287.3	0.07995	326.83	147.00
6.5	771.4	1286	0.09547	390.13	148.20
7.5	899.2	1284.9	0.11138	455.06	145.40
8	953.2	1284.9	0.11807	482.35	140.30
0.5	88.7	1300.6	0.01085	44.87	217.50
1.5	209	1295.4	0.02568	105.35	158.60
8	950	1284.3	0.11773	480.96	128.40

Coated Mode 4

accel (g)	Peak Velocity	Peak Frequency	Peak Displacement	Max Strain	Q
1	30.72	1685.1	0.00290	15.92	207.50
2	55.1	1683	0.00521	28.63	180.20
4	101.7	1679.4	0.00964	53.01	160.20
6	139.2	1676.9	0.01321	72.69	140.10
8	173.4	1675.4	0.01647	90.65	132.30
10	206.3	1674.2	0.01961	107.94	121.40
12	233	1672.9	0.02217	122.01	111.80
18	332.6	1670	0.03170	174.50	101.90
22	399.4	1667.7	0.03812	209.85	98.00
26	475.7	1666.9	0.04542	250.07	99.50
30	572	1665.5	0.05466	300.96	101.00
32	628.6	1664.9	0.06009	330.87	108.30
36	746.8	1663.5	0.07145	393.43	109.50
38	811.2	1662.9	0.07764	427.51	115.20
42	957.5	1661.6	0.09171	505.02	121.40
1	29.1	1684.3	0.00275	15.08	199.30
10	204.4	1672.8	0.01945	107.04	123.10
42	850.4	1661.7	0.08145	448.50	110.60

Bibliography

APS Materials, Inc., The Plasma Spray Process, January 2004, www.apsmaterials.com.

Baz, A. "Active Damping", *Encyclopedia of Vibration*, pp. 351-364. San Diego: Academic Press, 2001.

Cook, Robert D. and others. Concepts and Applications of Finite Element Analysis (4th Edition). New York: John Wiley & Sons, Inc. 2002.

Cowles, B. A. "High Cycle Fatigue in Aircraft Gas Turbines – an Industry Perspective", *International Journal of Fracture*, 80: 147-163 (1996).

Garrison, Brian, Editor. "Foreward", *High Cycle Fatigue Science and Technology Program 2000 Annual Report*. February 2001.

Grady, Joseph E. "Fundamentals of High-Cycle Fatigue", *Machine Design*, 71:86 (1999).

Green, Jeff, and Sophoclis Patsias, "A Preliminary Approach for the Modeling of a Hard Damping Coating Using Friction Elements", *Proceedings, 7th National Turbine Engine High Cycle Fatigue Conference*, May 2002.

Harris, Cyril M. *Shock and Vibration Handbook* (4th Edition). New York: McGraw Hill, 1996.

Ivansic, Frank T. *The Effect of a Hard Coating on the Damping and Fatigue Life of Titanium*. MS Thesis, AFIT/GAE?ENY/03-12. Department of Aeronautics and Astronautics, Air Force Institute of Technology (AU), Wright-Patterson AFB OH, March 2003

Kielb, R. and etal. "Advanced Damping Systems for Fan and Compressor Blisks", *Proceedings, 5th National Turbine Engine High Cycle Fatigue Conference*, May 2000.

Lazan, J. B. *Damping of Materials and Members in Structural Mechanics.* New York: Pergamon Press, 1968.

Lazan, J. B. "Energy Dissipation Mechanisms in Structures, with Particular Reference to Material Damping," *Paper presented at Colloquium on Structural Damping at the ASME Annual Meeting*. 2-34. New York: ASME, 1959.

Leissa, Arthur W. *Vibration of Plates*. Washington D.C.: GPO, 1969.

Meirovitch, Leonard. *Elements of Vibration Analysis*. Boston: McGraw-Hill, 1986.

Nashif, Ahid D. and Jones, David G. and Henderson, John P. *Vibration Damping*. New York: John Wiley & Sons, 1985.

Nicholas, T. and J. R. Zuiker. "On the Use of the Goodman Diagram for High Cycle Fatigue Design", *International Journal of Fracture*, 80: 219-235 (1996).

Patsias, Sophoclis, Geof R. Tomlinson, and Mark A Jones. "Initial Studies into Hard Coatings for Fan Blade Damping", *Proceddings, 6th National Turbine Engine High Cycle Fatigue Conference*, March 2001.

Patsias, Sophoclis, and Robin Williams. "Hard Damping Coatings: Material Properties and F.E. prediction methods", *Proceedings, 8th National Turbine Engine High Cycle Fatigue Conference*, April 2003.

Polytec Laser Doppler Vibrometer User Manual.

Soedel, Werner. *Vibration of Shells and Plates* (2nd Edition). New York: Marcel Dekker, Inc., 1993.

Shen, M.-H. Herman. "Development of a Free Layer Damper Using Hard Coatings", *Proceedings, 7th National Turbine Engine High Cycle Fatigue Conference*, May 2002.

Shipton, Mark. and Sophoclis Patsias. "Hard Damping Coatings: Internal Friction as the damping mechanism", *Proceedings, 8th National Turbine Engine High Cycle Fatigue Conference,* April 2003.

Torvik, Peter J., S. Patsias, and G. R. Tomlinson, "Characterising the Behavior of Hard Coatings: Comparisons from two Methodologies", *Proceedings, 7th National Turbine Engine High Cycle Fatigue Conference*, May 2002.

Torvik, Peter J, "Determining Material Properties of Nonlinear Damping Materials from System Response Data", *Proceedings, 8th National Turbine Engine High Cycle Fatigue Conference*, April 2003.

Ungar, E. E. "Damping Materials", Encyclopedia of Vibration, pp. 327-331. San Diego: Academic Press, 2001.

Vita

Christopher M. Blackwell was born in Pensacola, FL. In 1995 he was born-again when he accepted Jesus Christ as his Lord and Savior. He attended the University of Florida on an Air Force ROTC scholarship and graduated with honors and a degree in Mechanical Engineering in 1999.

Second Lieutenant Chris Blackwell completed his first assignment at the Air Force Research Laboratory, Wright Patterson, Ohio. While there he served as the lead structural analyst for the Compressor Aero Research Lab. He also managed the lab's research facility and personnel. When not in uniform, Lt Blackwell earned an MSA from Central Michigan University in 2002 with a perfect 4.0 GPA. He also met and married his beautiful wife.

In the fall of 2002 Lt. Blackwell was selected to attend the Air Force Institute of Technology to earn a Masters of Science in Aeronautical Engineering. While at AFIT his first son was born. After graduation Captain Blackwell will report to the Air Logistics Center at Hill AFB, Ohio.

REPORT DOCUMENTATION PAGE

Form Approved
OMB No. 074-0188

1. REPORT DATE *(DD-MM-YYYY)*	**2. REPORT TYPE**	**3. DATES COVERED** *(From – To)*
12-03-2004	**Master's Thesis**	Jun 2003 – Mar 2004

4. TITLE AND SUBTITLE

THE EVALUATION OF THE DAMPING CHARACTERISTICS OF A HARD COATING ON TITANIUM

5a. CONTRACT NUMBER

5b. GRANT NUMBER

5c. PROGRAM ELEMENT NUMBER

6. AUTHOR(S)

Blackwell, Christopher M., Captain, USAF

5d. PROJECT NUMBER

5e. TASK NUMBER

5f. WORK UNIT NUMBER

7. PERFORMING ORGANIZATION NAMES(S) AND ADDRESS(S)

Air Force Institute of Technology
Graduate School of Engineering and Management (AFIT/EN)
2950 Hobson Way, Building 641
WPAFB OH 45433-7765

8. PERFORMING ORGANIZATION REPORT NUMBER

AFIT/GAE/ENY/04-M03

9. SPONSORING/MONITORING AGENCY NAME(S) AND ADDRESS(ES)

Dr. Charles Cross
AFRL/PRTS
1950 5th Street Bldg. 252 DSN: 656-5530
WPAFB OH 45433-7251

10. SPONSOR/MONITOR'S ACRONYM(S)

11. SPONSOR/MONITOR'S REPORT NUMBER(S)

12. DISTRIBUTION/AVAILABILITY STATEMENT

APPROVED FOR PUBLIC RELEASE; DISTRIBUTION UNLIMITED.

13. SUPPLEMENTARY NOTES

14. ABSTRACT

This research evaluates the damping characteristics of magnesium aluminate spinel, $MgO+Al_2O_3$, (mag spinel) on titanium plates. The material and aspect ratio were chosen to approximate the low aspect ratio blades found in military gas turbine fans. The plates were tested with a cantilevered boundary condition, using electrodynamic shaker excitation. The effective test area of each specimen was 4-1/2 in. x 4-1/2 in. Mag spinel was applied to both sides of the plate, at a thickness of .01 in., and damping tests were run at room temperature. The effect of the coating was evaluated at the 2nd bending mode (mode 3) and the chordwise bending mode (mode 4). A scanning laser vibrometer revealed the frequency and shape of each mode for the plates. Sine sweeps were used to characterize the damping of the coated and uncoated specimens for the modes tested. The coating increased damping nonlinearly for both modes tested.

15. SUBJECT TERMS

Vibration, High Cycle Fatigue, Damping, Fatigue, Titanium, Magnesium Aluminate Spinel, Resonance, Resonance Frequency,
Resonance Mode, Finite Element Analysis

16. SECURITY CLASSIFICATION OF:			**17. LIMITATION OF ABSTRACT**	**18. NUMBER OF PAGES**	**19a. NAME OF RESPONSIBLE PERSON**
a. REPORT	**b. ABSTRACT**	**c. THIS PAGE**			Dr. A. N. Palazotto (ENY)
U	**U**	**U**	**UU**	116	**19b. TELEPHONE NUMBER** *(Include area code)* (937) 255-3636, e-mail: Anthony.Palazotto@afit.edu

Standard Form 298 (Rev. 8-98)
Prescribed by ANSI Std. Z39-18